# TriBeam System for Multimodal Data

M.P. Echlin[1], A. Mottura[2], J.C. Stinville[1], M.S. Titus[1], S. Krämer[1], M. DeGraef[3], P. Gumbsch[4], T.M. Pollock[1]

[1] *Materials Department, University California at Santa Barbara, USA*
[2] *School of Metallurgy and Materials, University of Birmingham, UK*
[3] *Carnegie Mellon University, Pittsburgh, PA*
[4] *Karlsruhe Institute of Technology, Karlsruhe, Germany*

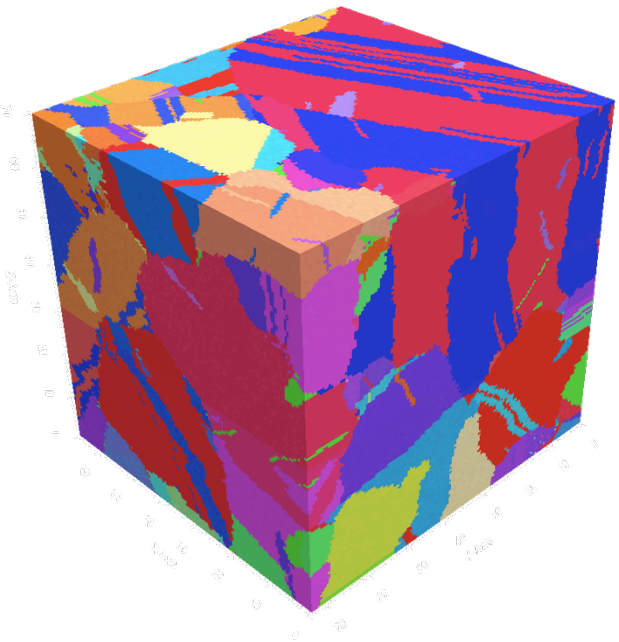

Acknowledgements:
M. Straw, M. Groeber (AFRL), M. Jackson (BlueQuartz), J.P. McDonald (Dow), S.M. Yalisove (UM), Pollock Group, GE, FEI Company

# Sensitivity of Material Properties on Volume

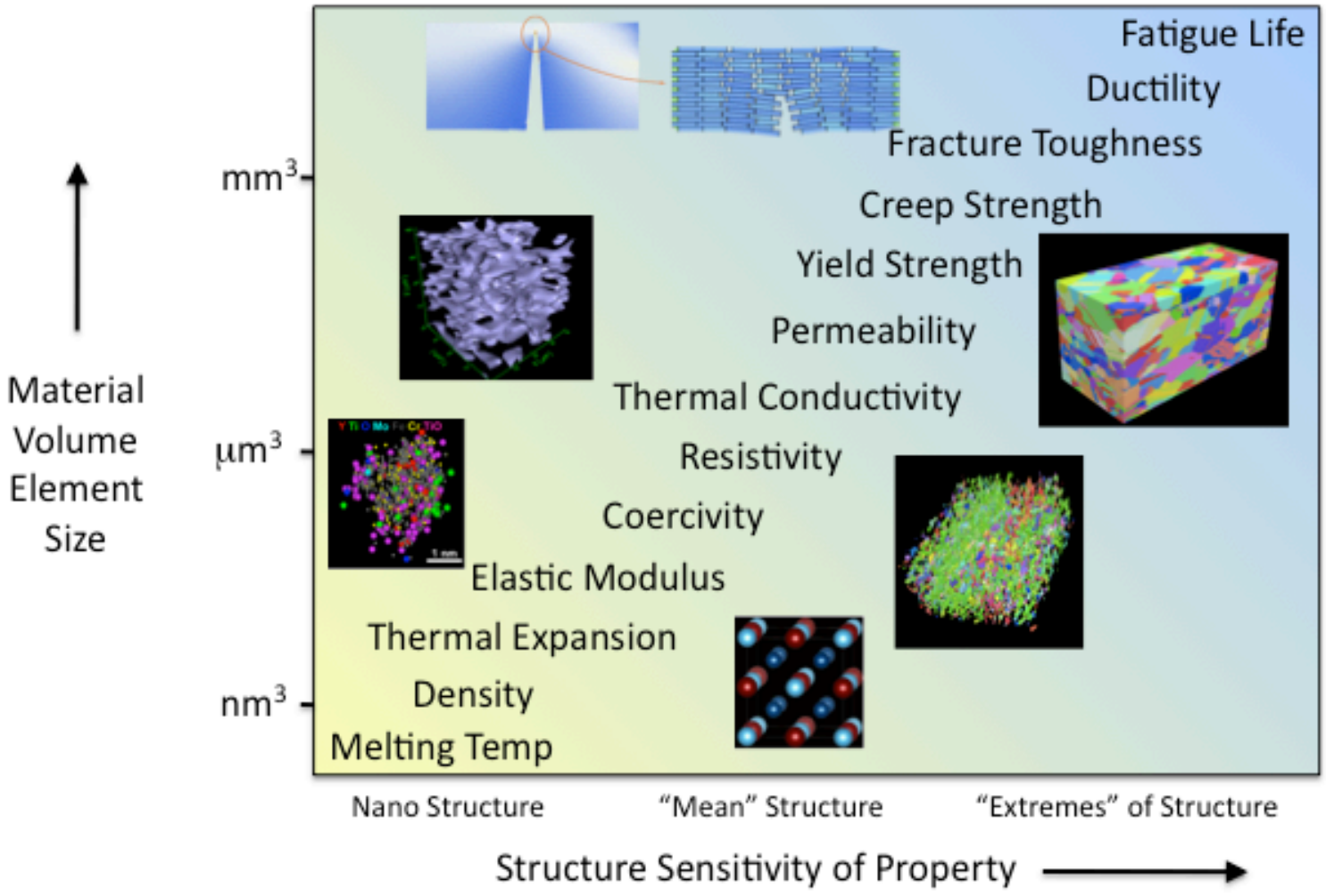


We ***need*** more volume(s)!

# Femtosecond Lasers and Tomography

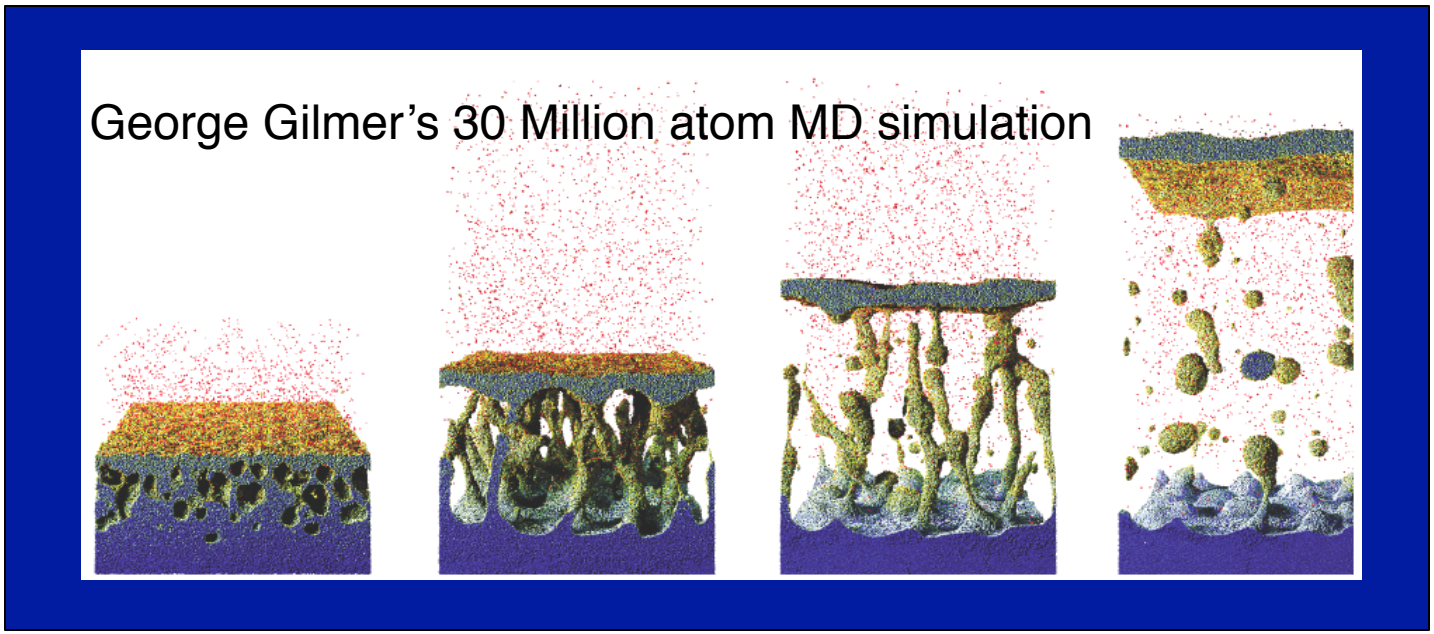


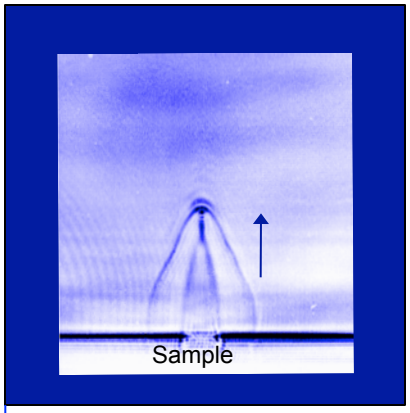


- 150fs laser pulse; ablation occurs much later (ns)
- Ablated layer 30 – 50nm in thickness, kHz repetition
- Collateral damage very limited (no melting)
- Same process occurs in wide range of materials (metals, semiconductors, ceramics, polymers)
- Layer by layer ablation *ex-situ* in air or *in-situ* in vacuum

J.P. McDonald, S. Ma, T. M. Pollock, S. M. Yalisove, *J Appl Phys,* 103, 093111 (2008).

# 3-D Data Acquisition Techniques

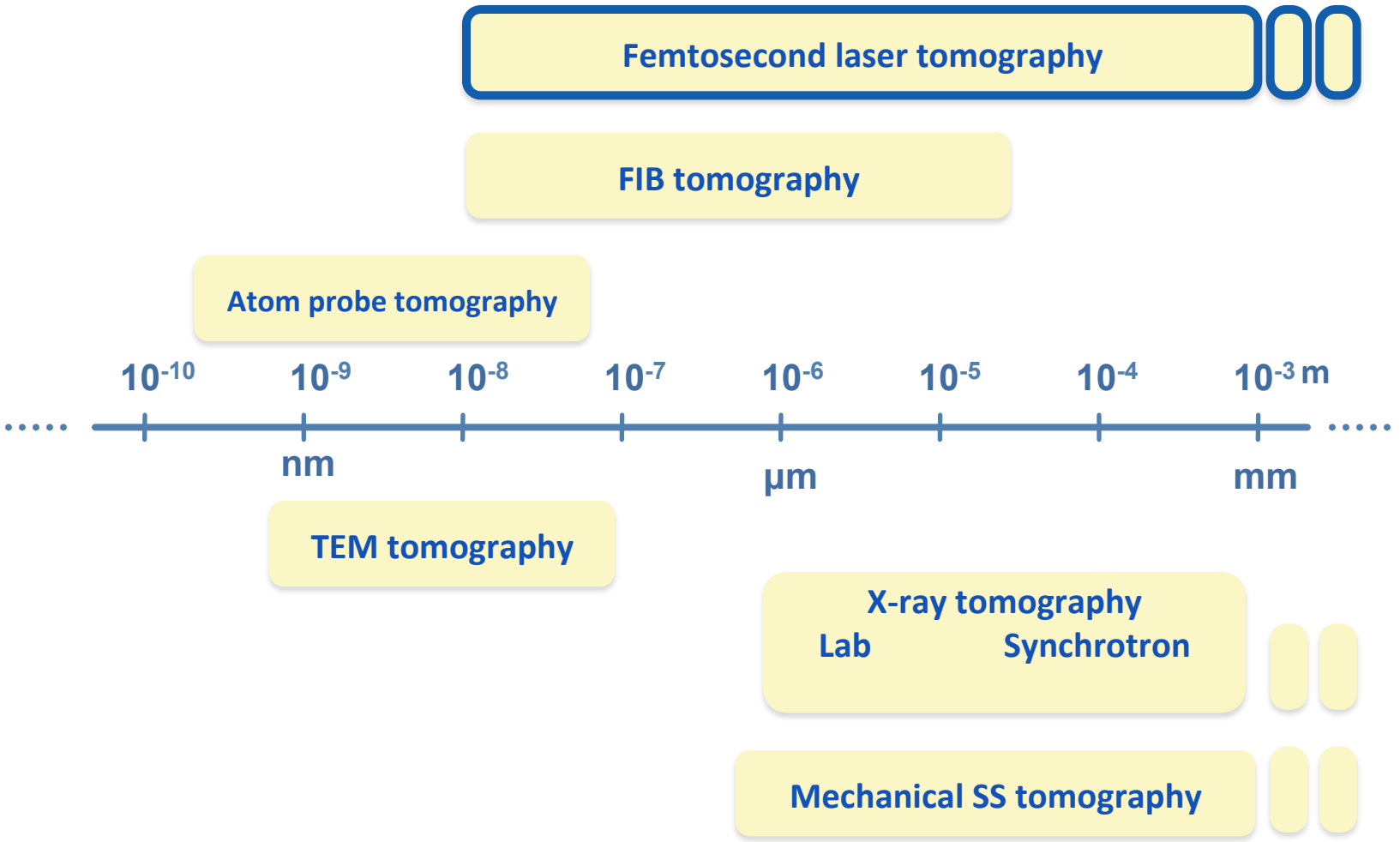

# 3-D Data Acquisition Techniques

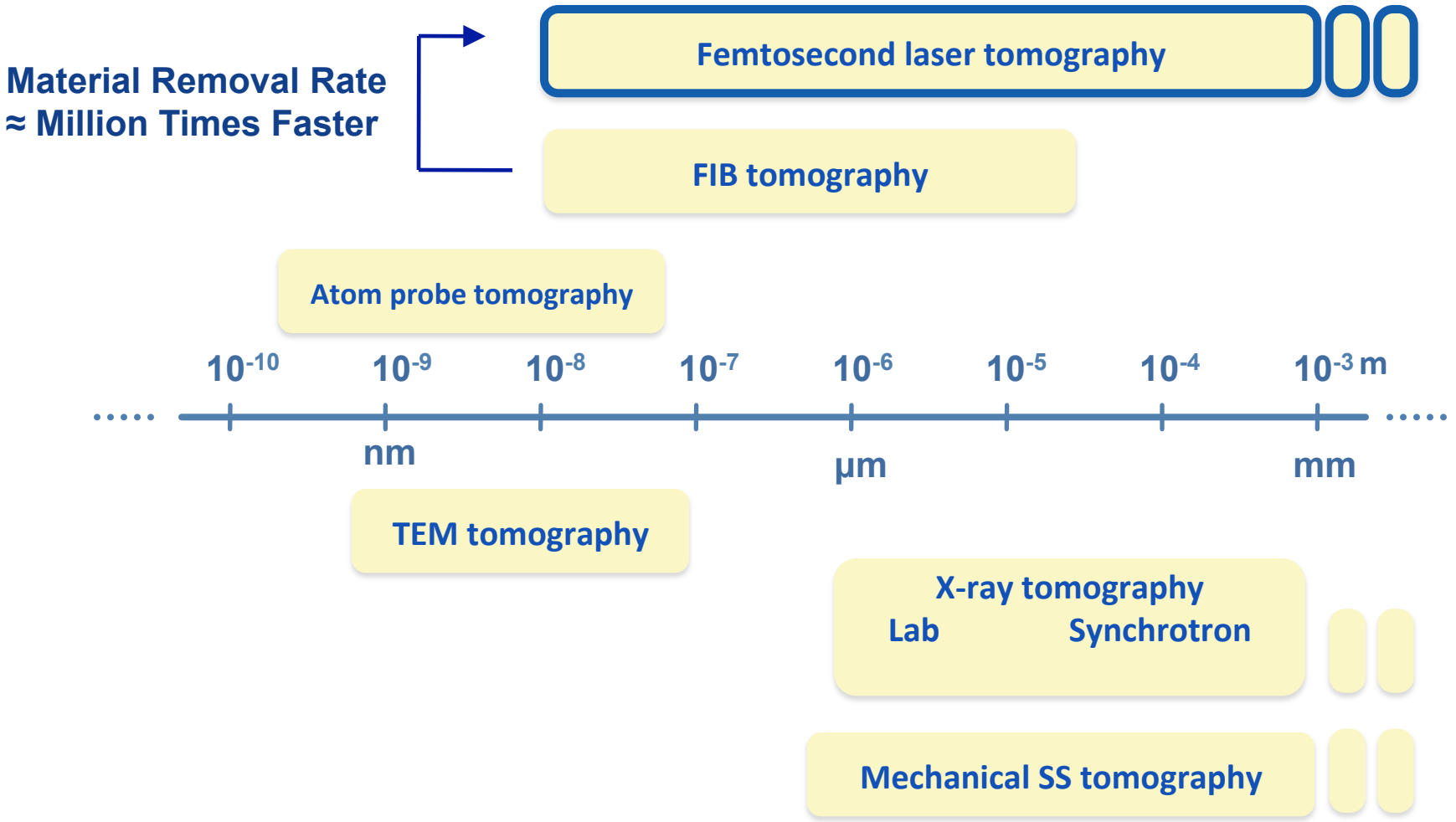

## Detectors and imaging

- SE, BSE, EDS, EBSD

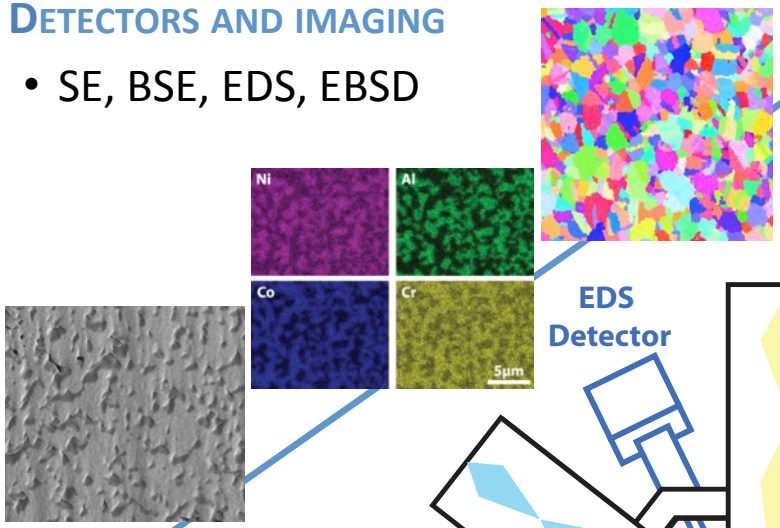


## Laser delivery

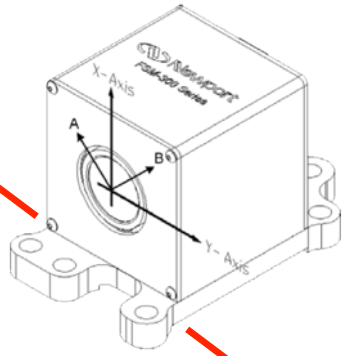


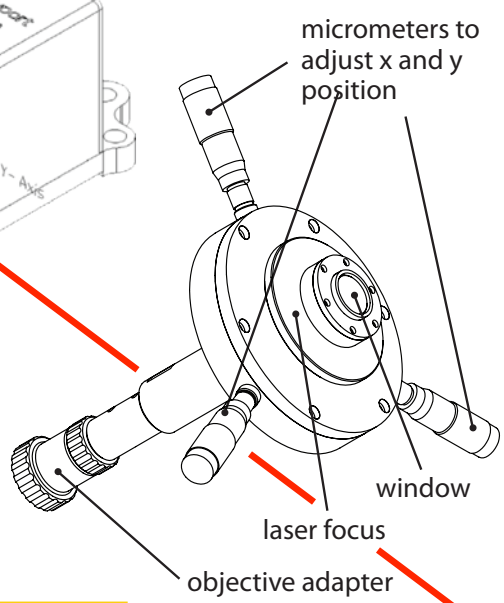


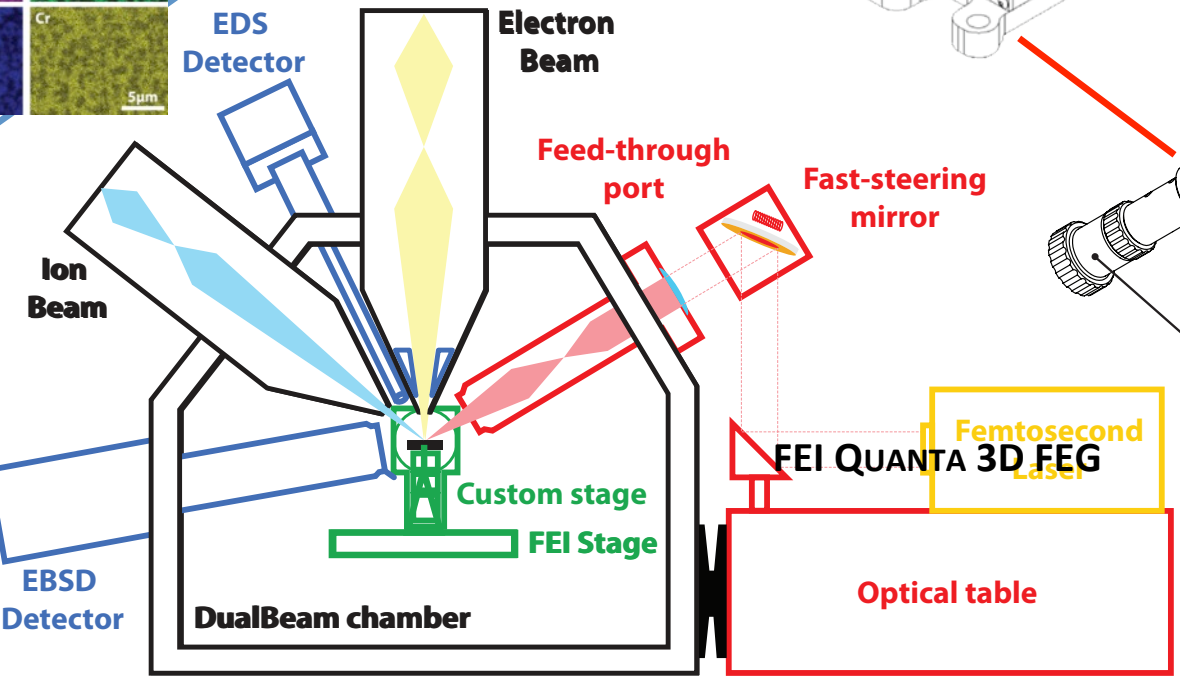


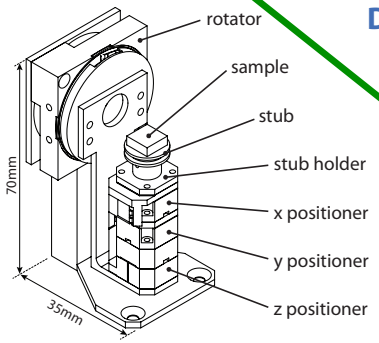


- Full eucentric rotation
- nm-resolution

## Sample positioning

- 780 nm
- 150fs pulses
- 1kHz repetition rate
- Material removal with negligible heat affected zone
- $10^5$-$10^6$ faster at removing material compared to ion beam

## Femtosecond laser

# TriBeam System

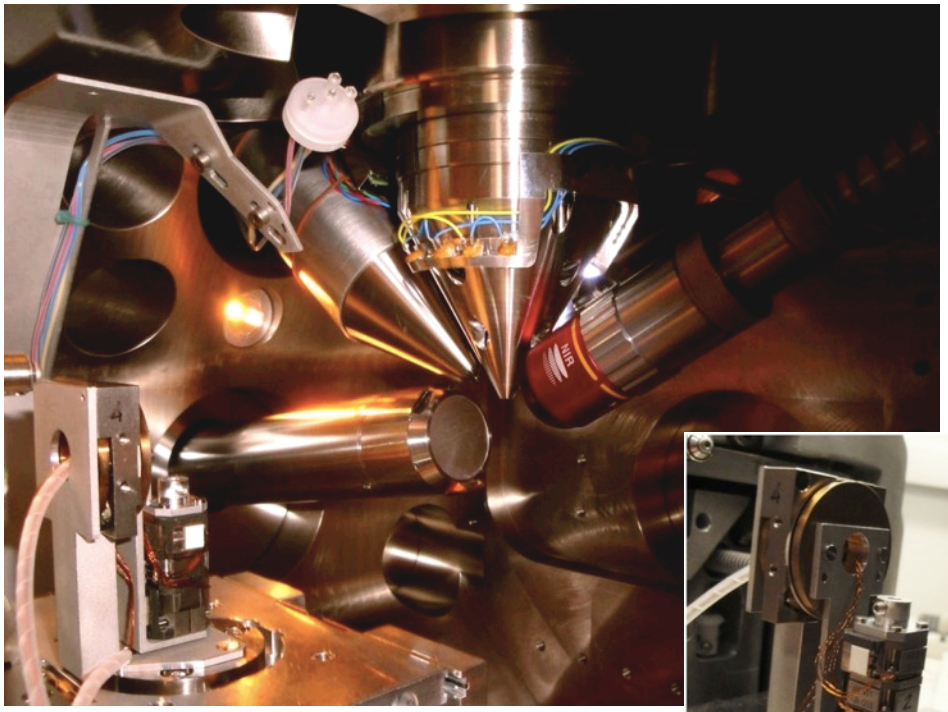

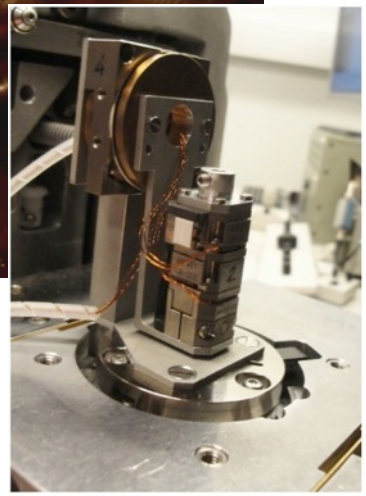

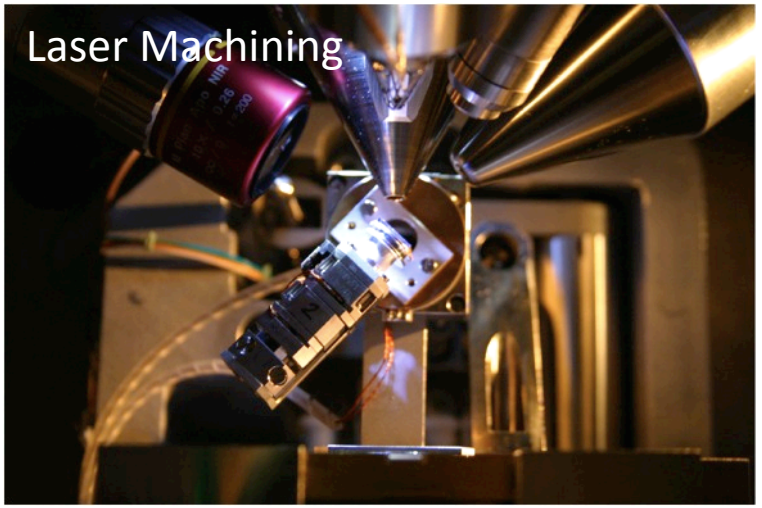


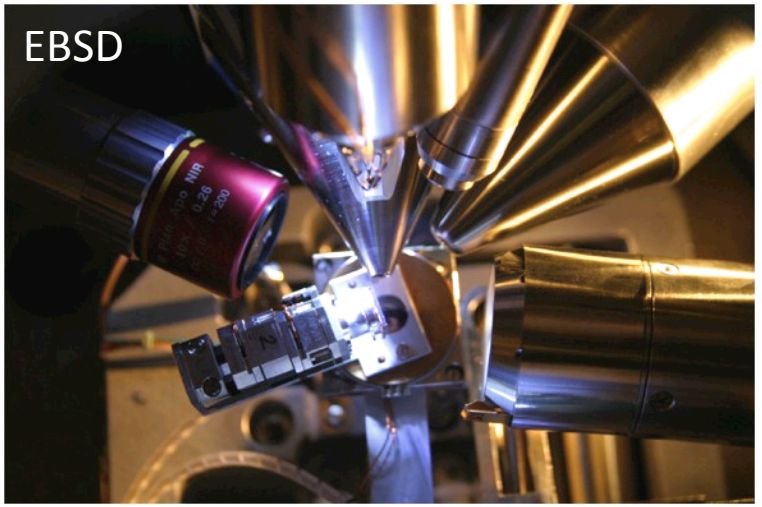


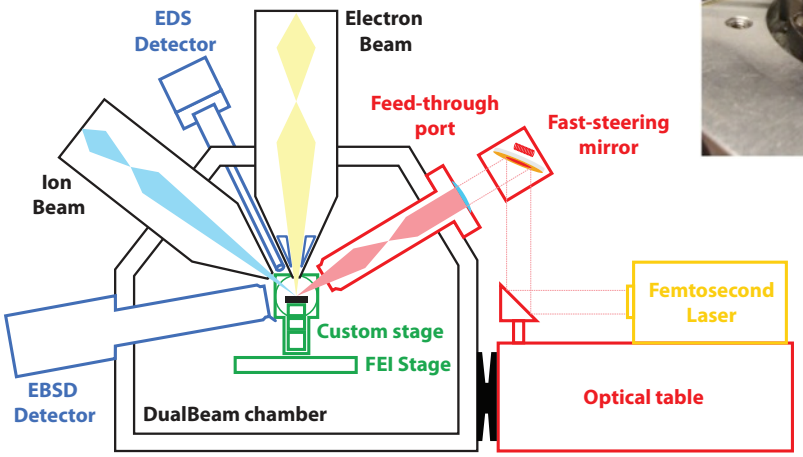


*M. Echlin, A. Mottura, C. Torbet, T.M. Pollock. RSI (2012)*

# Delivering the Beam

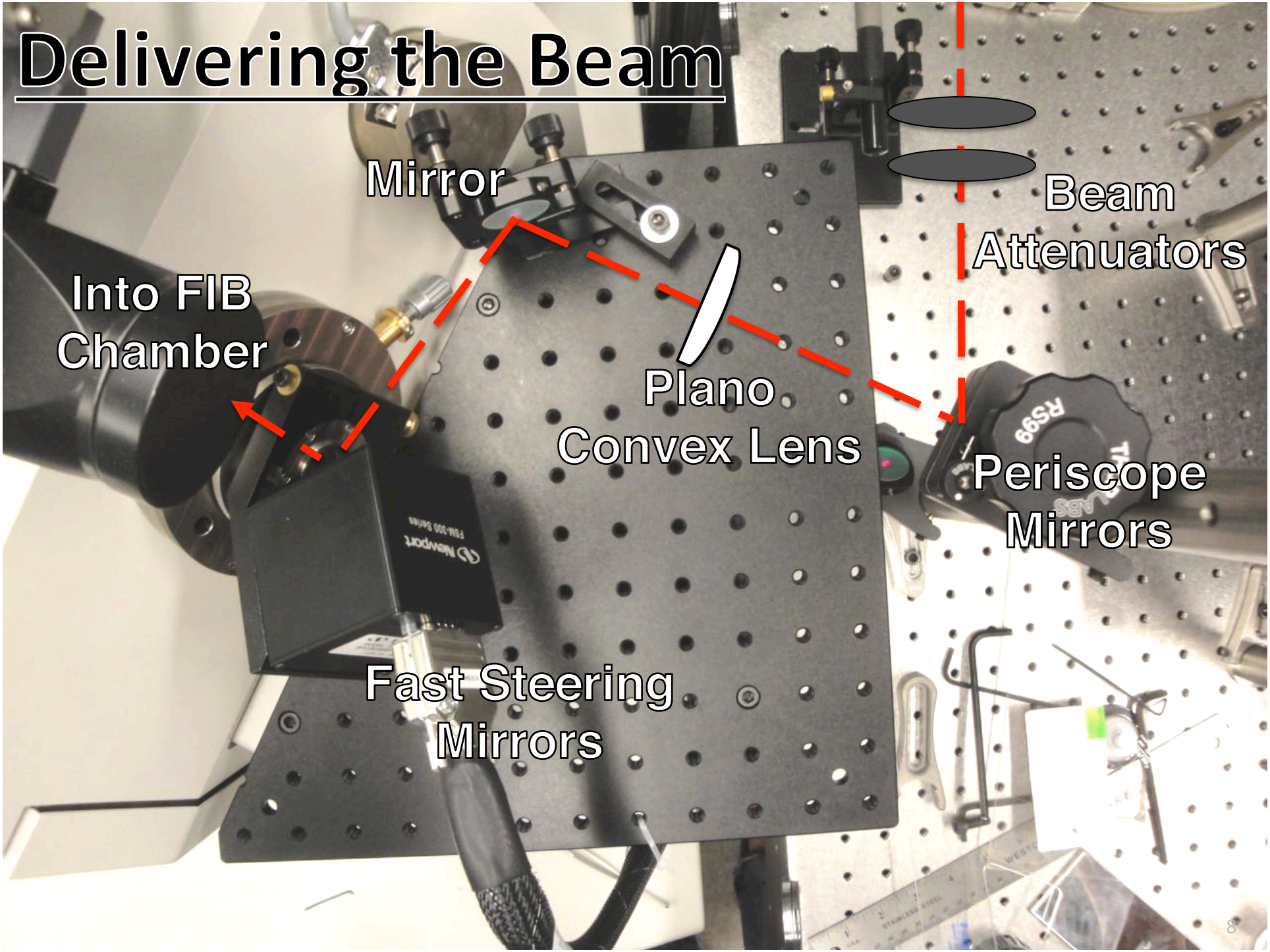

# Laser in Vacuum / Eucentric Point

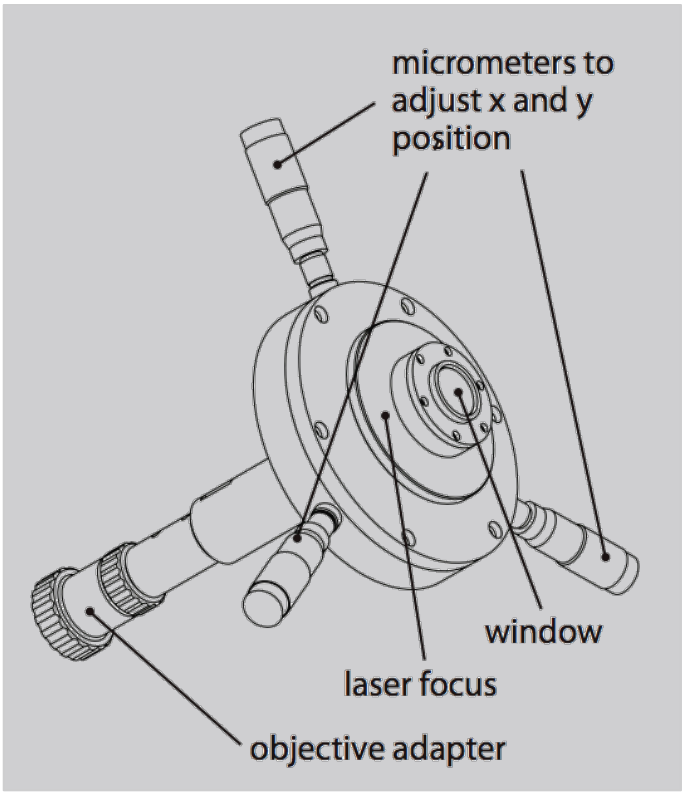


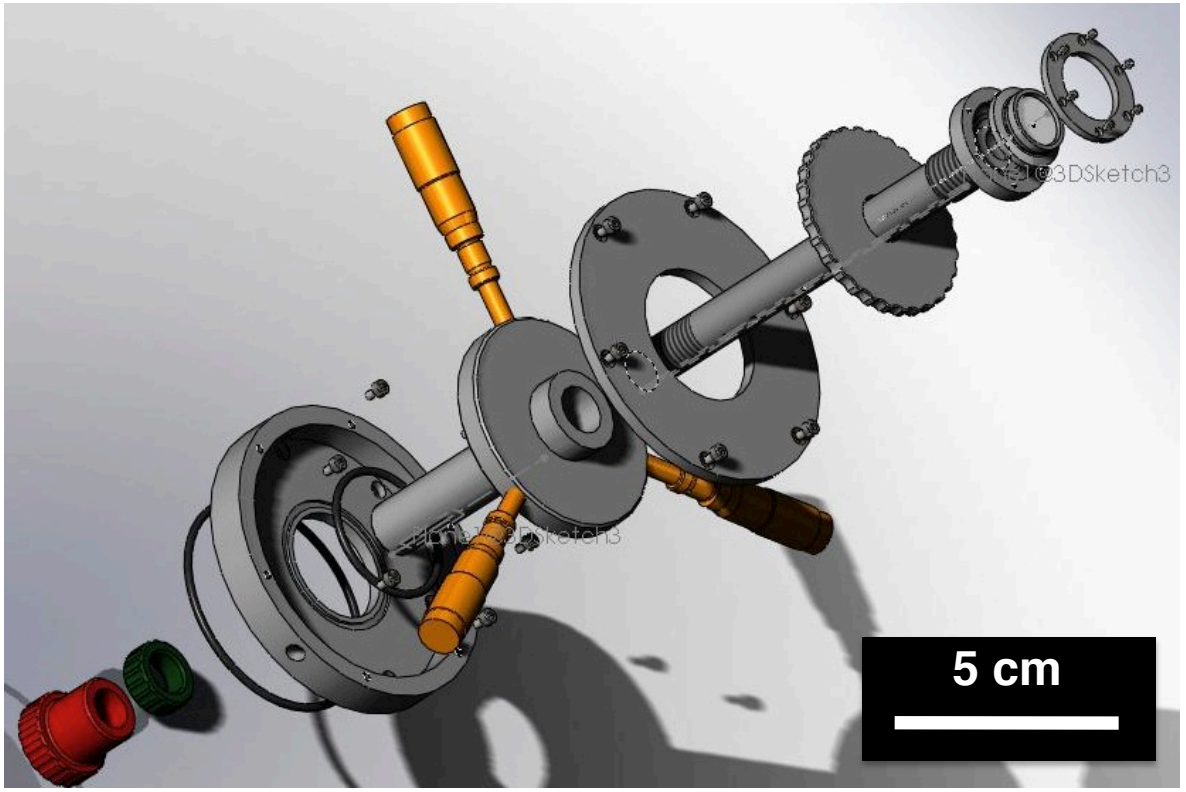


- Micrometer adjustments for X and Y positioning
  - Target laser to eucentric position
- Microscope objective position can be changed
  - Focus laser beam to eucentric position
- Adjustments can be made in vacuum

# W-Cu Applications

**Aerospace – Mach 5+**
Hypersonic Vehicles

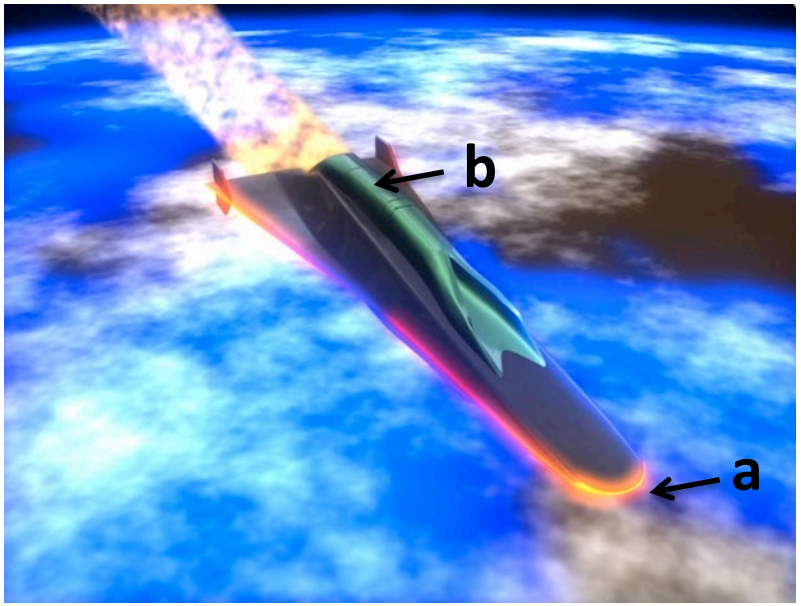


a) Leading edge - Ablative structural material. 2700°C at leading edge.
b) Combustor – thermal management via ablative cooling. 3000°C inside combustor

**Fusion – Power Generation**
ITER Tokomak Blanket
Module Heat Sinks

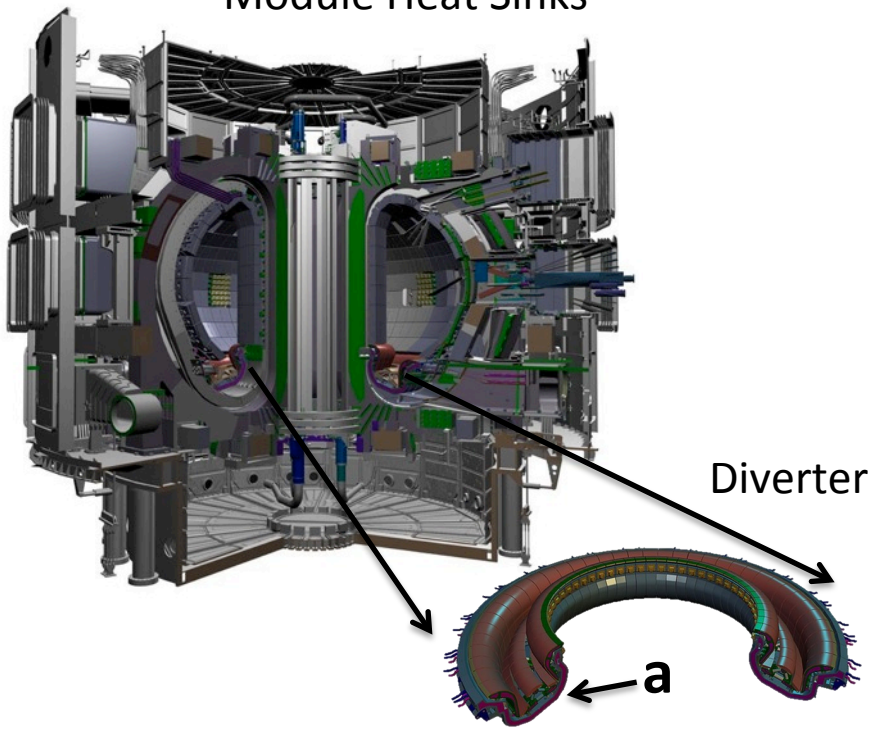


a) Thermal management material – heat sinking below plasma facing material or use under pulsed fusion events, extracts heat withstand up to 3000°C over a 20 year lifetime.

*[1] http://phys.org/news180844091.html*

*[2] http://www.iter.org/mach*

# Materials for High Heat Flux Environments

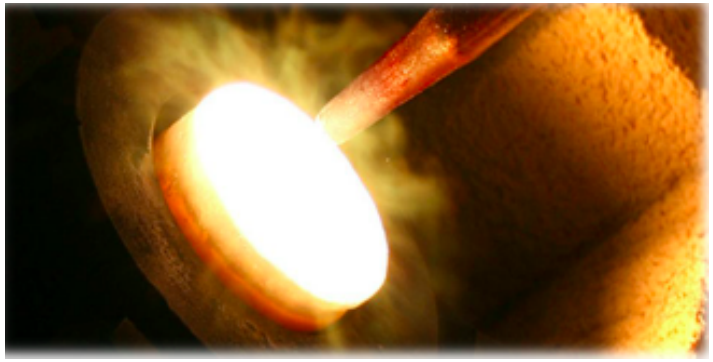

**Interpenetrating W – Cu Composites**

- Ablation of Cu phase provides cooling under high heat fluxes
- CuW used for thrust vectoring, experience extremely high temperatures (>2000°C)
- Want to Measure Permeability, Sv, $V_f$ directly in 3D

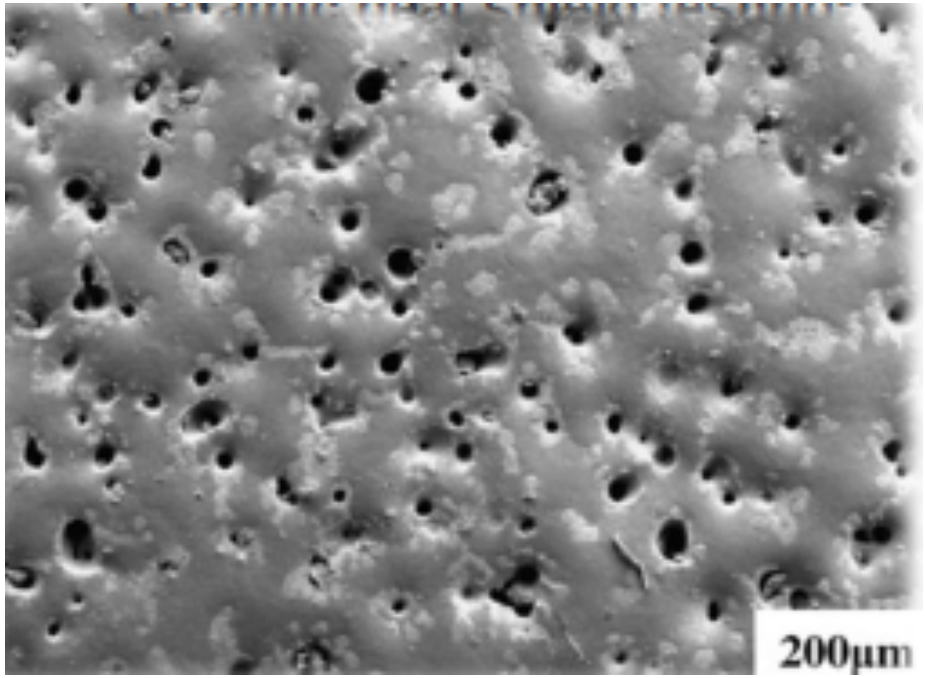


Following High Heat Flux Ablation

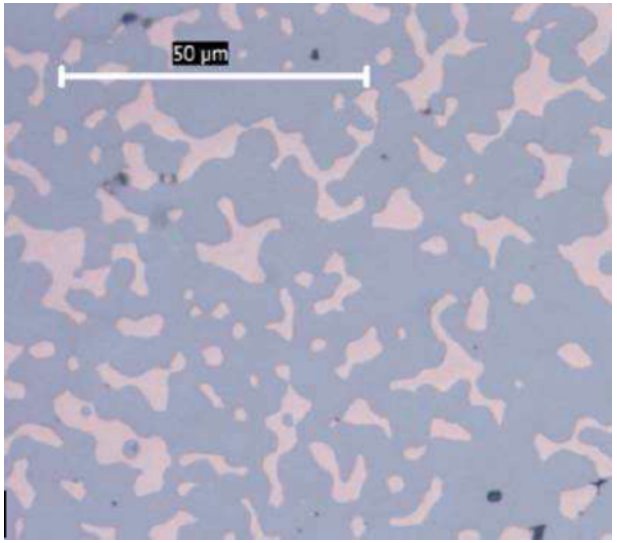


W-Cu Composite

# Schematic of Laser Ablation

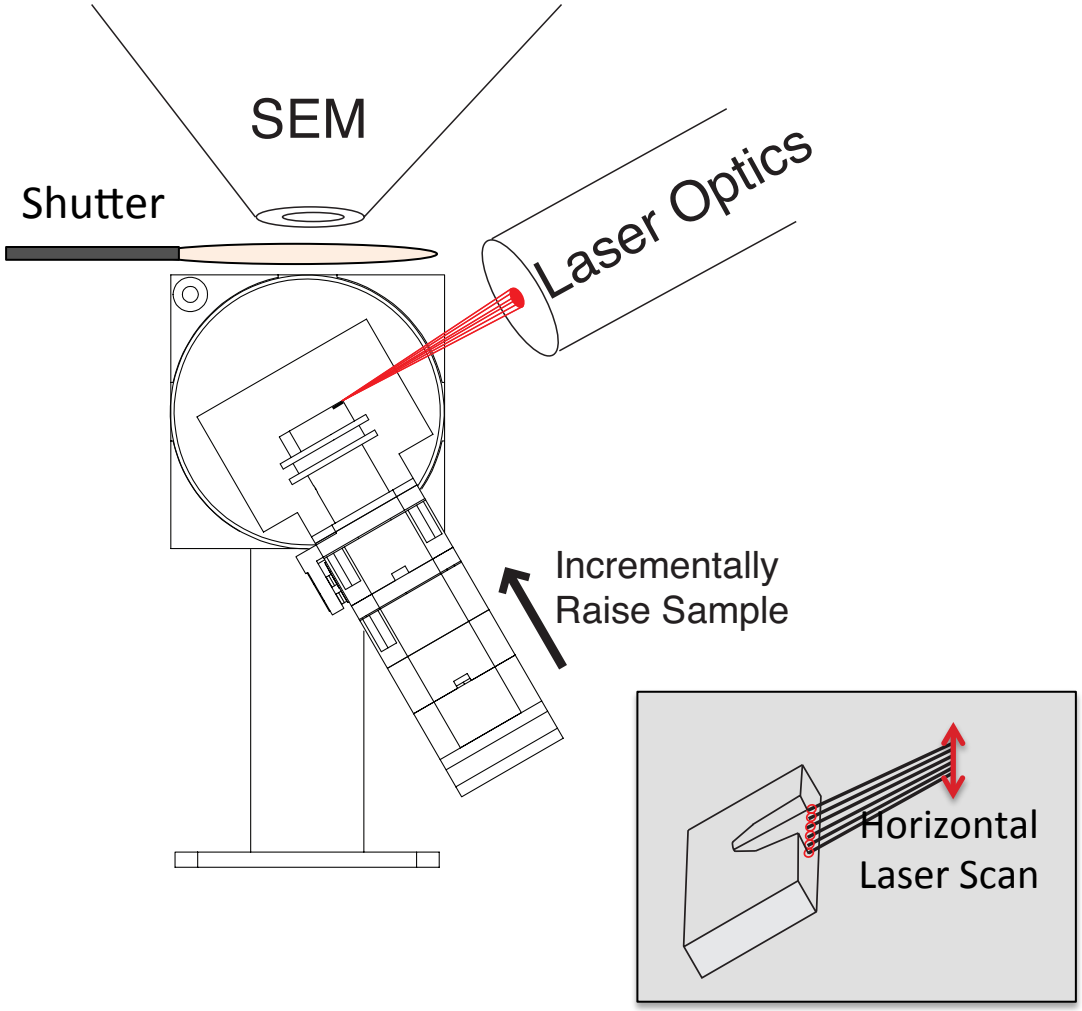


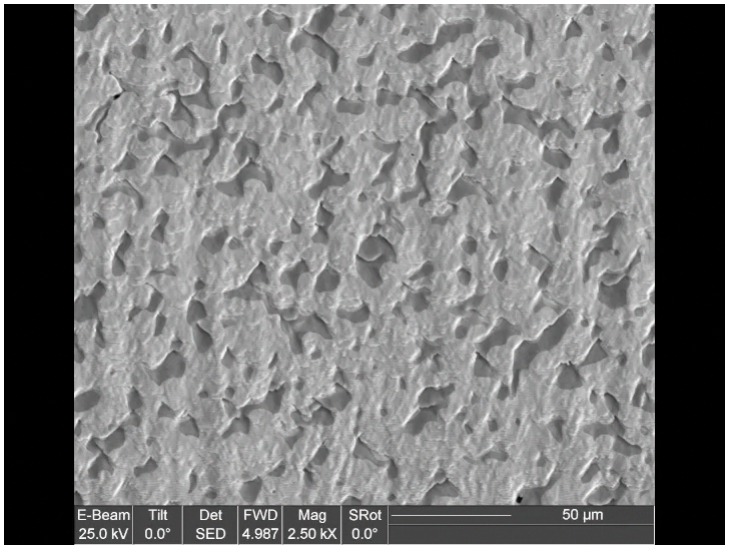


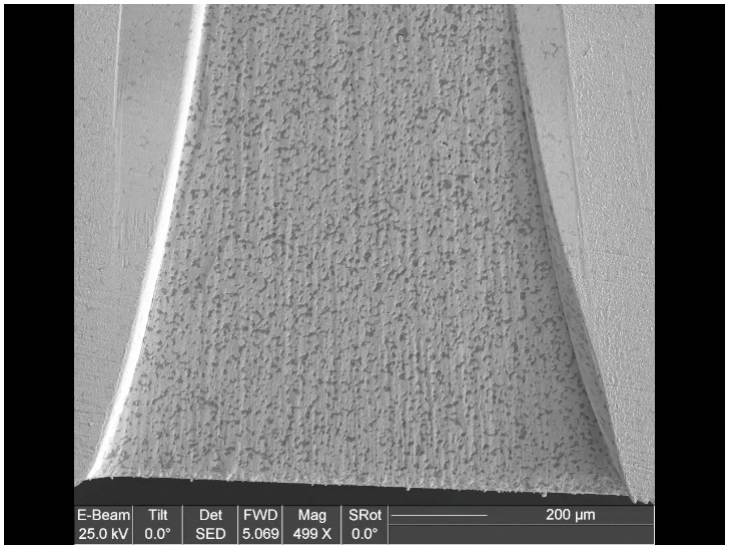


Machining time per slice = 25 s
3-D dataset acquisition time = 48 h.

# WCu Image Processing and Segmentation

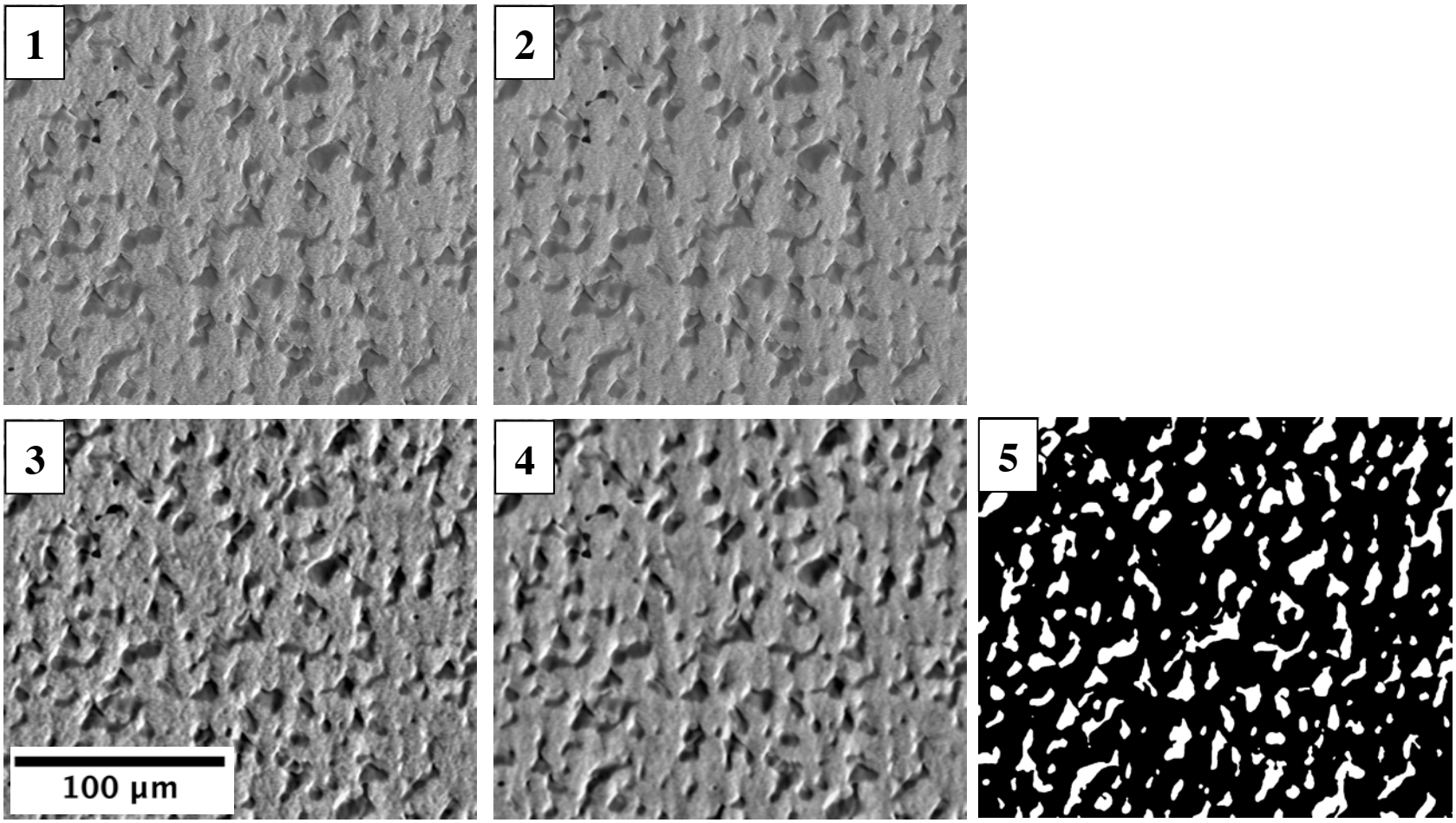


(1) Raw secondary electron image as captured by the TriBeam
(2) 3D median filter
(3) FFT bandpass filters for horiz. high frequency LIPSS and vert. low frequency curtaining
(4) 3D Gaussian filtering
(5) Batch EM-MPM segmentation using initialized areas

# Serial Sectioning: Cu15W

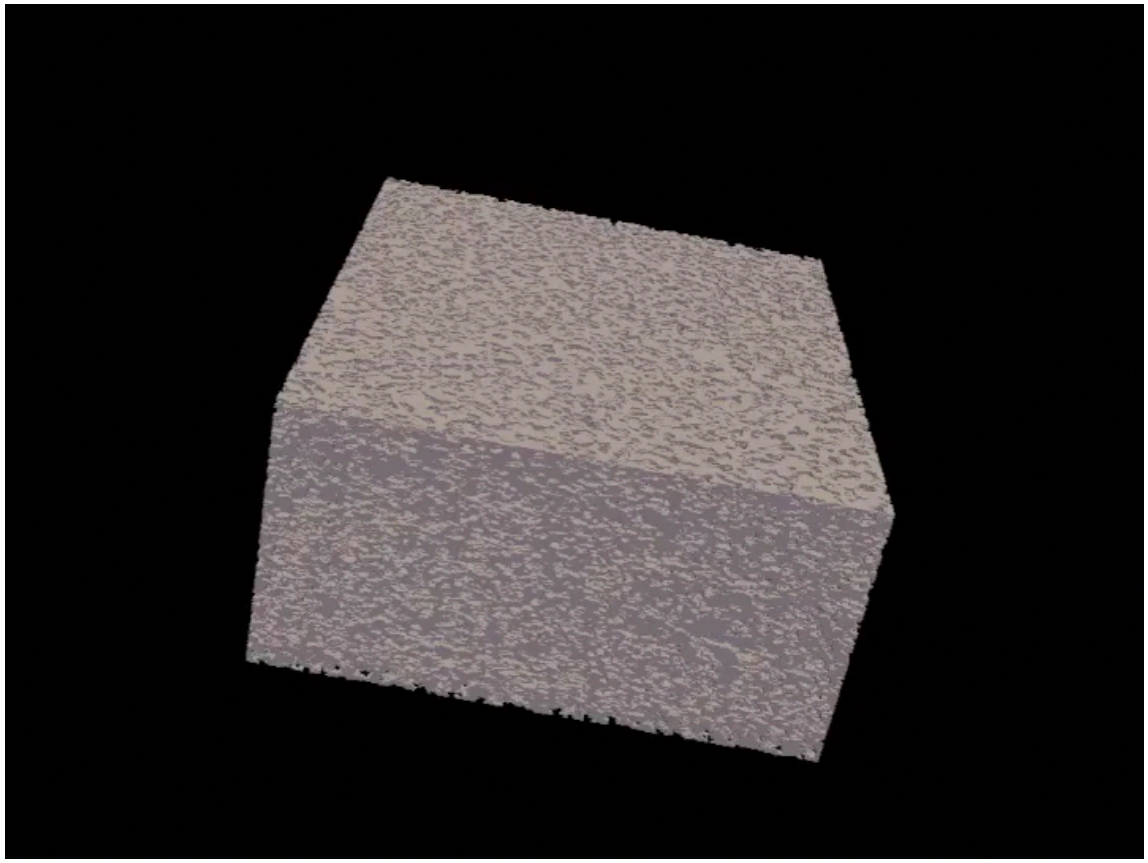

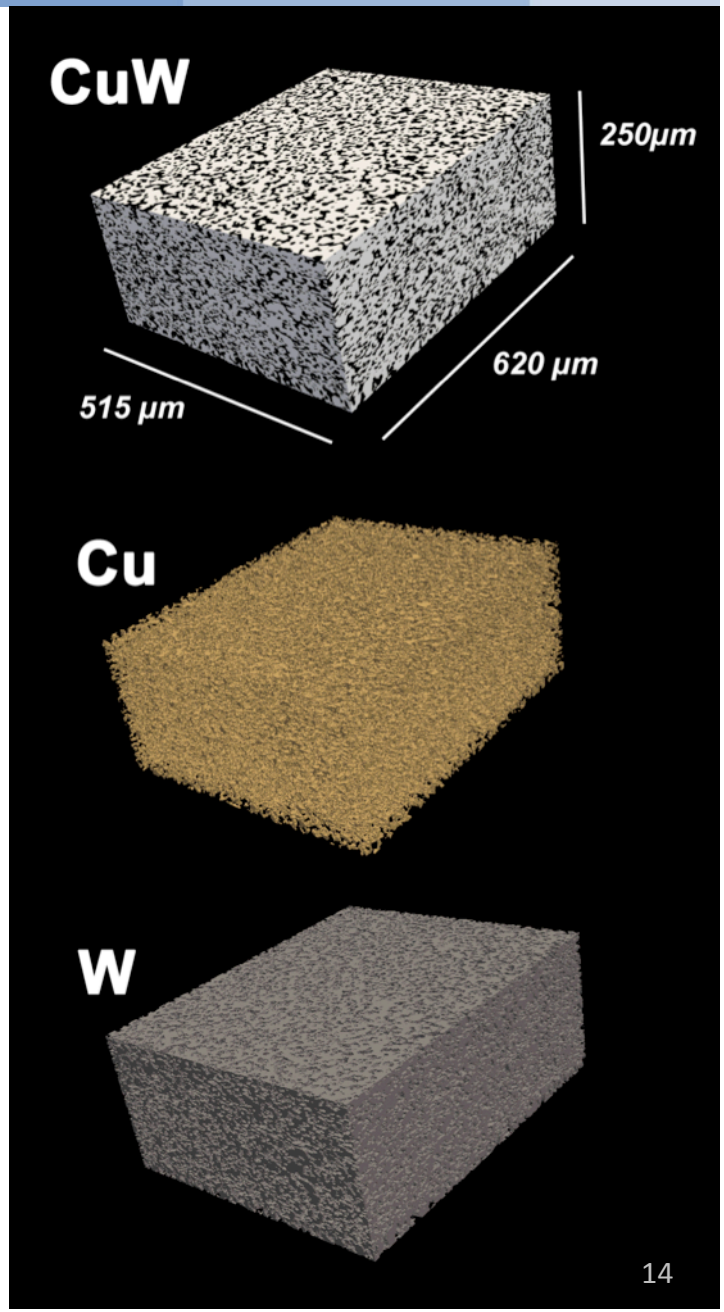


- Cu volume fraction measured 28 vol%
- Nominal Cu composition is 15 wt% (27.5 vol%)
- 1000 SE images collected
- Interconnected Cu phase
- 2D Dilation / Erosion shows potential segmentation error of less than +/-4%

# MVE sampling in WCu

## Example Volume Element Samplings

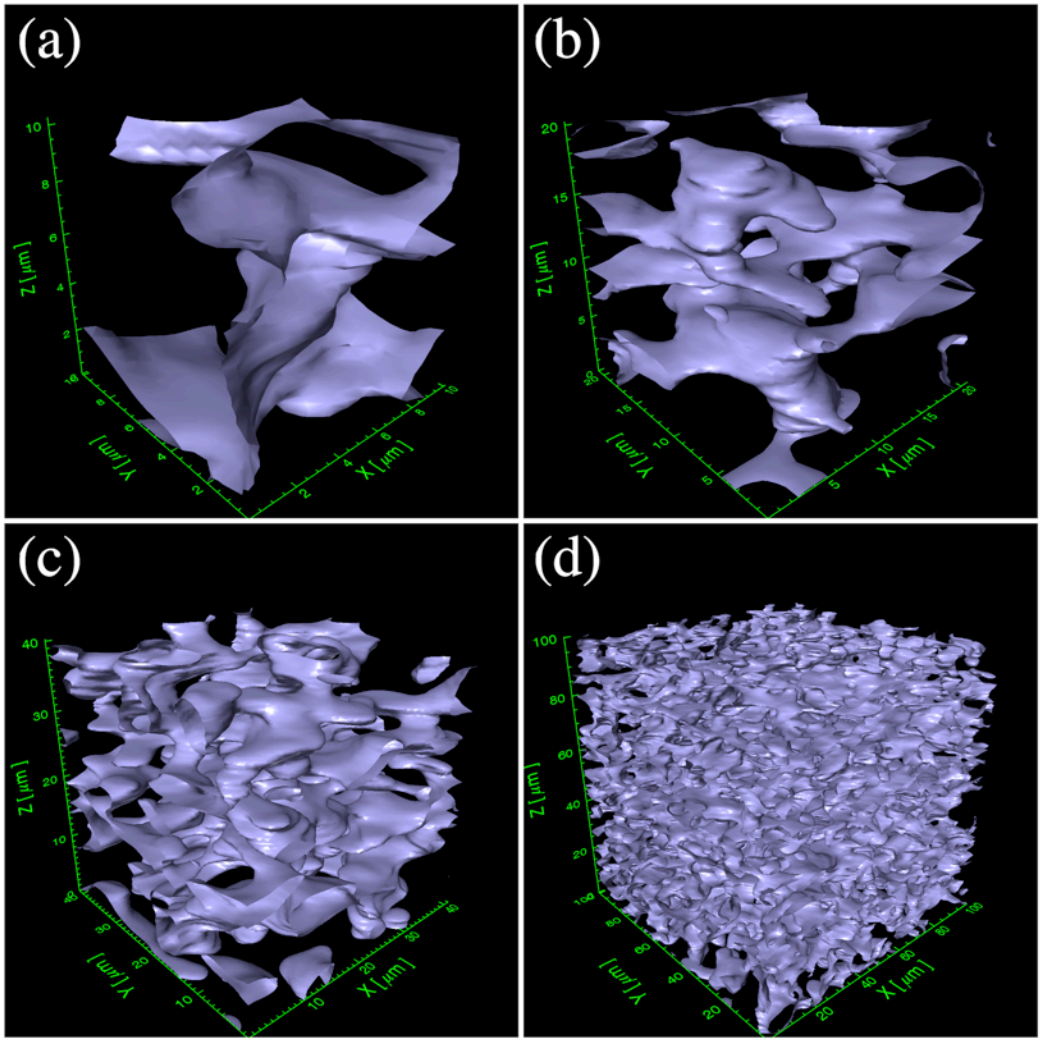


## Sampling Methodology

- Random volumes selected from with edge sizes ranging from 10µm-160µm
- $V_f$, $S_v$ measured for each sample
- K calculated from $V_f$, $S_v$ using the Kozeny-Carmen model
- Compute variability in $V_f$, $S_v$, K to determine MVE size and PVE dependency
- Select desired bounds on K to set the PVE size which in turn sets the MVE size

# WCu Mesh Smoothing

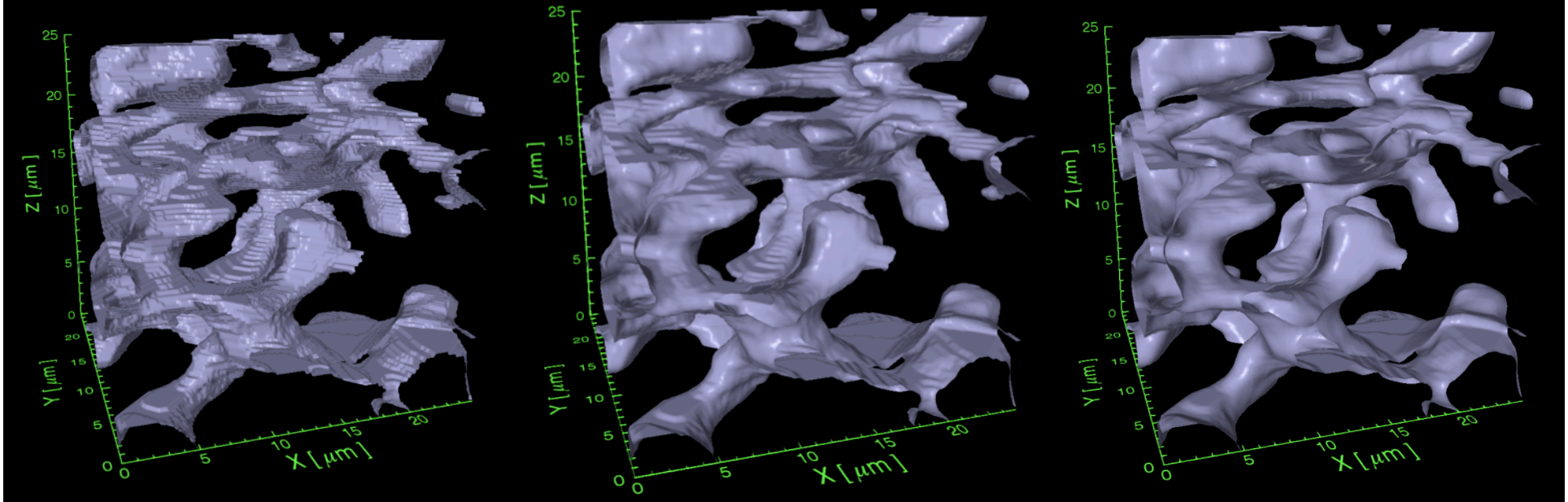


- $S_v$ has dependence on smoothing
- Convergence is not affected by smoothing
- Small regions of connectivity unperturbed

# MVE Sampling for Property Convergence

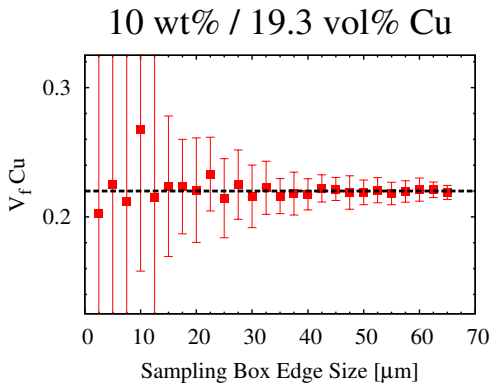


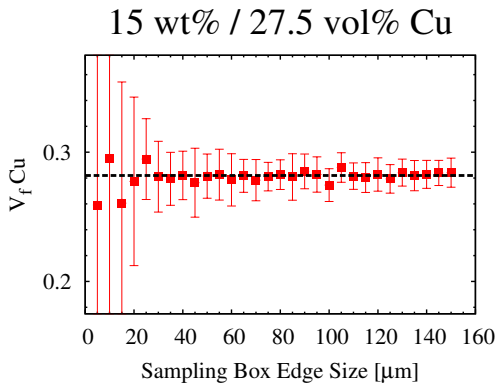


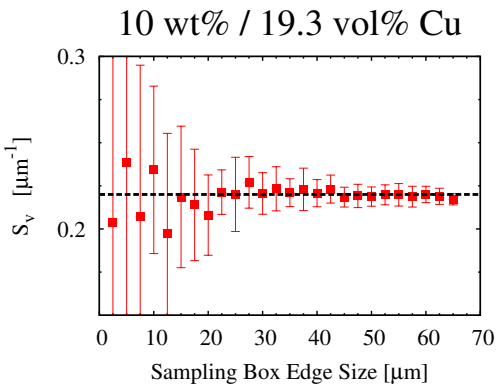


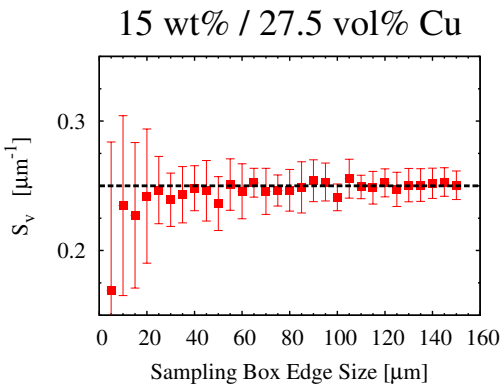


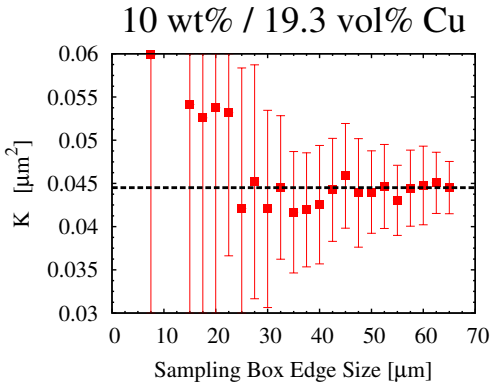


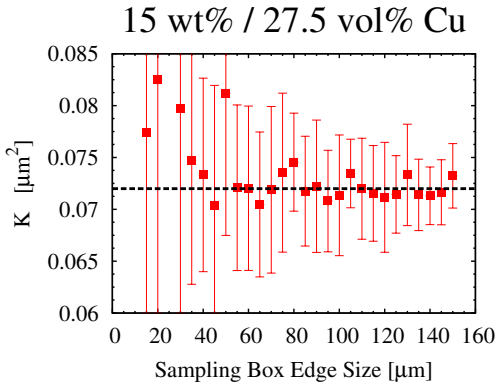


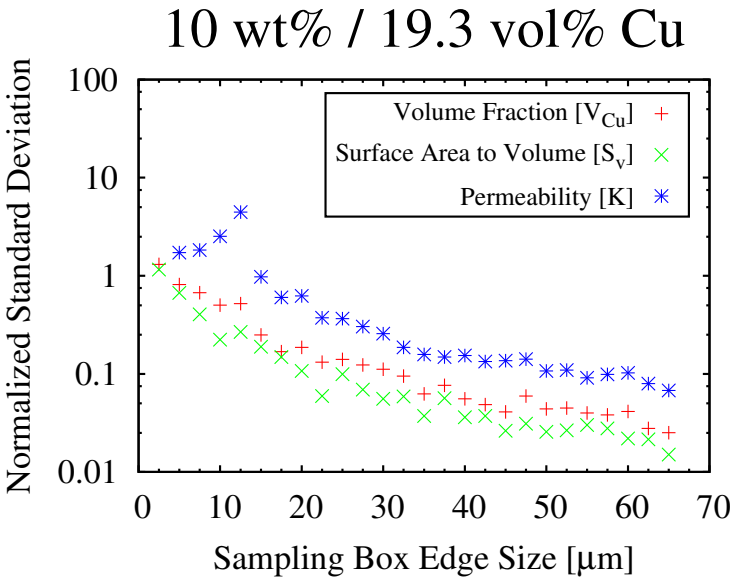


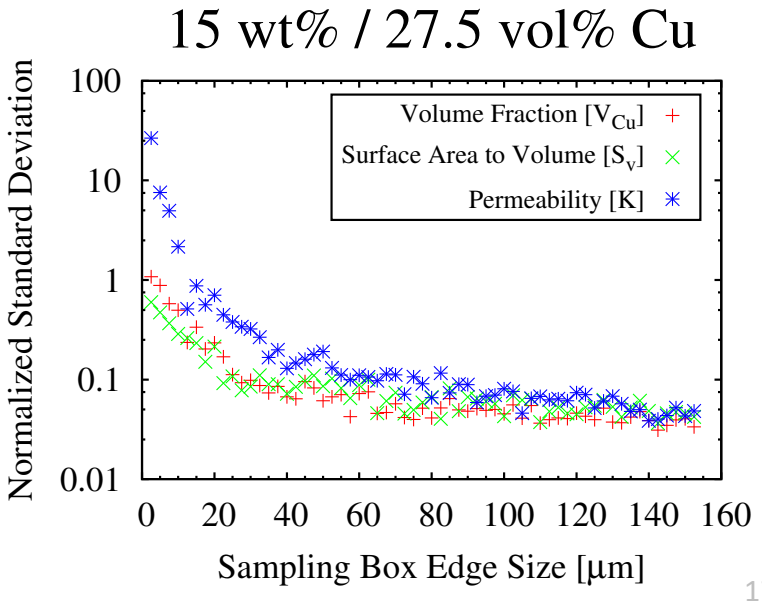

# Representative Volumes

**Microstructural Volume Elements (MVE) –** The volume necessary to define the microstructure of interest

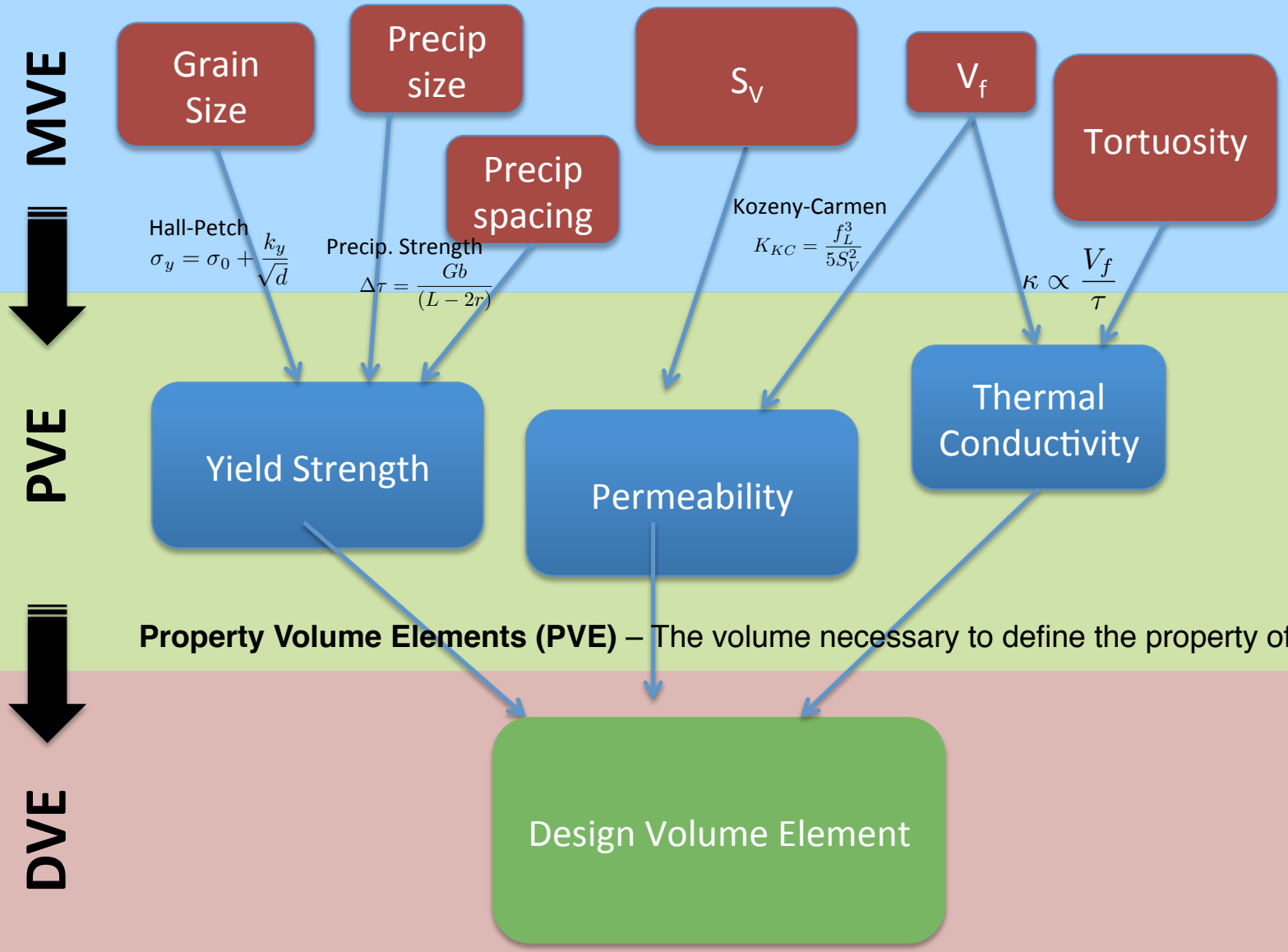


**Property Volume Elements (PVE)** – The volume necessary to define the property of interest

**Design Volume Element (DVE)** – Volume necessary for convergence of all relevant PVEs

# PVE for Permeability

**Fluid Flow (Darcy's law):**

$$Q = \frac{-KA}{\mu}\frac{P_b - P_a}{L}$$

$$q = \frac{-K}{\mu}\nabla P$$

**Permeability Calculation (Kozeny-Carmen):**

$$K_{KC} = \frac{f_L^3}{5S_{GV}^2(1-f_L)^2} = \frac{f_L^3}{5S_V^2}$$

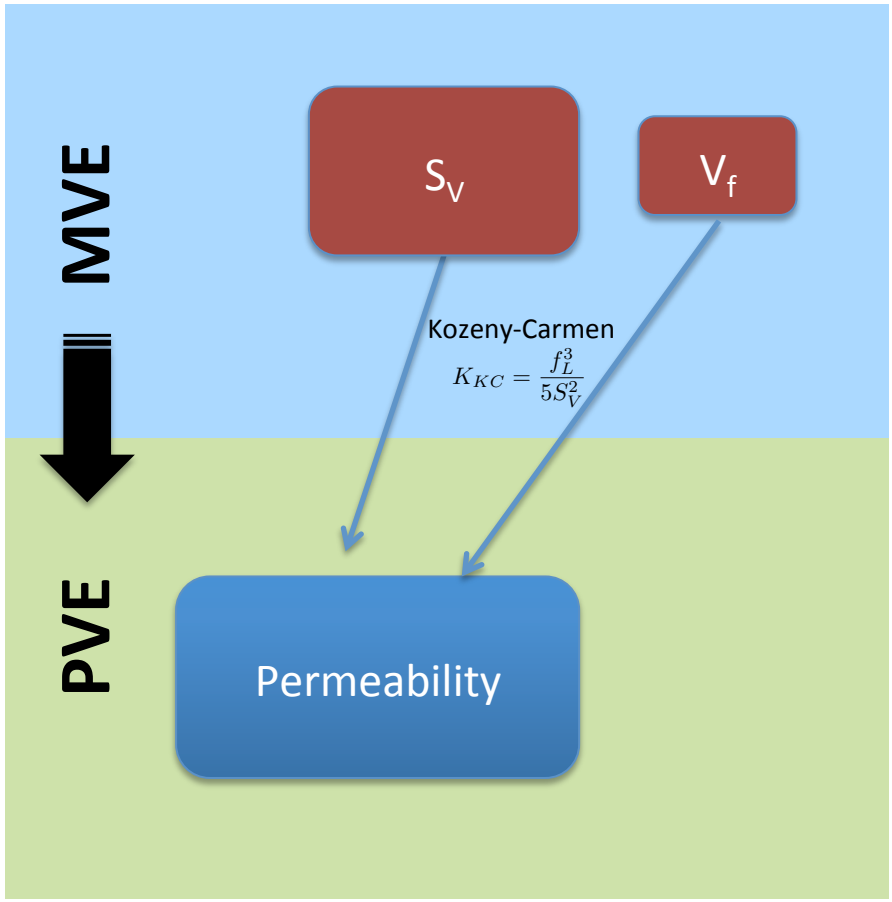

# FEA Compression Testing

## Mises stresses in the W Matrix

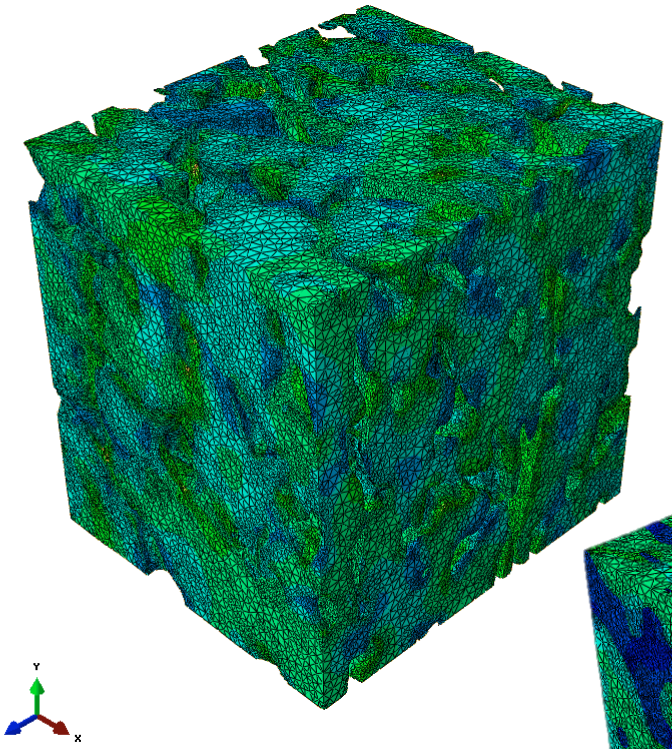

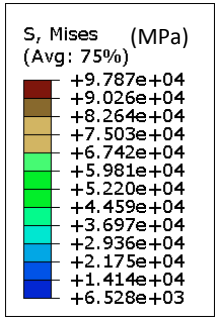


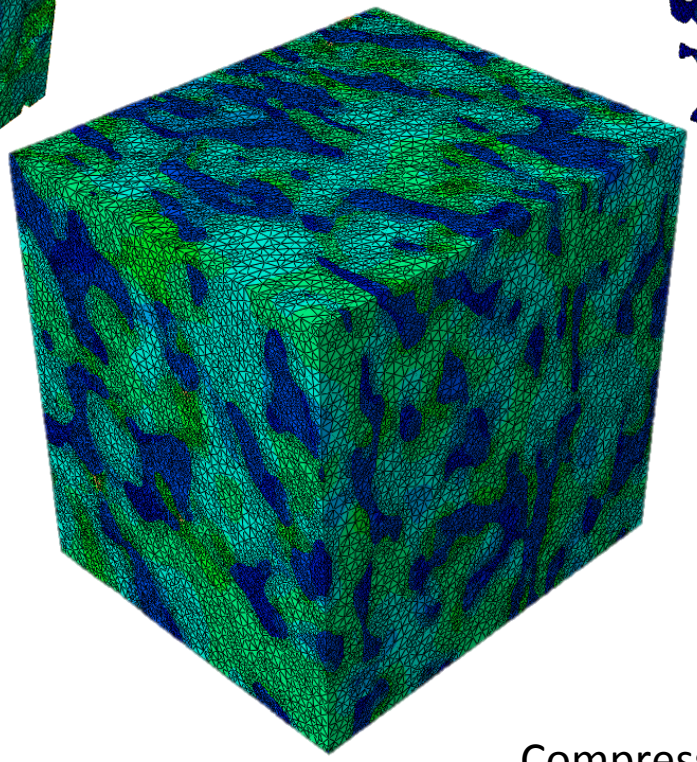

## Mises stresses in the Cu

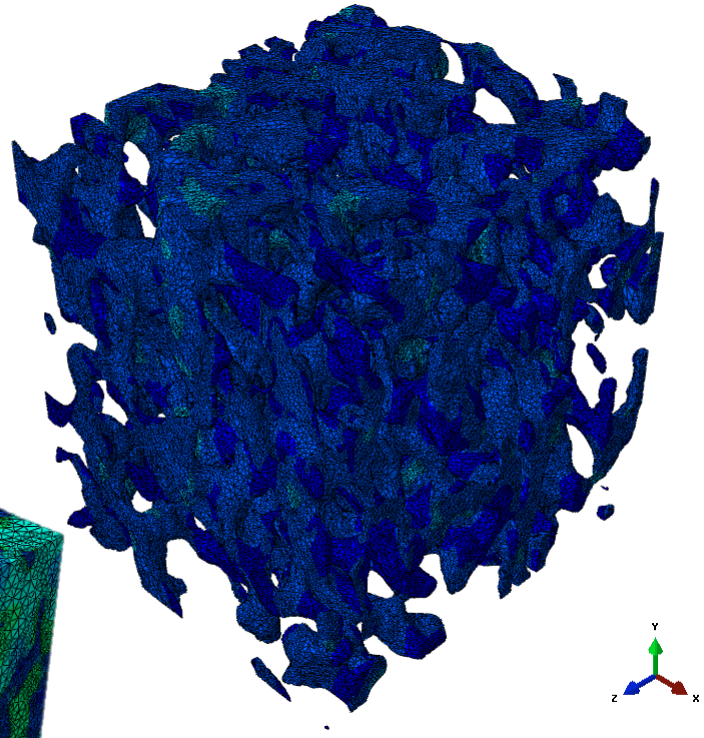

Most of compressive load carried in W matrix due to higher stresses in stiffer material.

Significant strength reduction expected past the melting point of copper

WCu 15wt% Cu
60um x 60um x 60um
Compressed in X direction to 10% strain

*Mignone, P. et al. University of Melbourne. Unpublished*

# Meshless Method: Lattice Monte Carlo

## 19.3 vol% Cu

***200x200x128: 5M Voxels***

## 27.5 vol% Cu

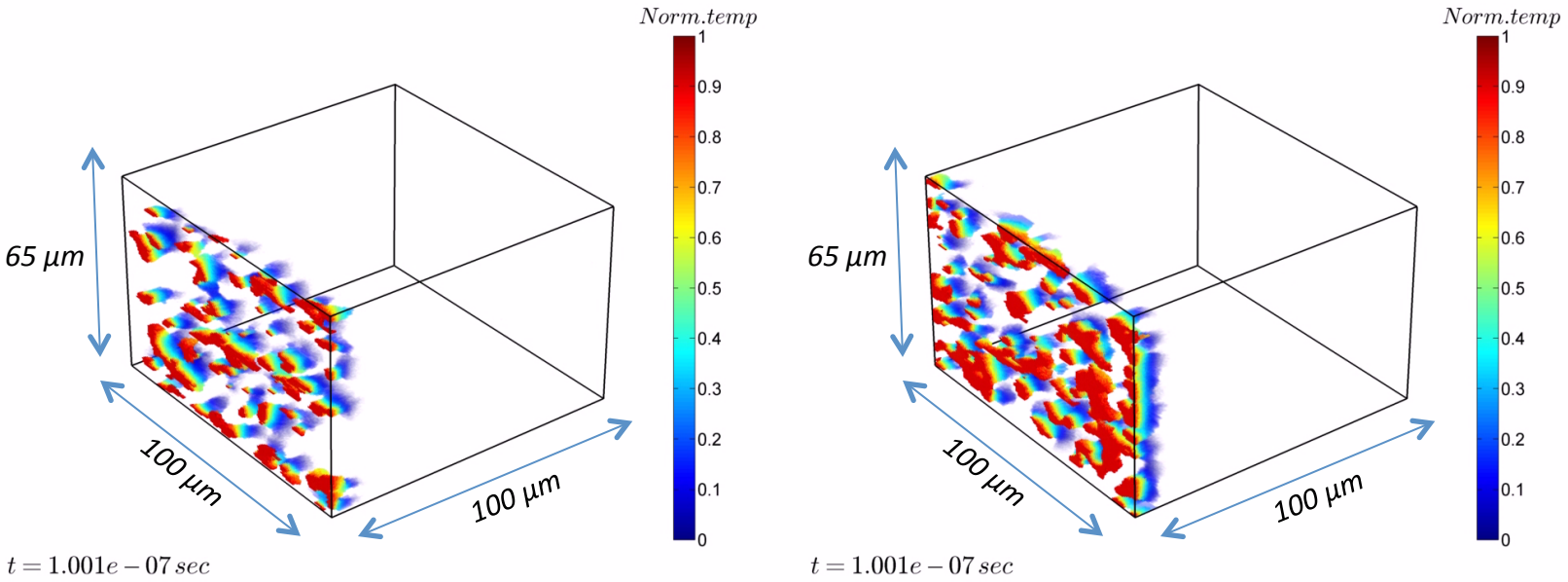


- Modeled thermal diffusion using random walk of heat particles
- Segmented datasets (binary, ternary, …) inherently suited for cubic/cuboid grid-based simulation methods
  - No meshing required → faster iterative workflow
- Novel GPU-based LMC code, ***cudaLMC***, speeds up transient LMC conduction analysis by 160x over a single CPU core*

***Comparison between 3.0GHz Intel CPU vs cudaLMC v1.2 running on Tesla K20 GPU (2013), M. Wang et al (publication in progress)**

# EBSD from Femtosecond Laser Ablated Surfaces

Laser Ablated Mg Alloy - AXJ-530

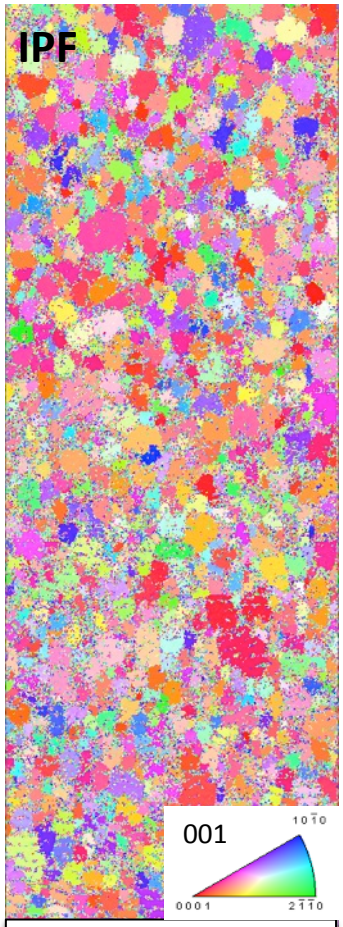


Laser Ablated Ni Alloy - Rene88DT

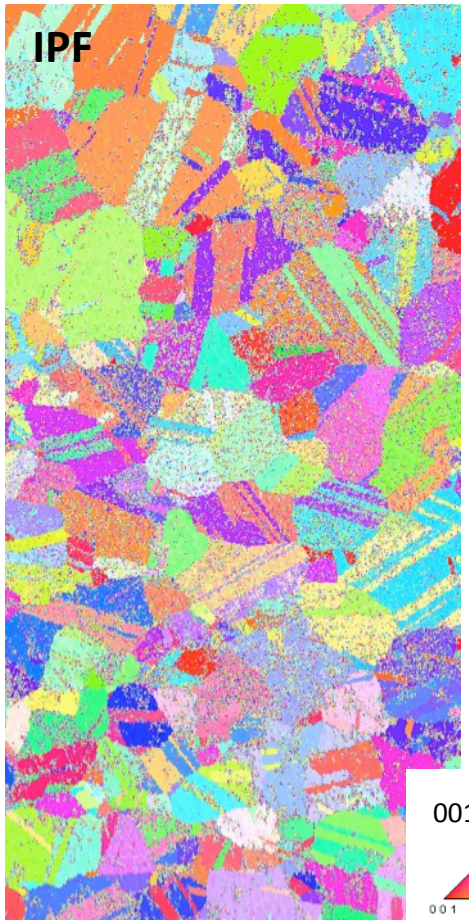


Laser Ablated Strontium Titanate

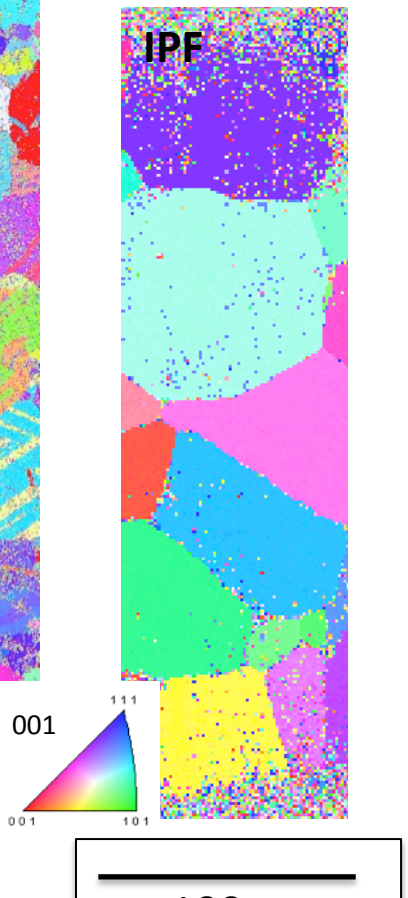


**Laser Ablated Rene88DT**

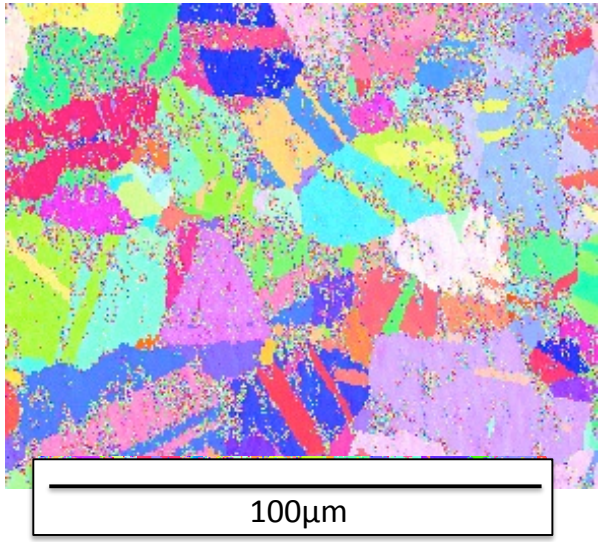


**Laser Ablated + FIB Milled**

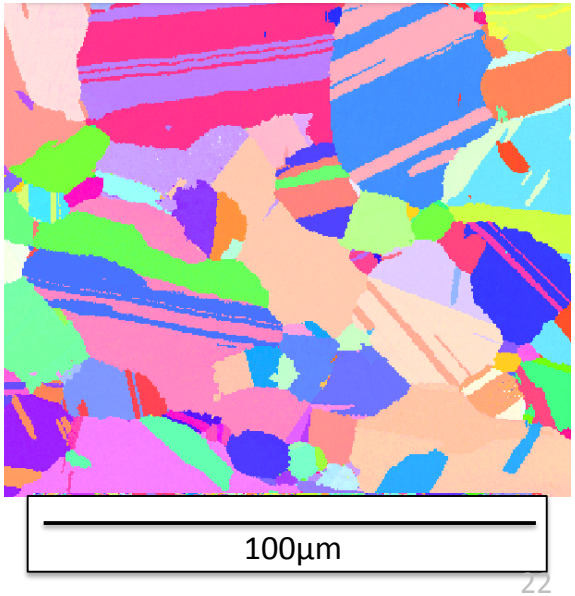

# Femtosecond Laser / FIB 3-D: Ti – 6Al – 4V

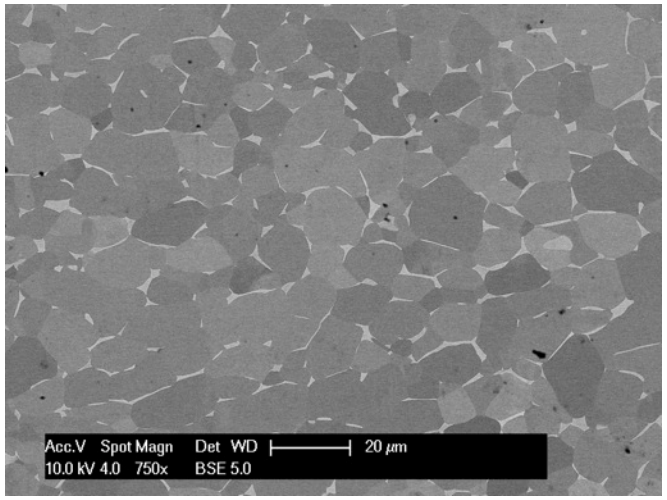


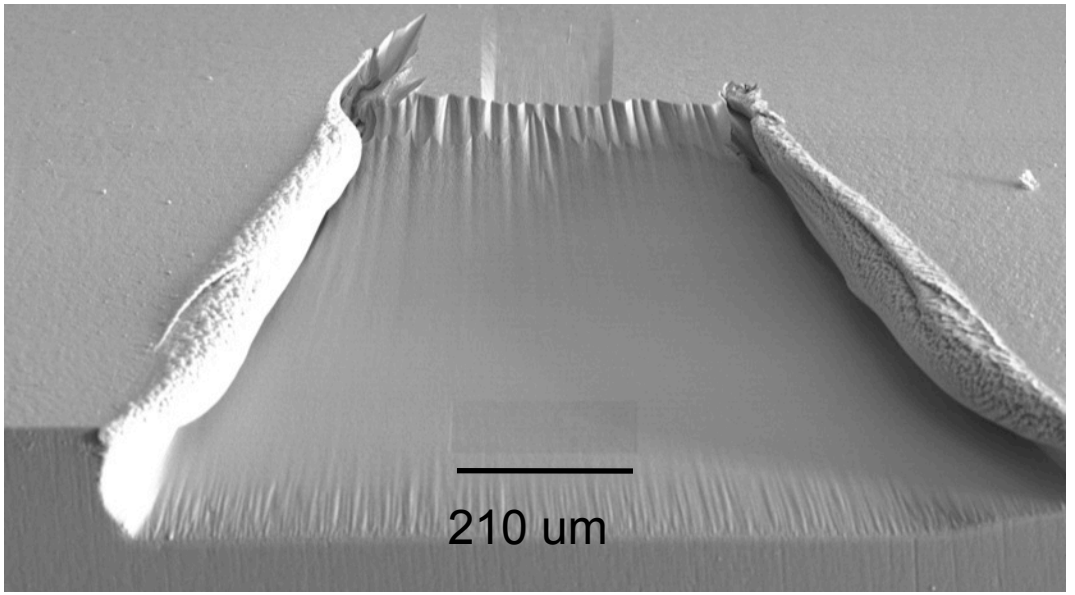


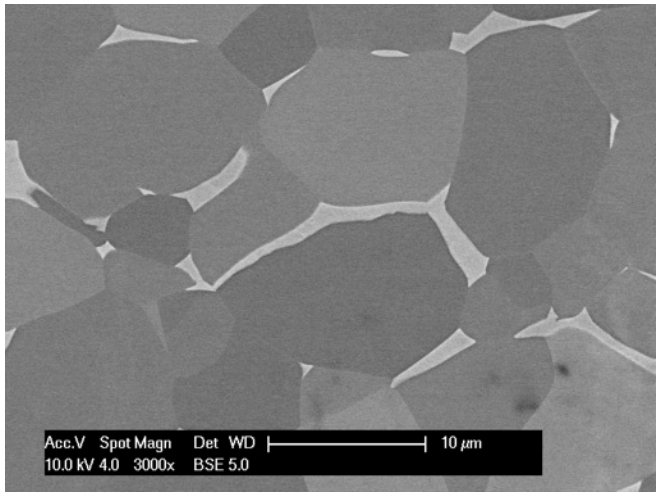


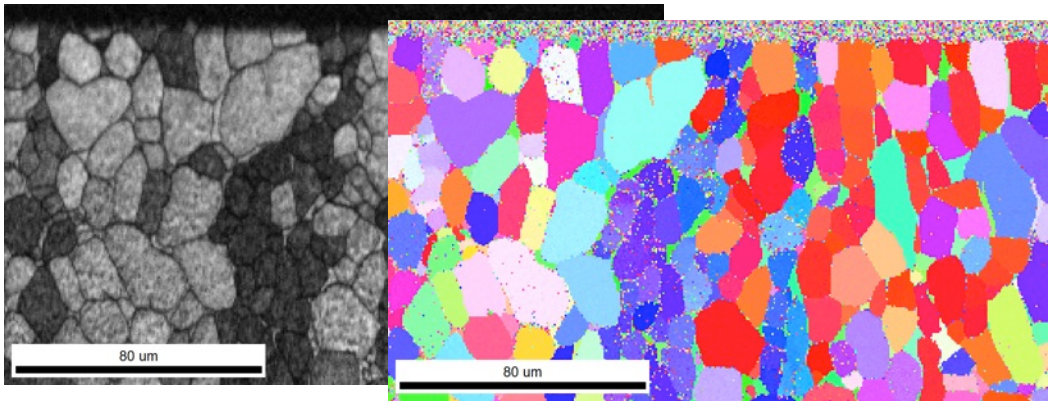

# Ti-6Al4V 3D EBSD – Ion Cleaning

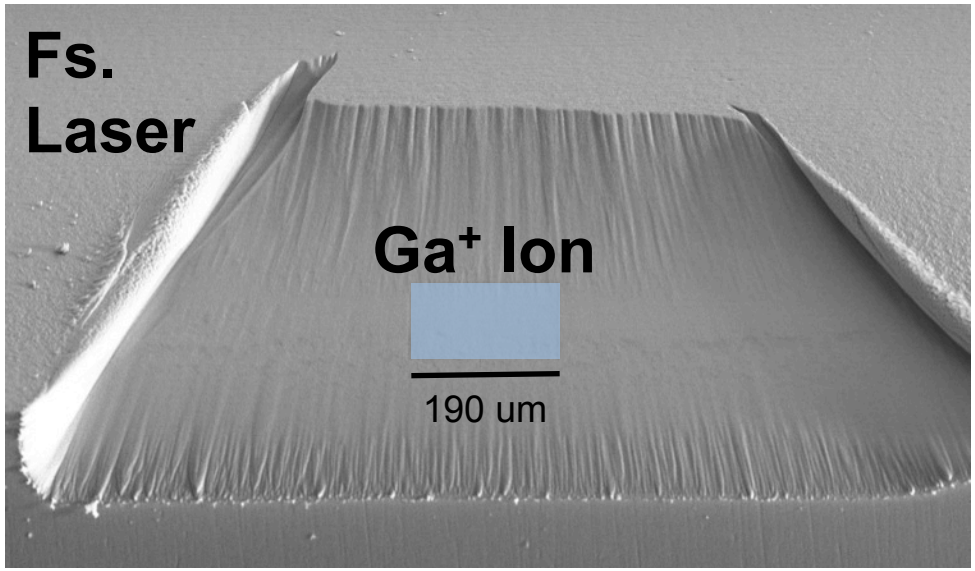


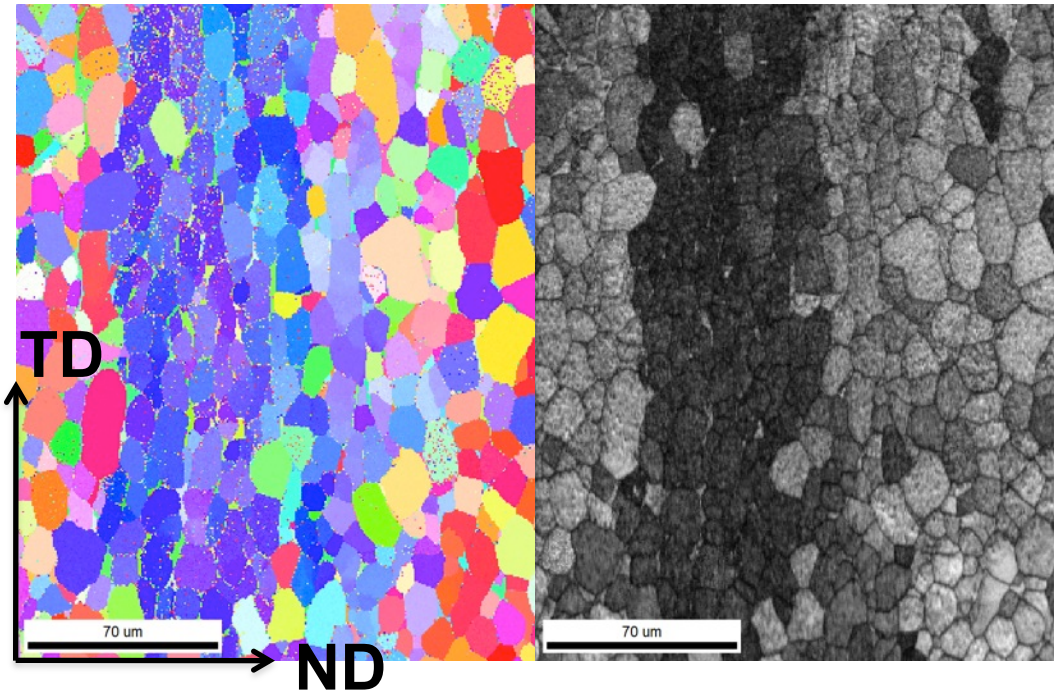


- Fs. laser ablated Ti64 surfaces do not produce high contrast diffraction patterns
- <10° surface parallel 20 nA ion cleaning was performed (5-10 minutes)
- Diffraction pattern contrast dependent on ion polishing angle ($Ga^+$ damage)
- Diffraction patterns are collected from ion polished surface
- Microtextured region of alpha grains was collected
- Beta grain are indexed

# Ti – 6Al – 4V: Texture and Morphology

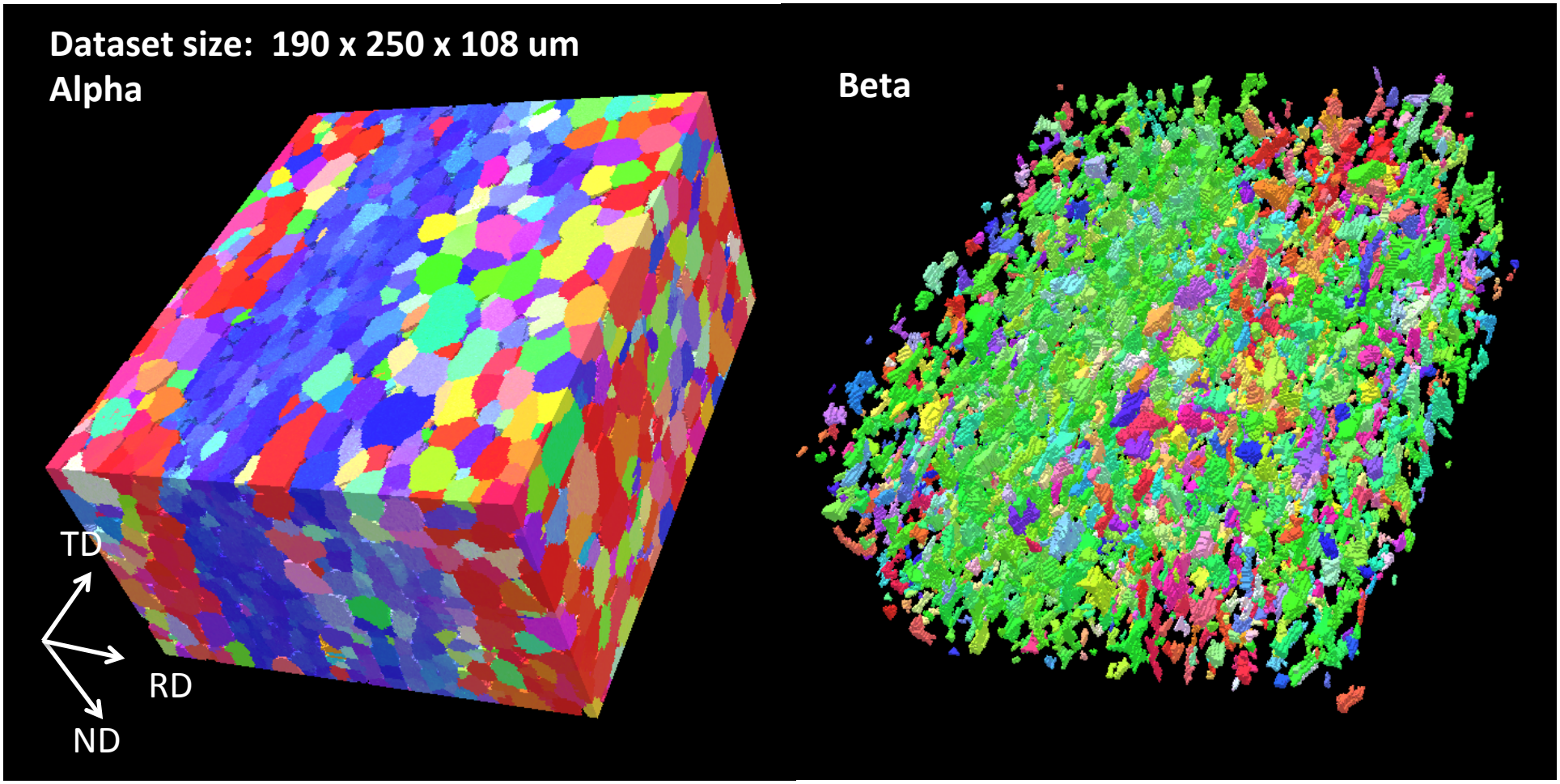


**Dataset size: 190 x 250 x 108 um**
**Z-resolution: 1 um XY-resolution: 0.6 um**

# Ti – 6Al – 4V: Texture and Morphology

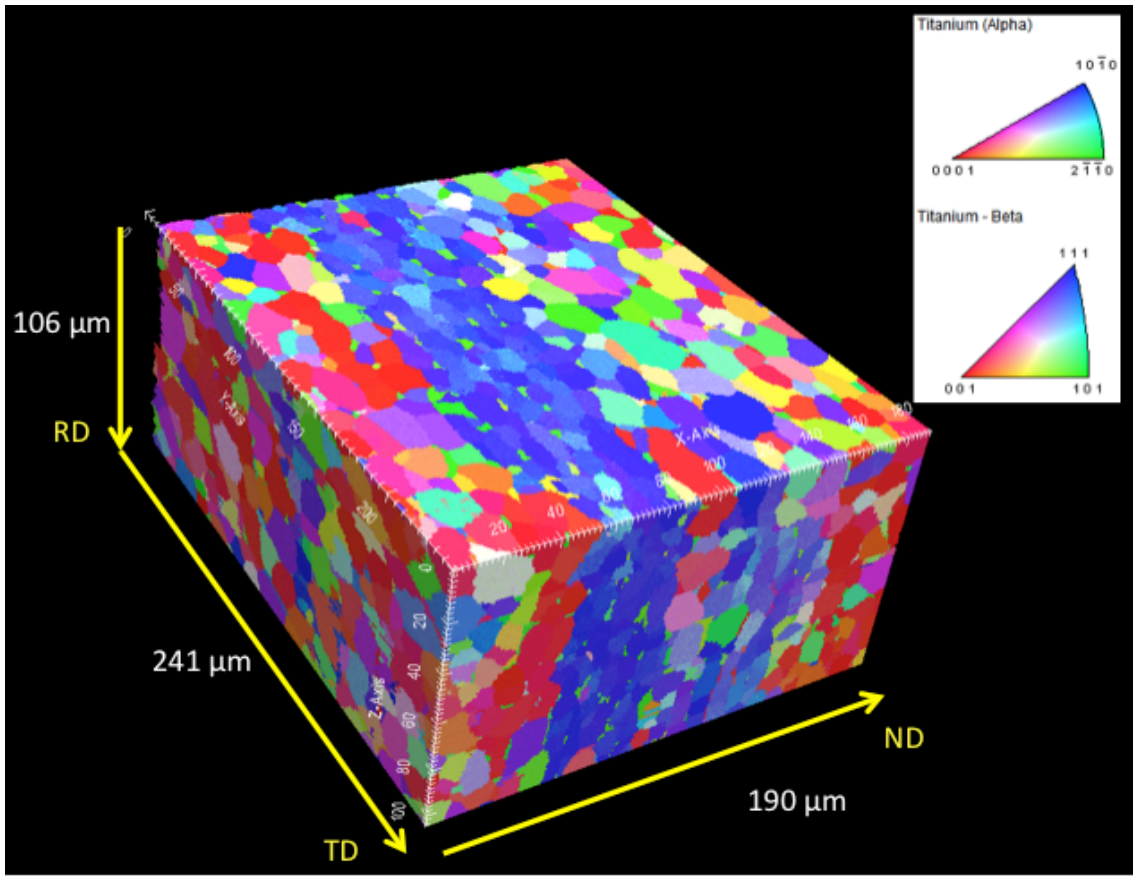


α-phase

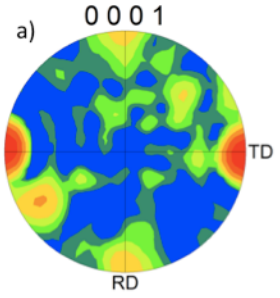


β phase

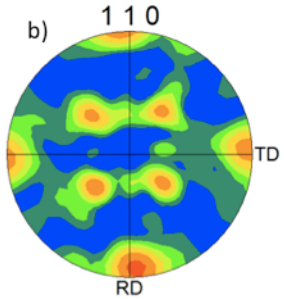


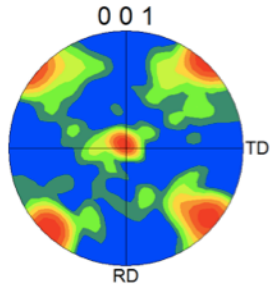


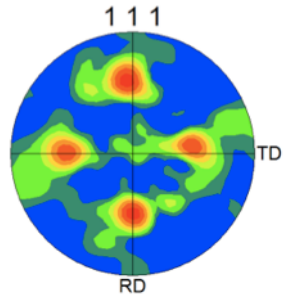


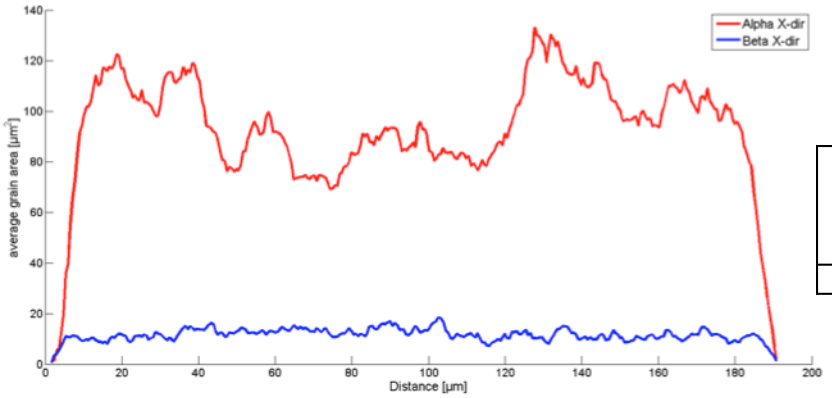


| Total No of grains | No. of grains used for statistics | No. α grains | No. of β grains | Volume fraction α phase | Volume fraction β phase | Grain fraction α phase | Grain fraction β phase |
|---|---|---|---|---|---|---|---|
| 8893 | 6645 | 2484 | 4161 | 0.9353 | 0.0647 | 0.3738 | 0.6262 |

# Laser Ablated Pedestals

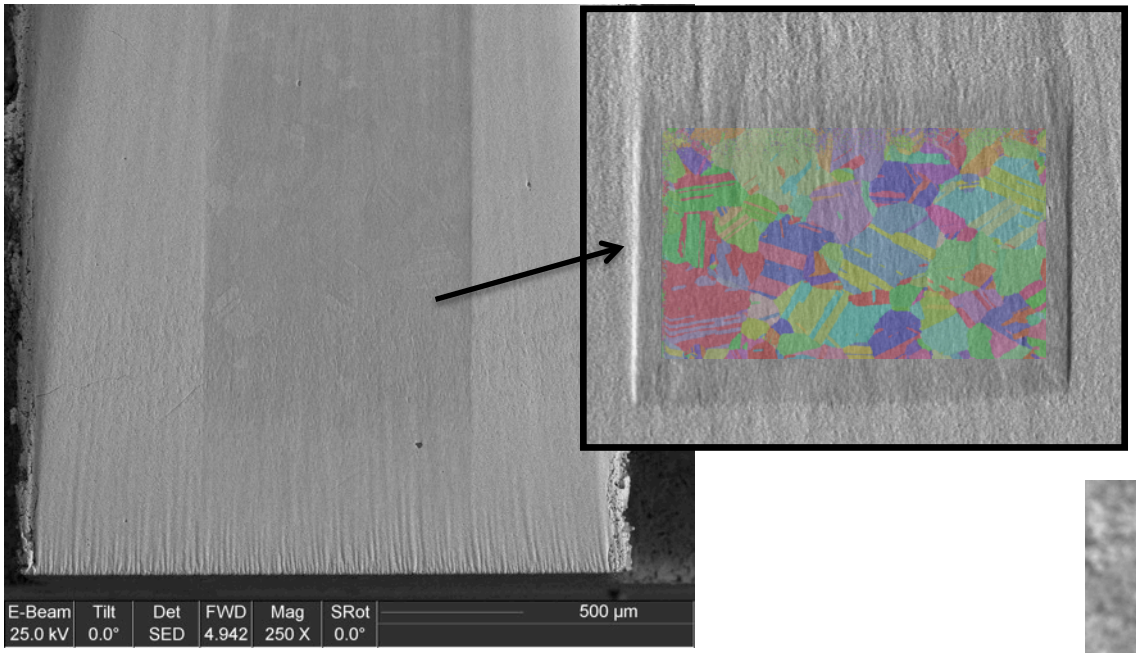


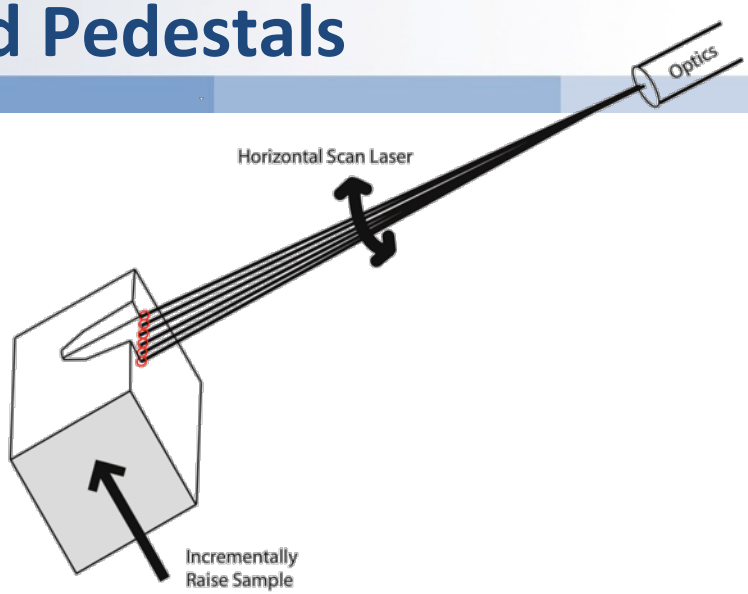


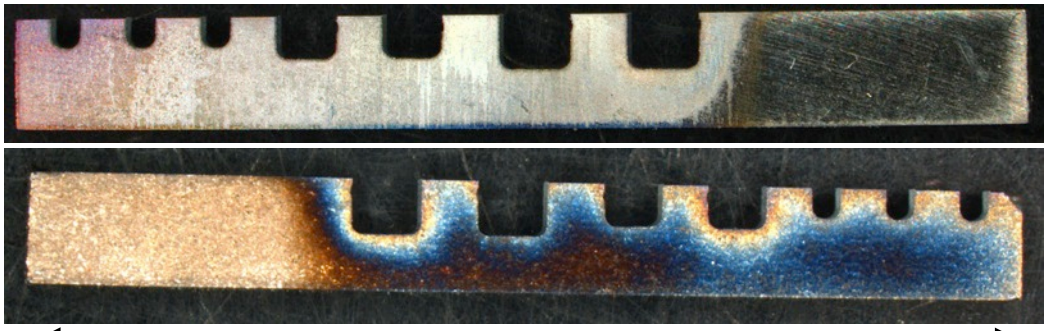

13.4 mm

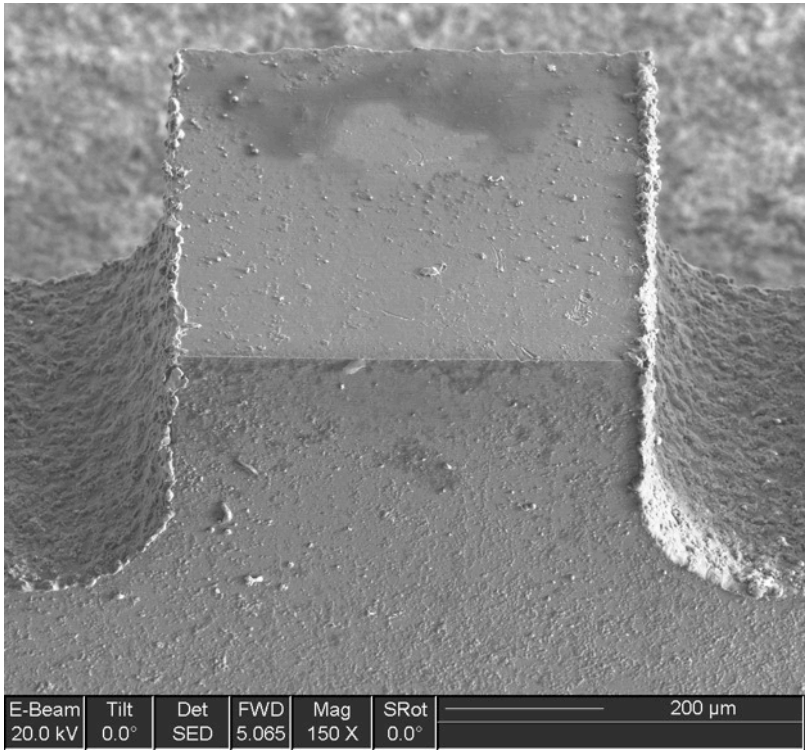

# Example: Nickel Base Alloys for Turbine Engines

- Turbine Blades and Disks of Ni-base alloys are critical components
- Properties that limit their performance are “Structure Sensitive” Properties such as Fatigue and Fracture
- Submicron features in $mm^3$ to $cm^3$ volumes of material

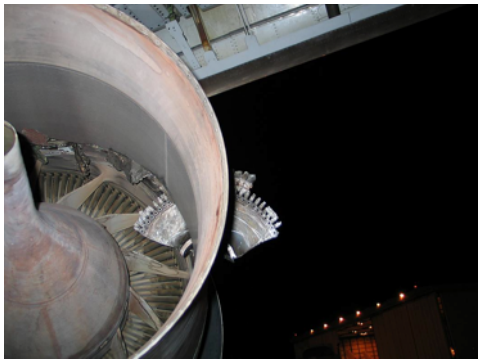

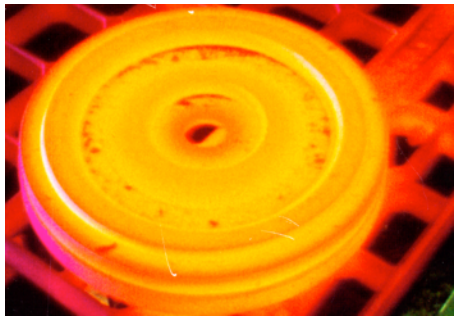

Chemical composition of René 88DT (weight percent)

| Cr | Co | Mo | W | Al | Ti | Nb | C | B | Ni |
|---|---|---|---|---|---|---|---|---|---|
| 16 | 13 | 4 | 4 | 2.1 | 3.7 | 0.7 | 0.03 | 0.015 | Bal |

# Fatigue Behavior of Polycrystalline René 88DT

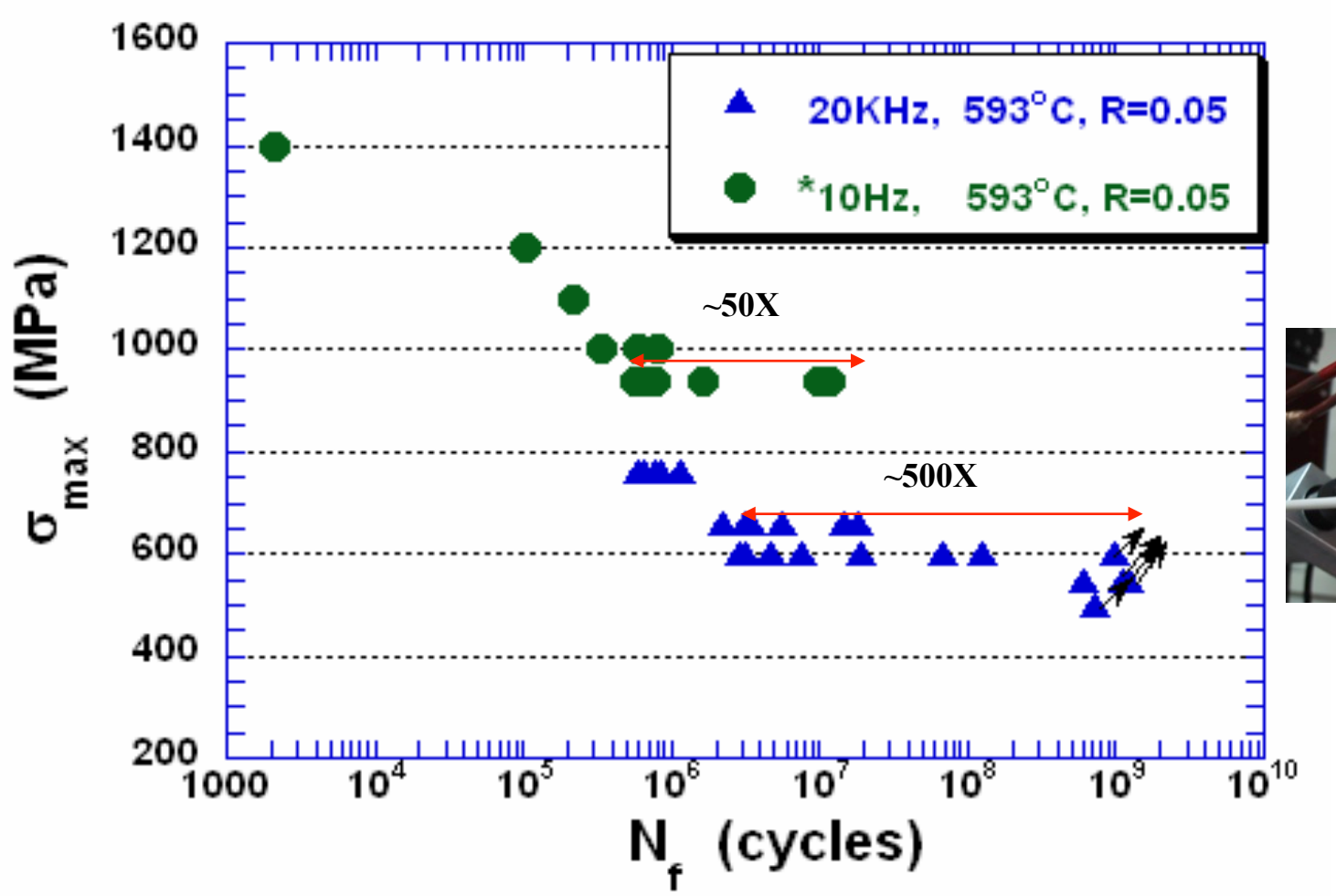


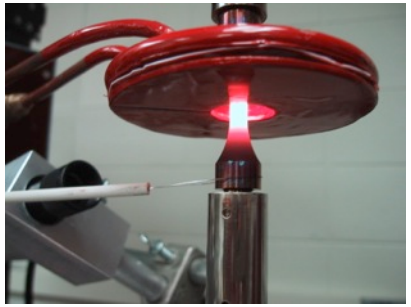

J. Miao, T.M. Pollock and J.W. Jones, *Acta Materialia* 60, 2840, (2012).

# What Material Volume Element Controls Fatigue?

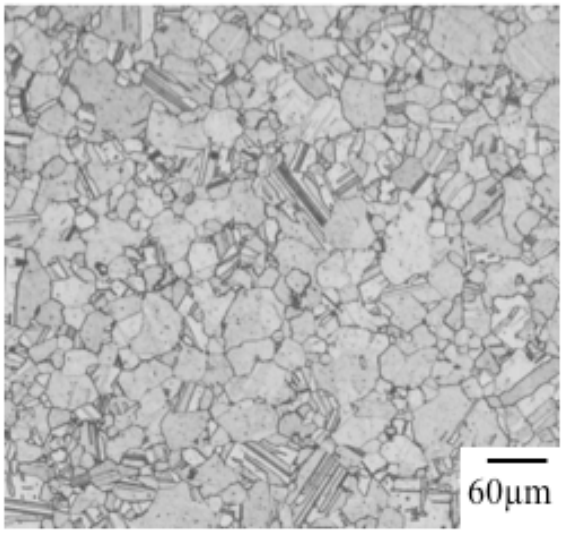


- Forged pancake
- Average grain size ~20μm
- Large grains at the tail of the distribution

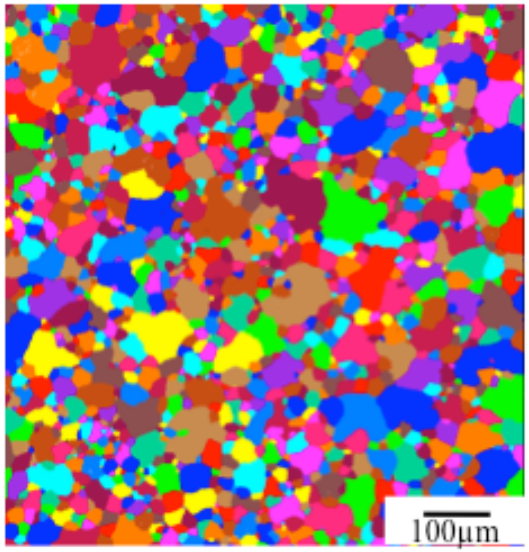


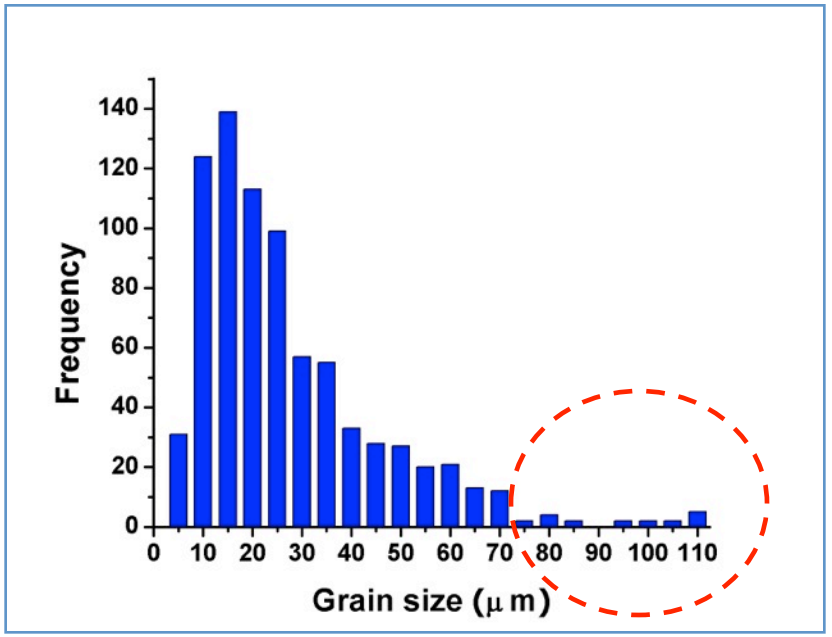

# 3-D Characterization of Initiation Sites

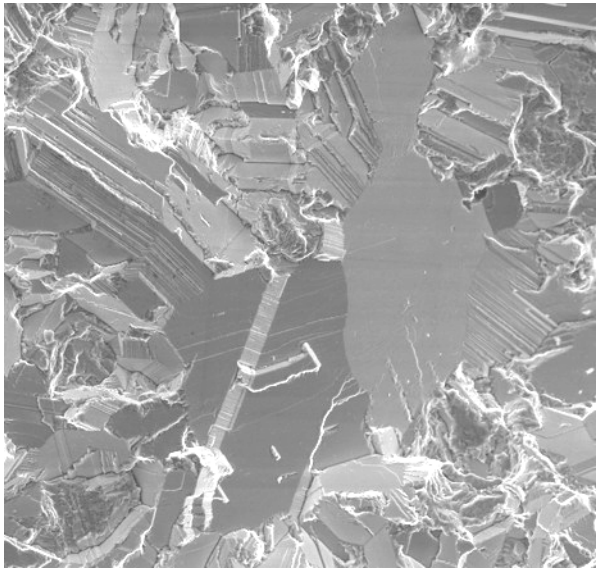

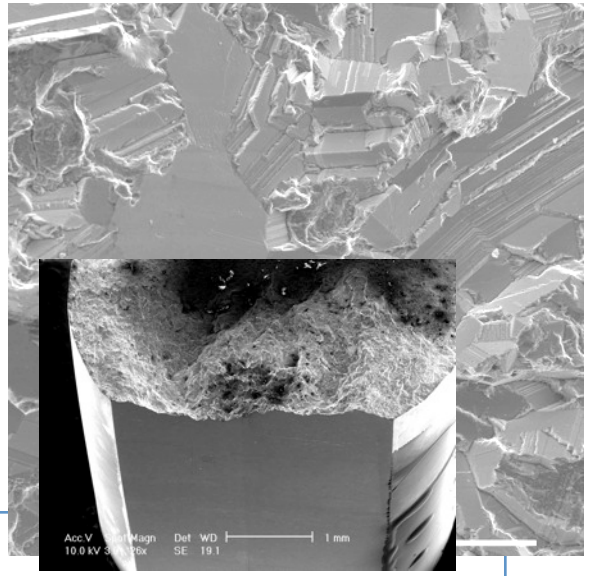

$\sigma_{max}$= 600 MPa, $N_f$ = 3.16x10$^6$

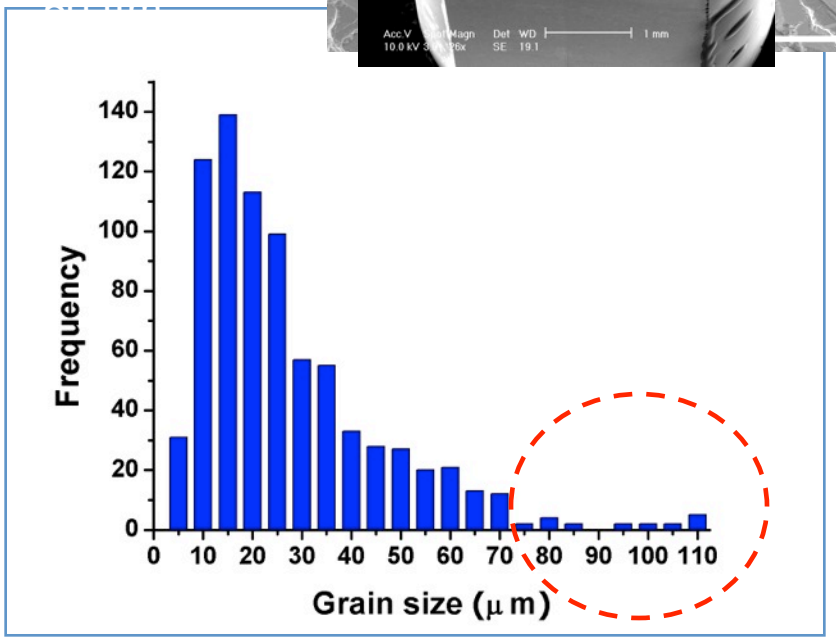


**Large crystallographic facets at crack initiation sites are transgranular and produced by strain localization on slip planes prior to crack formation**

# Fatigue Crack Initiation

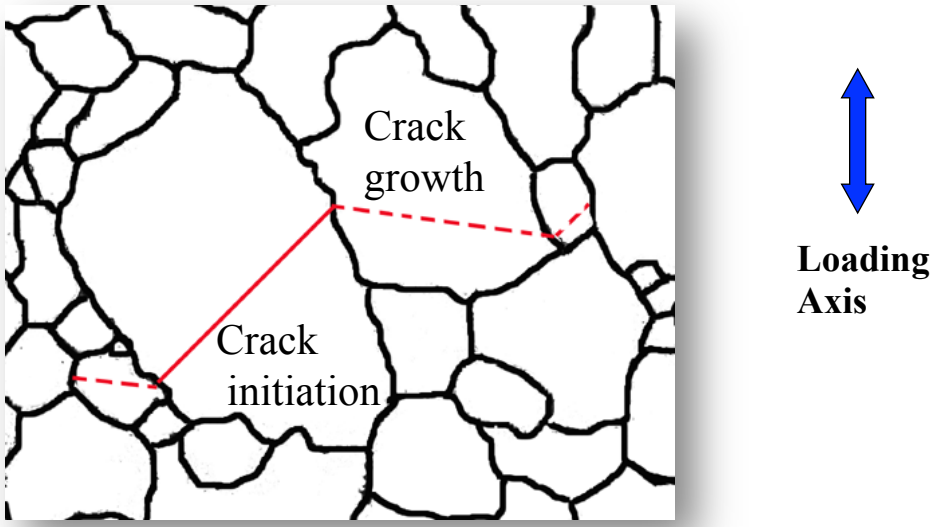


**Critical microstructure features:**

- Large grain (more than two times larger than the average grain size).
- Favorably Oriented for Slip (Schmid Factor > 0.45)
- Favorably Oriented Twin boundaries

**AND**

- Neighboring grains misoriented by < 20 degrees with high SF

# Cracks Initiate Parallel to Twins

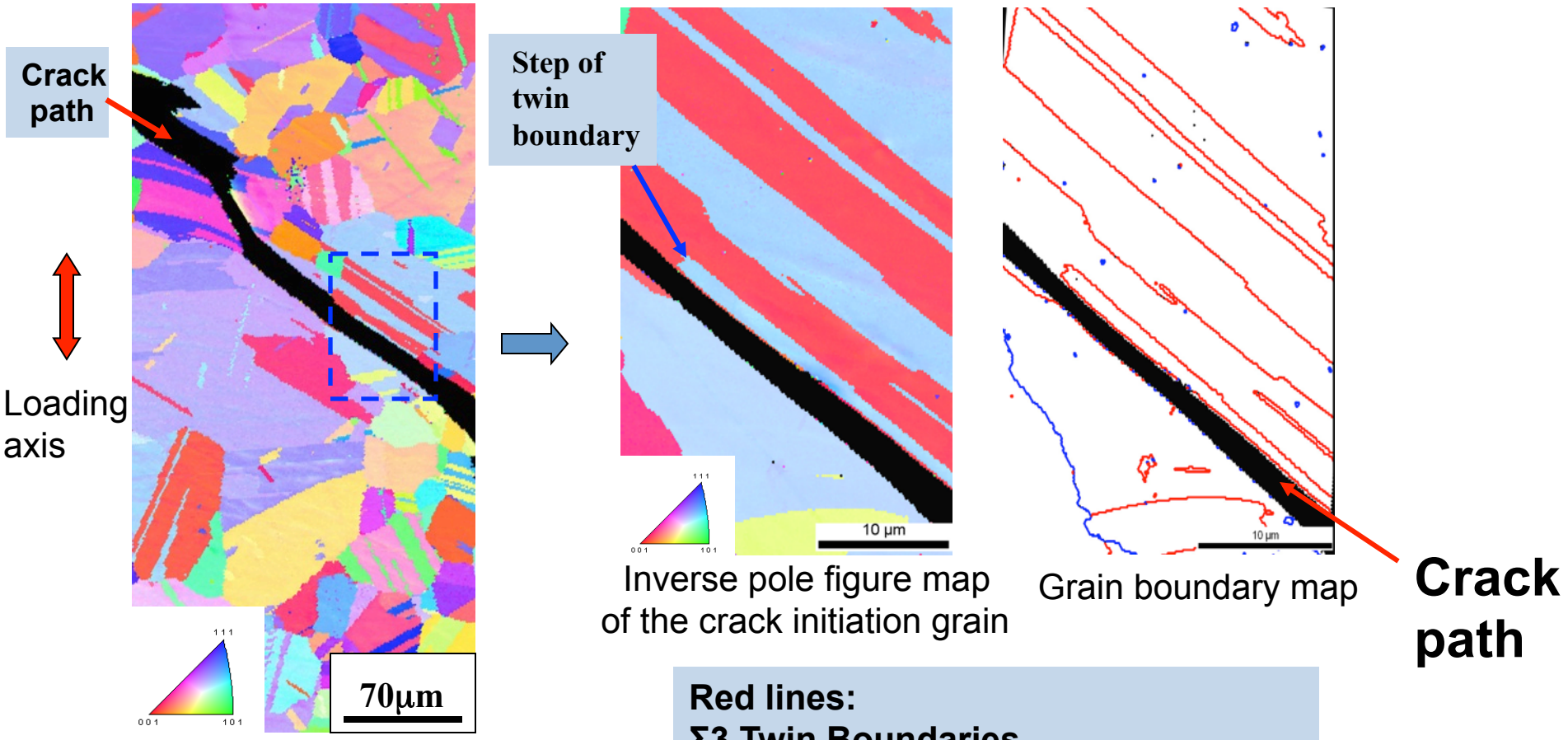


**Inverse pole figure map**

**Red lines:**
**Σ3 Twin Boundaries**

**Blue lines:**
**Random large angle boundaries**

# TriBeam 3-D Characterization of Rene 88

Step size 0.3 μm in X-Y and 0.75 in Z
(240×150×200 $\mu m^3$)

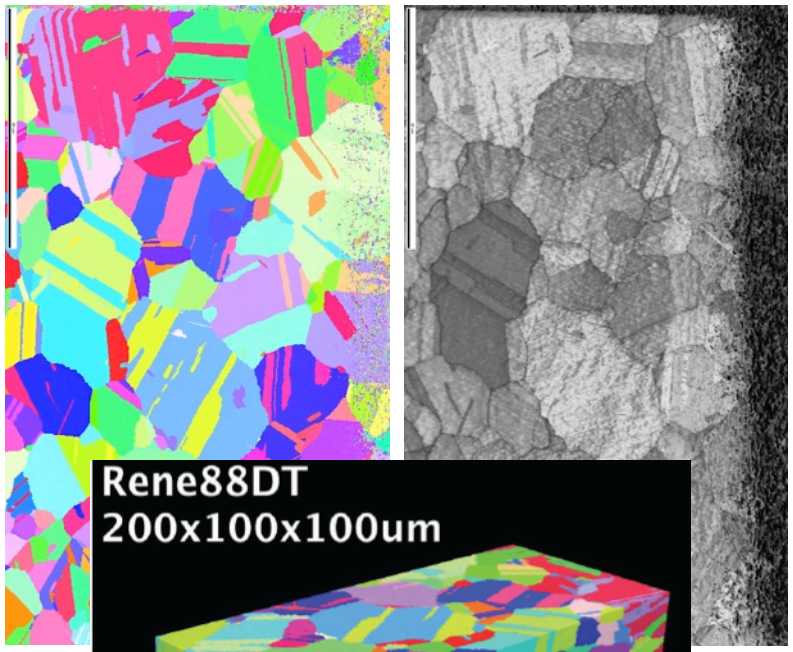

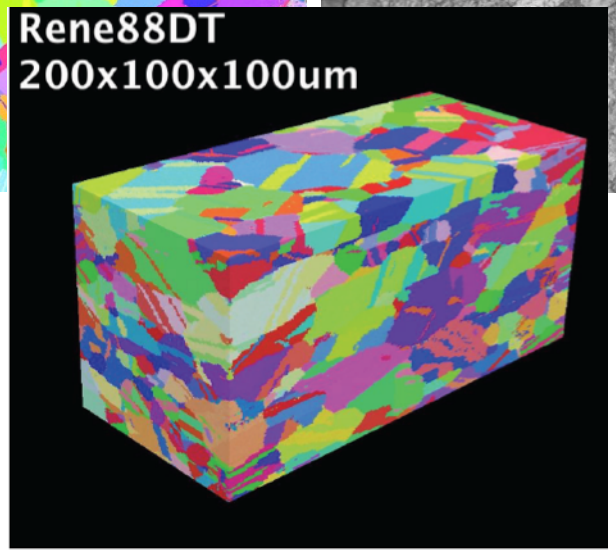


Medium resolution to have a huge volume

Step size 0.1 μm in X-Y and 0.5 in Z
(70×100×75 $\mu m^3$)

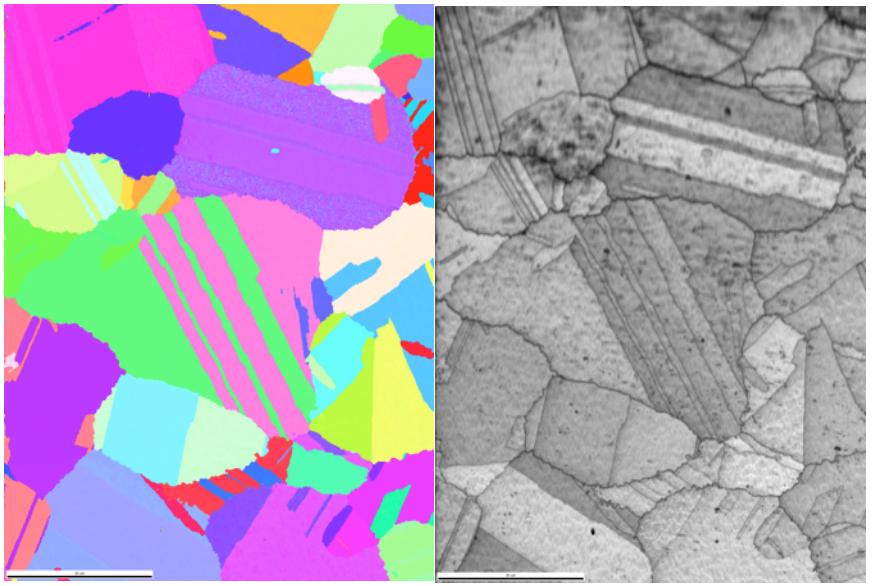

High resolution to describe the grain-twin boundaries

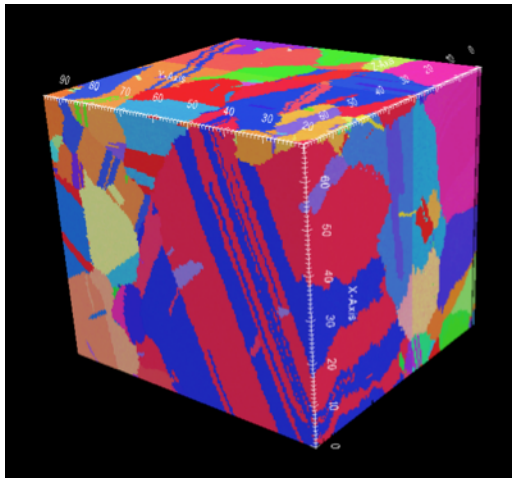

# Tri Beam Dataset for René 88DT

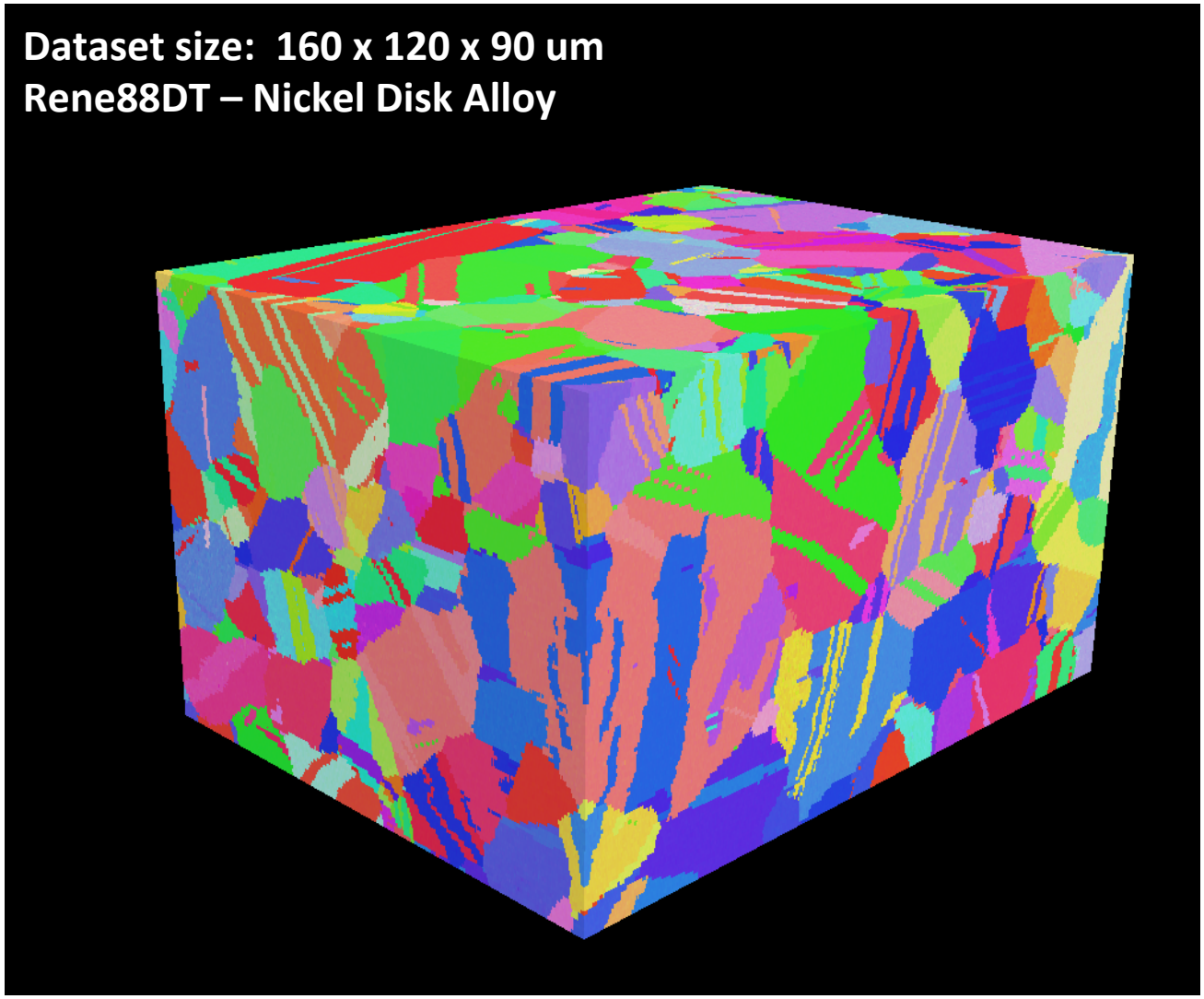


- 100h Dataset
- Laser + FIB (30 kV, 10˚, 20nA)
- 8x8 camera binning @ 375indexed pts/s
- Avg CI ≈ 0.5

UC SANTA BARBARA engineering

The convergence of research and innovation.

# Rene88DT Clustering: Highly Connected

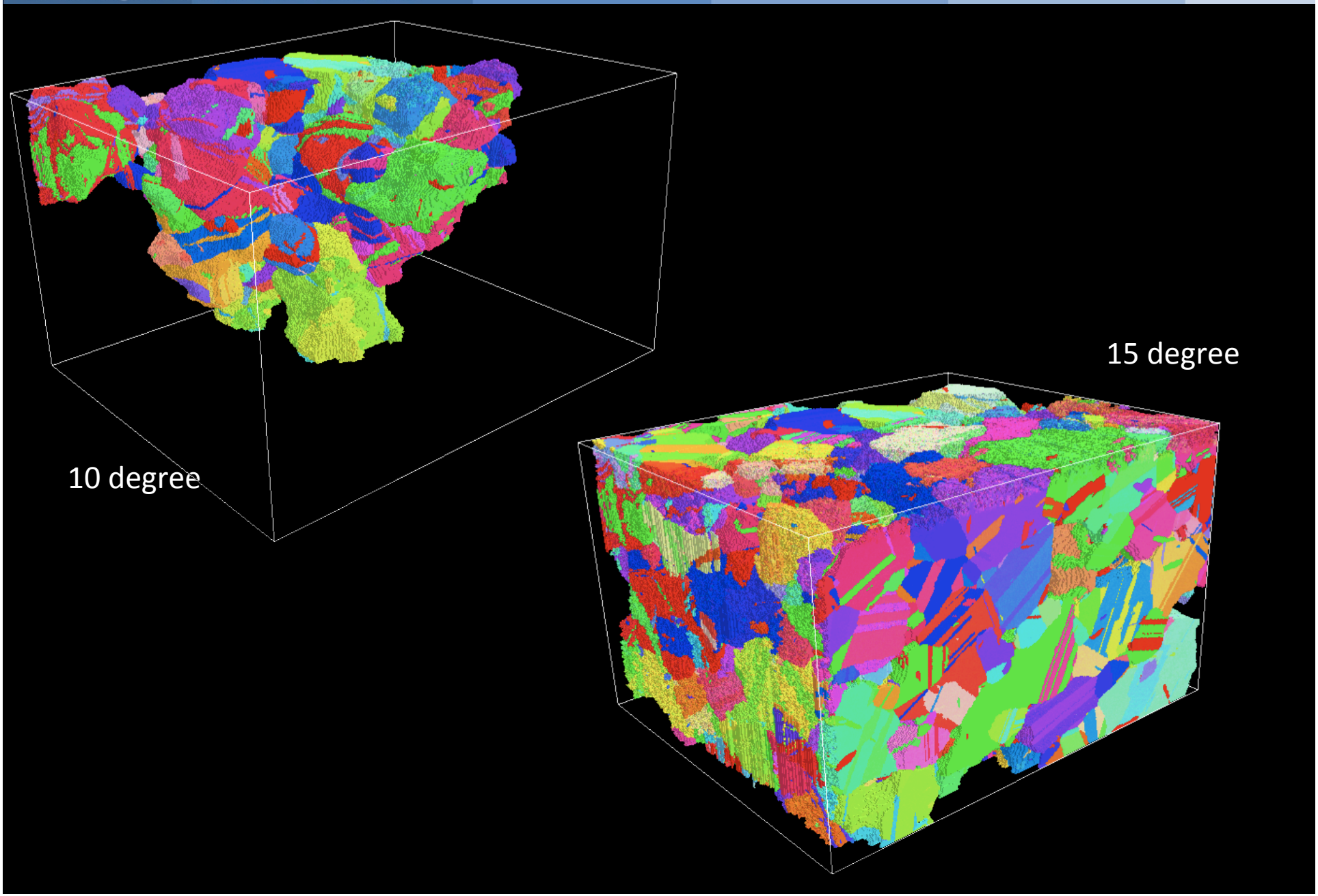

# Identifying Large Grains and Large Twins

**Dataset size: 160 x 120 x 90 um**
**Rene88DT – Nickel Disk Alloy**

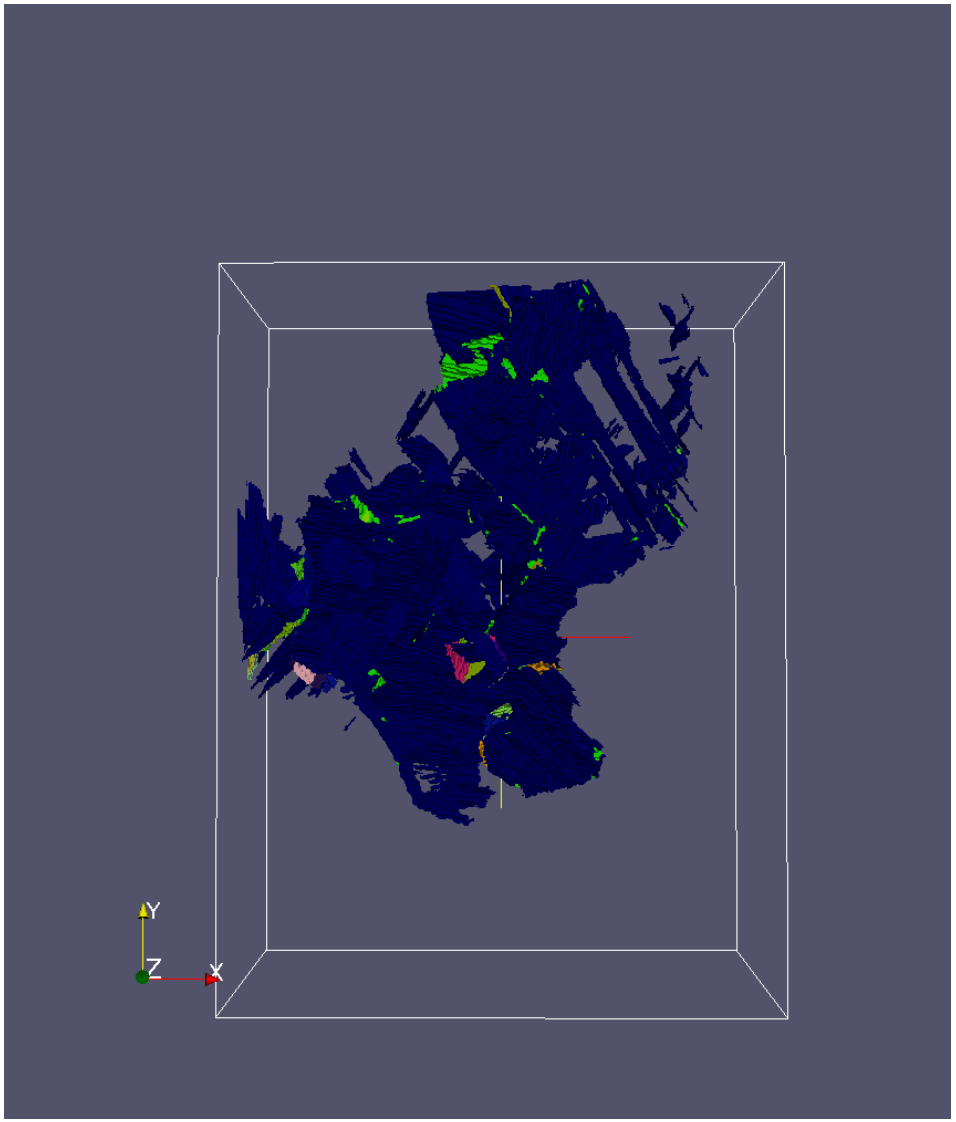


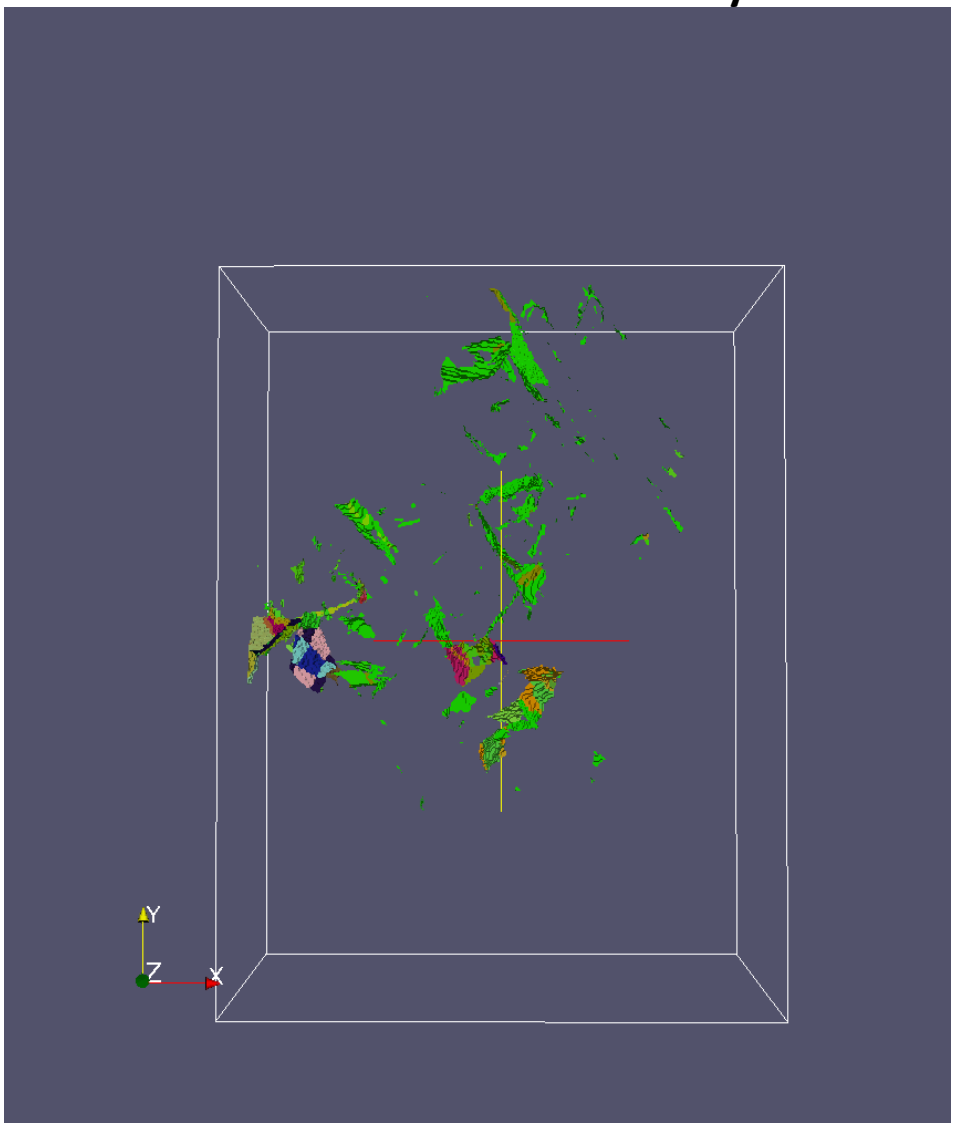

# Length of Slip Band?

## Single Grain, Twins Oriented Regions in Color

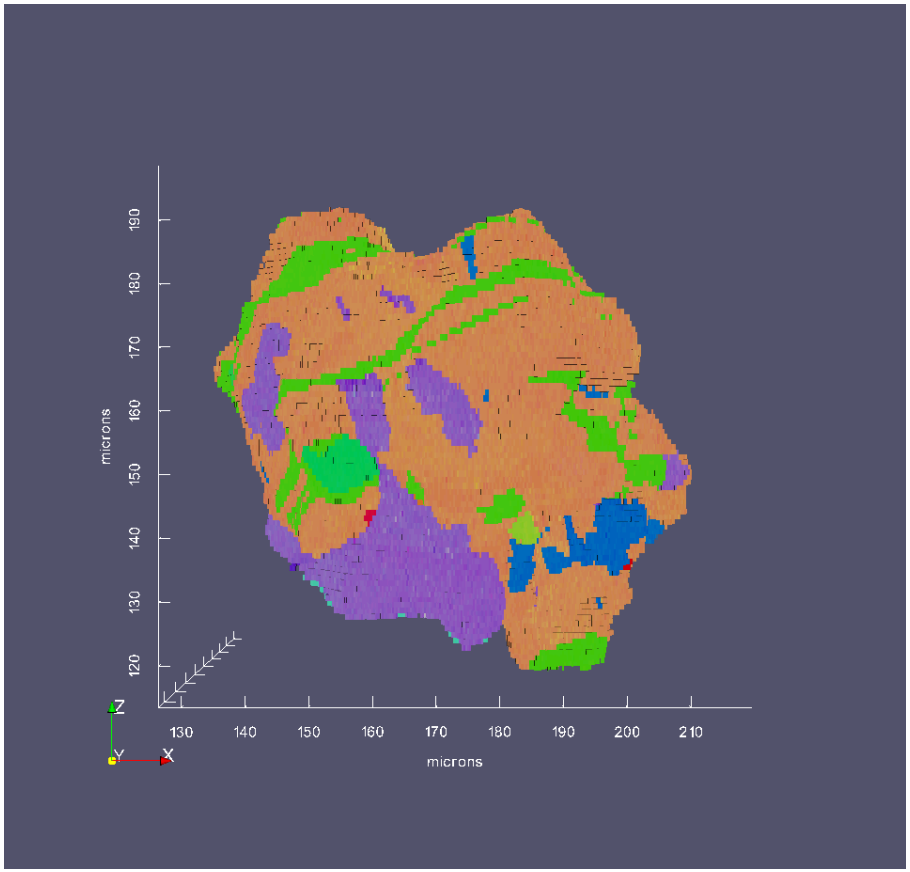


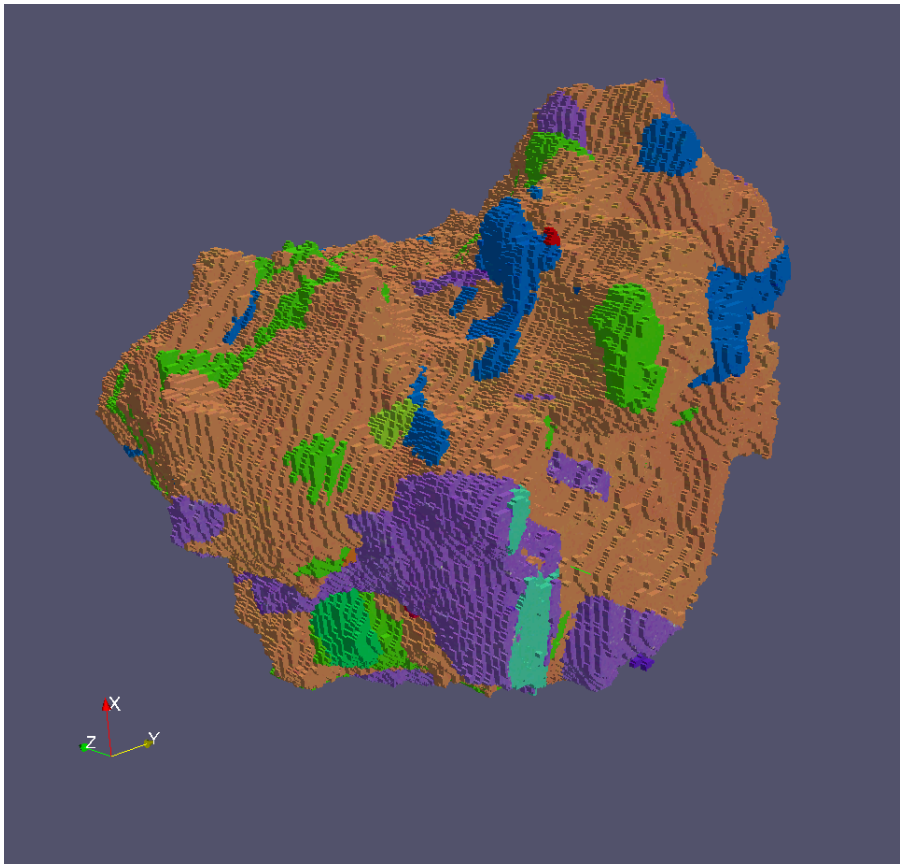


Dream 3-D Reconstructions: dream3d.bluequartz.net

# Visualizing Twin and Boundary Surfaces

**Dataset size: 160 x 120 x 90 um**
**Rene88DT – Nickel Disk Alloy**

*Twins Removed*

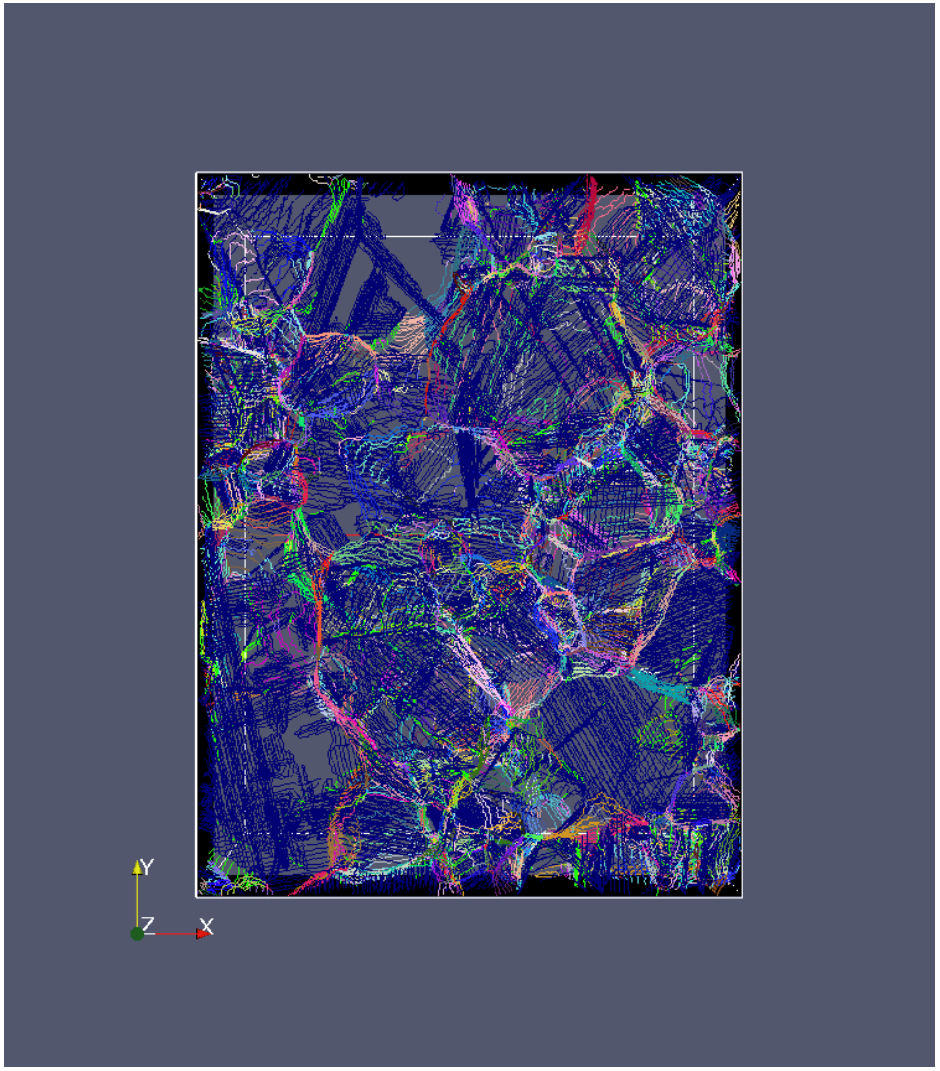


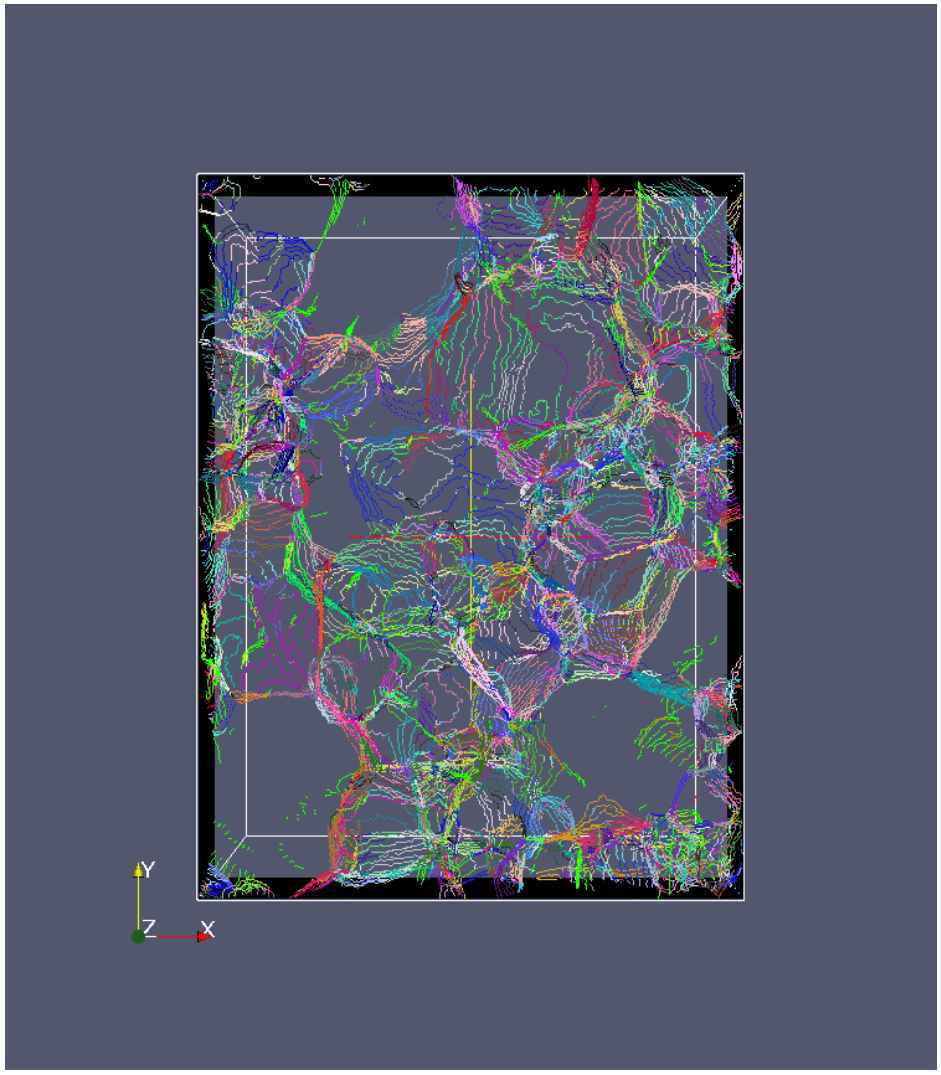


Identify large twin boundary surface favorably oriented for slip AND adjacent grains that crack can propagate into

# Mulitphase Thermoelectrics in the TiNi1+xSn System

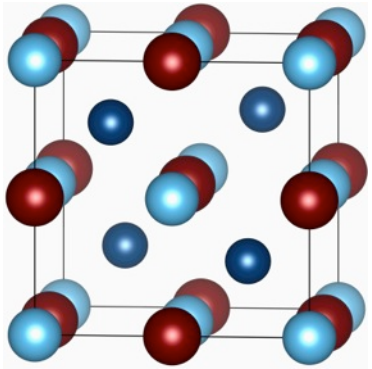

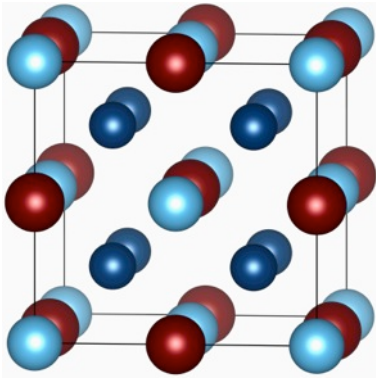

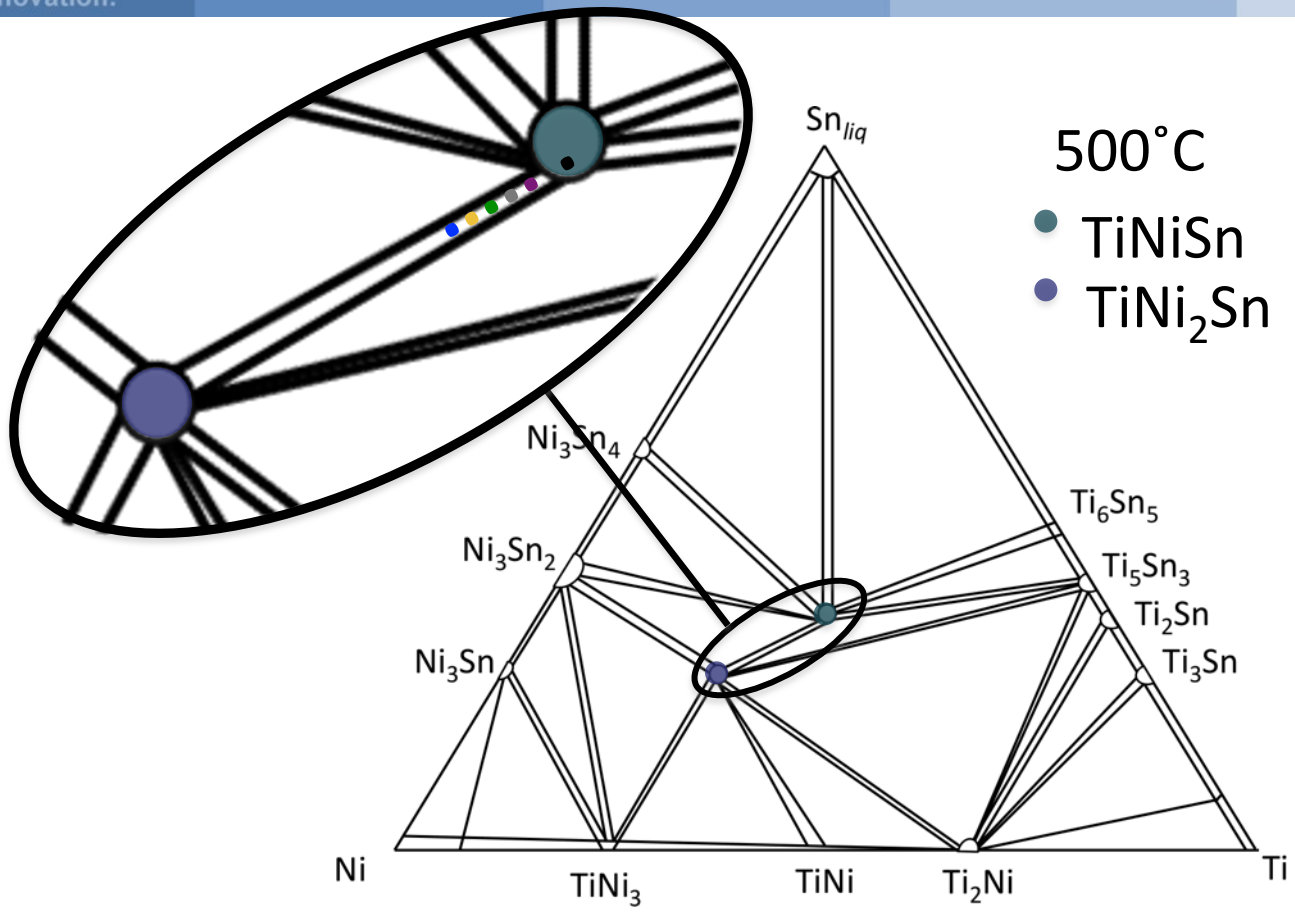


- Half Heusler TiNiSn is thermoelectric and the Heusler is metallic $TiNi_2Sn$
- There is a two-phase field between them
- Similar structures, 3% lattice mismatch

Douglas *et al. Appl. Phys. Lett.* **101** (2012) 183902(1–4).

# The Full Heusler Phase Improves Thermoelectric *ZT*

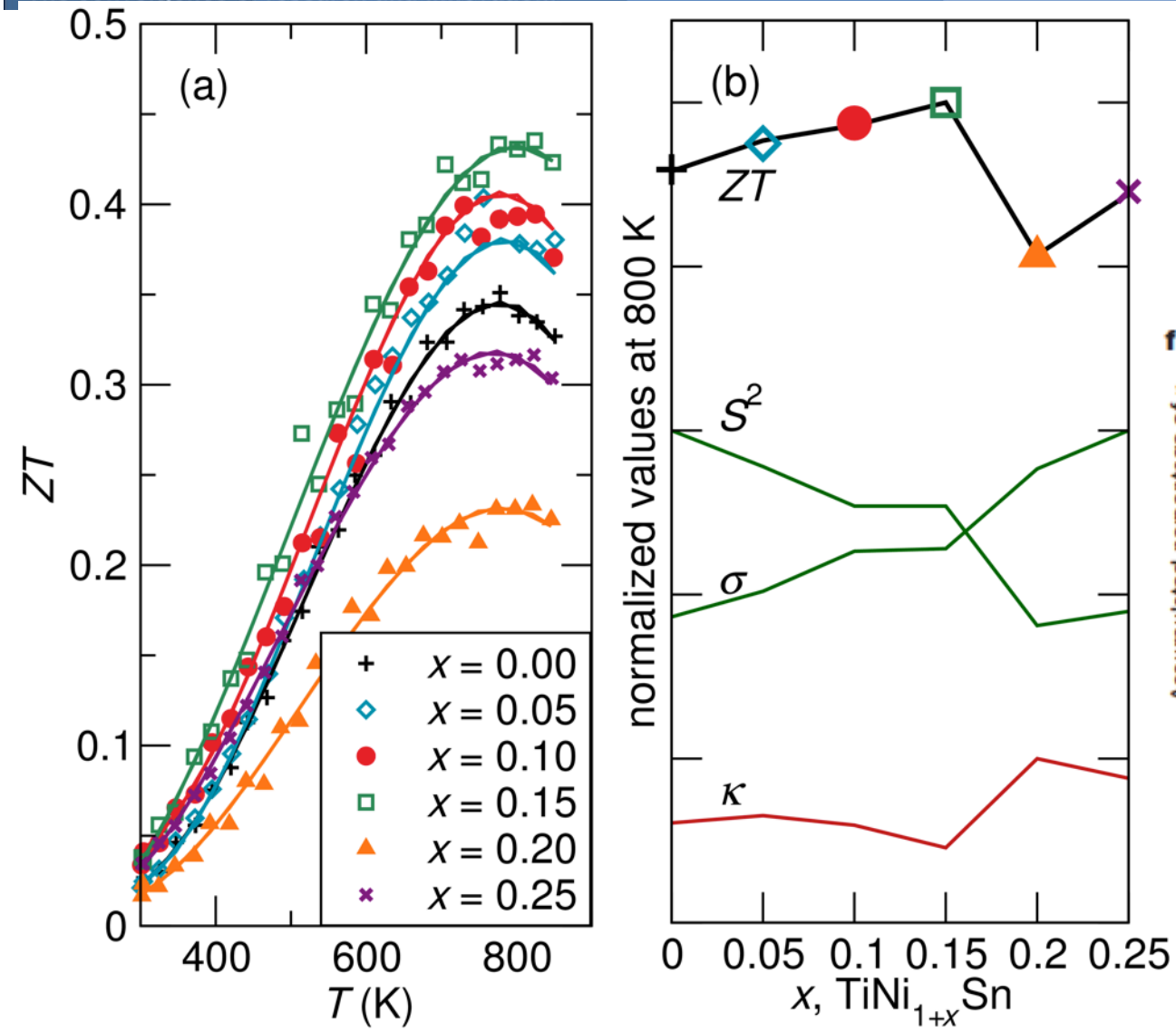


Figure of Merit

$$ZT = \frac{S^2\sigma}{\kappa}T$$

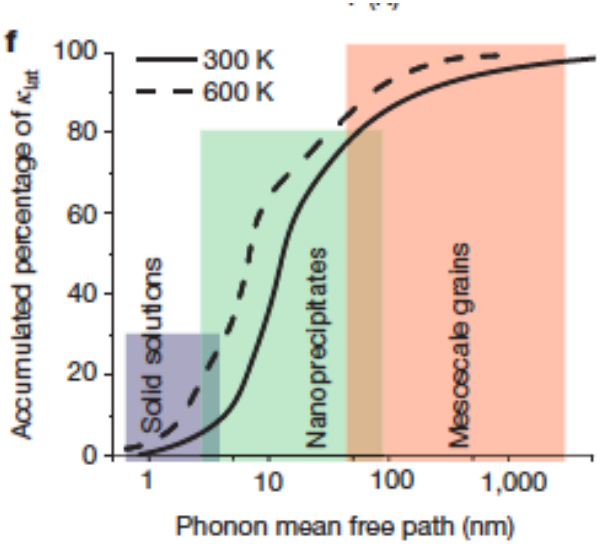


Biswas *et al*, *Nature* 489, 2012

Douglas *et al. Appl. Phys. Lett.* **101** (2012) 183902(1–4).

# Hierachy of Interfaces and Lengthscales TiNi1+xSn

[Dark grey: half-Heusler; light grey: Heusler]

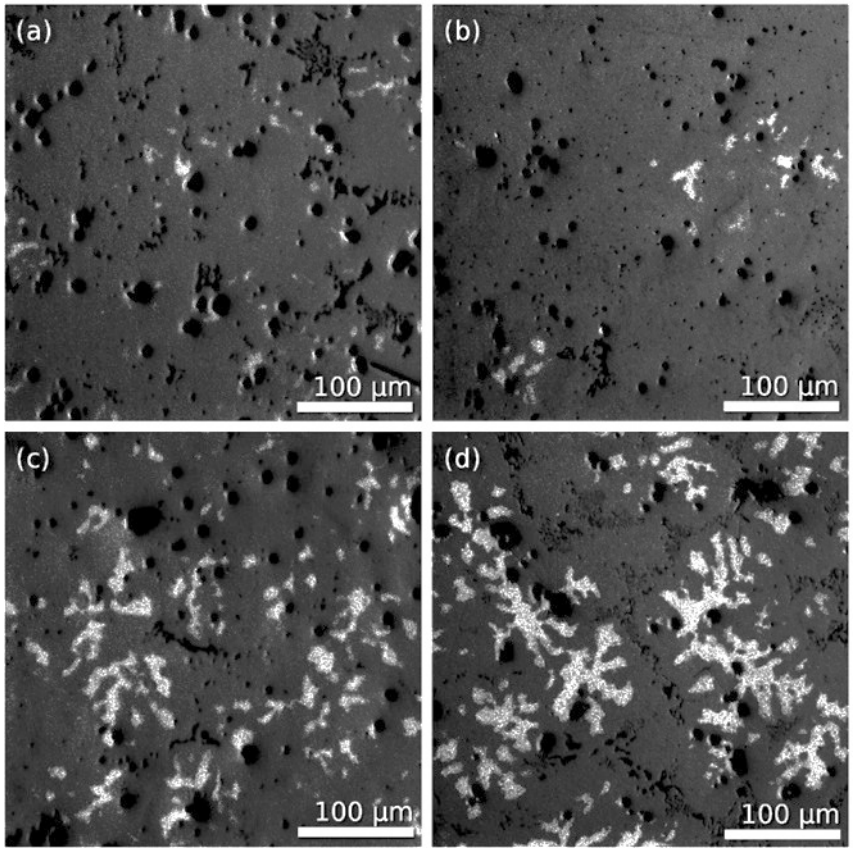


Dendritic Heusler phase

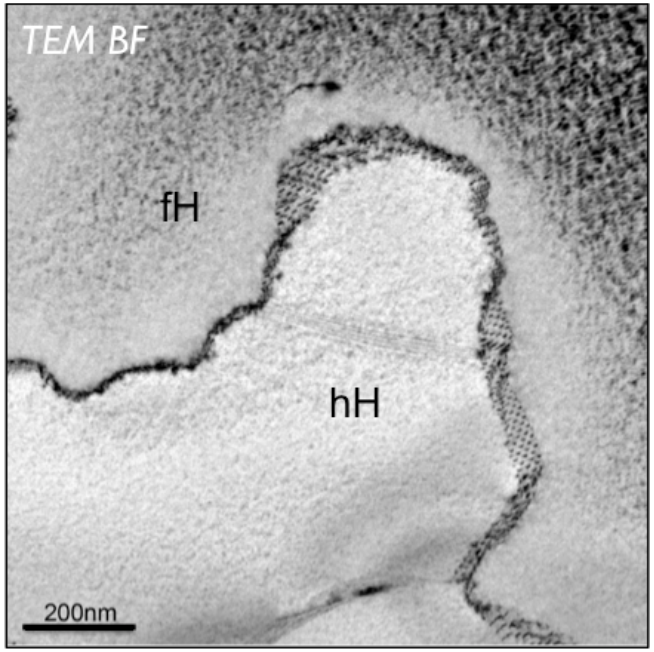


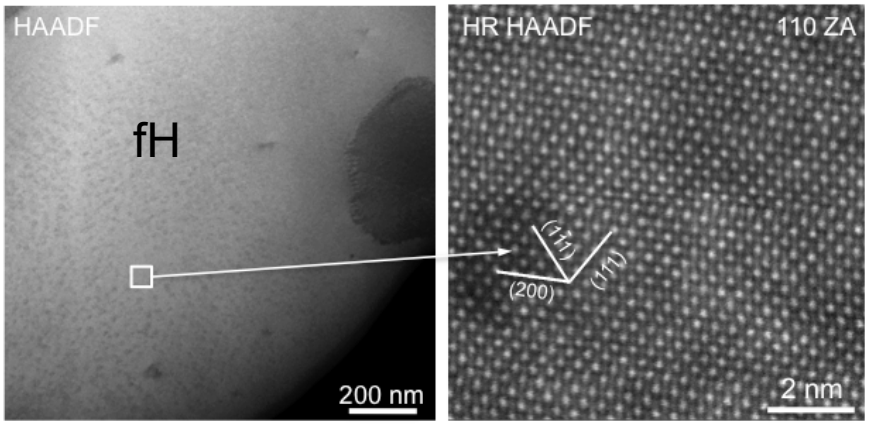


Small coherent precipitates

# Topological Arrangement of Phases

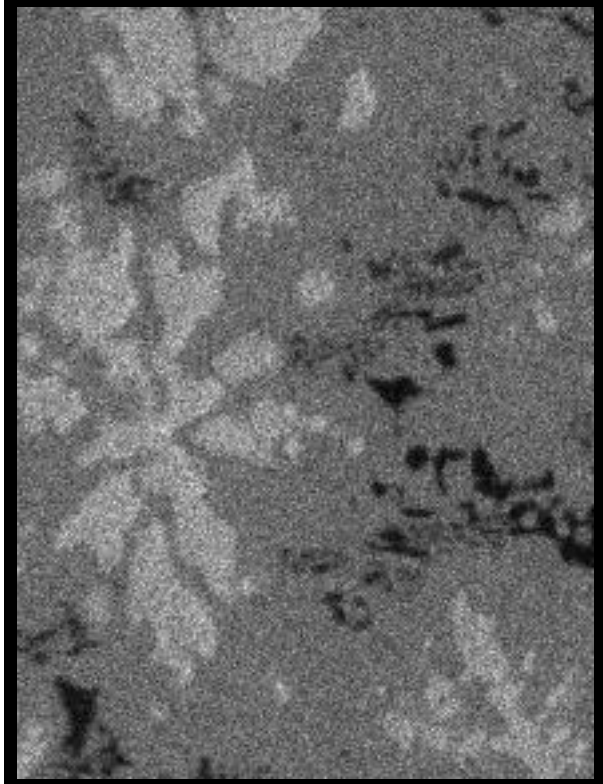

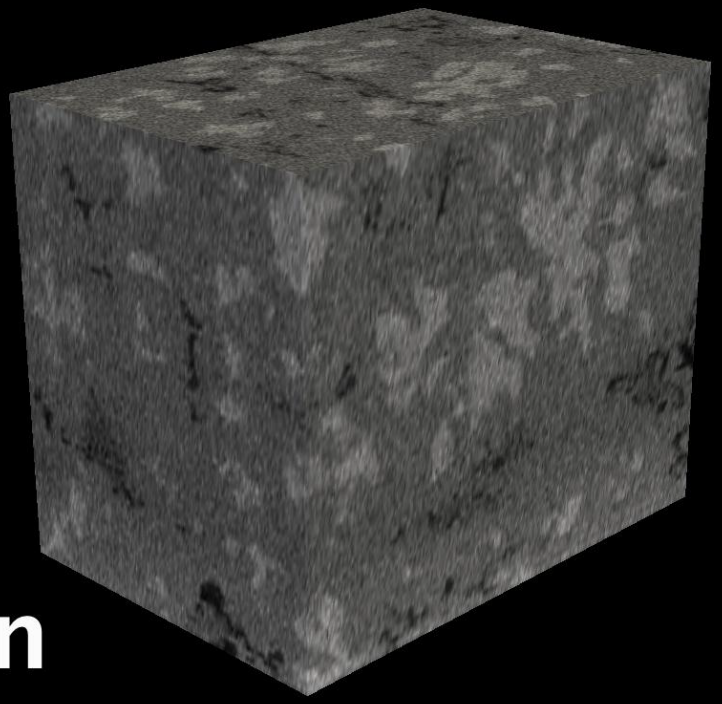

NiTiSn
200x170x140um

FH = Light phase;  Mid tone Gray = hH;  TiSn = Dark

# NiTiSn Phase arrangement

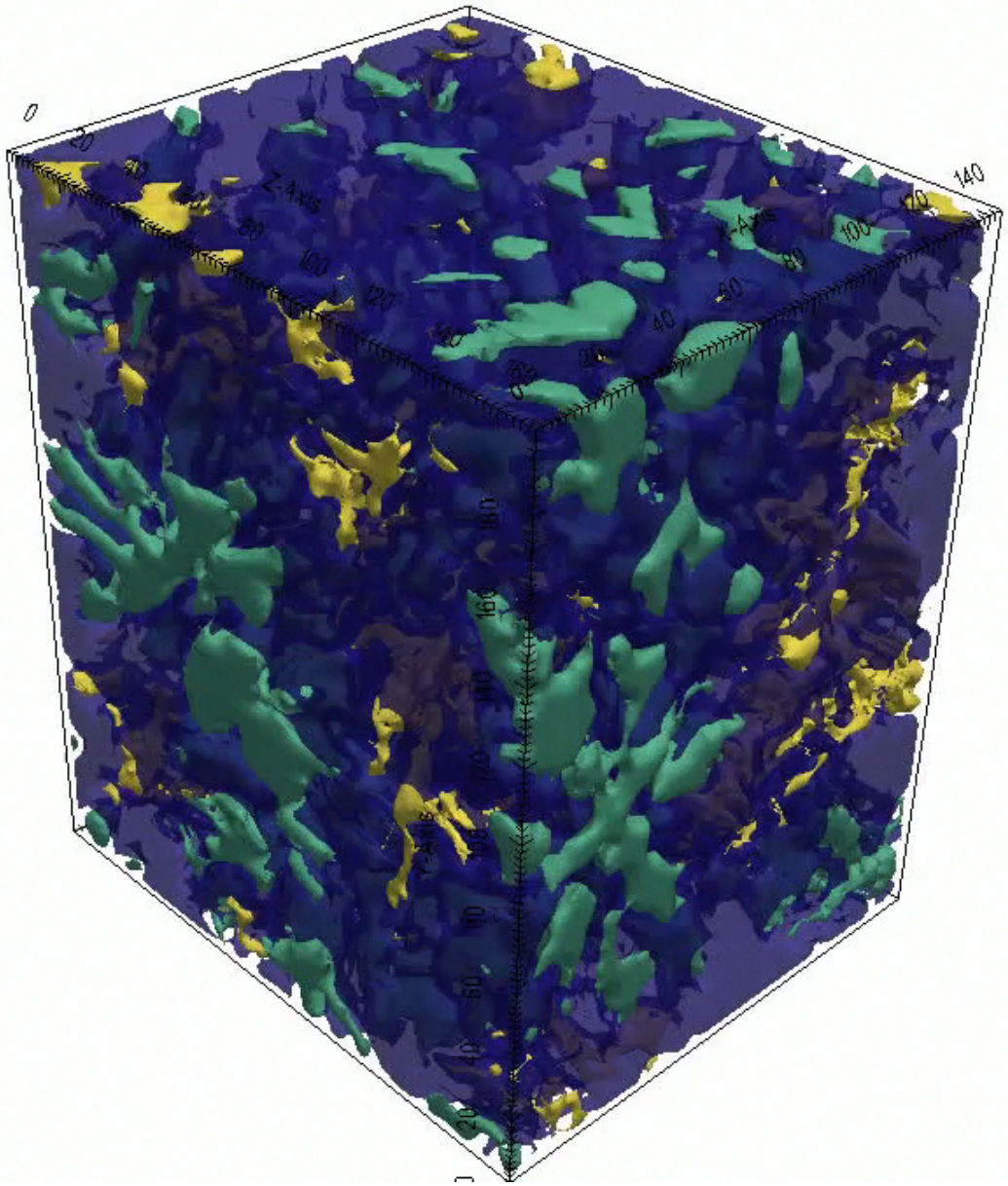


Y – TiSn
(7%)
G – Heusler
(20%)
B – Half-Heusler
(73%)

# $TiNi_{1+x}Sn$: $x$ = 0.20: TriBeam-studies

Tribeam: Multimodal information

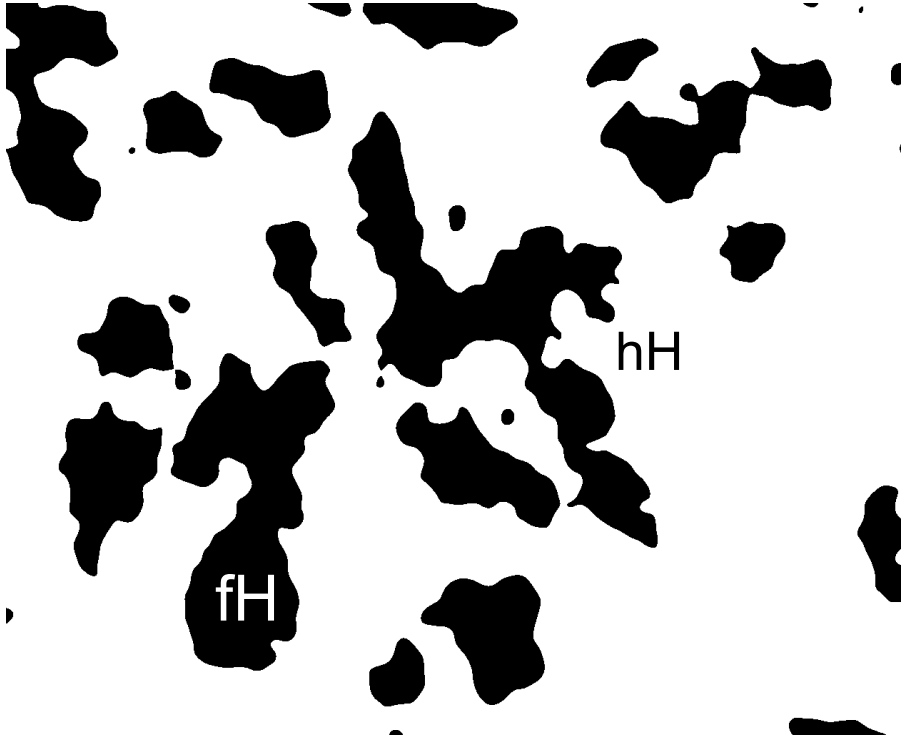


EDS Phase ID (Ni)

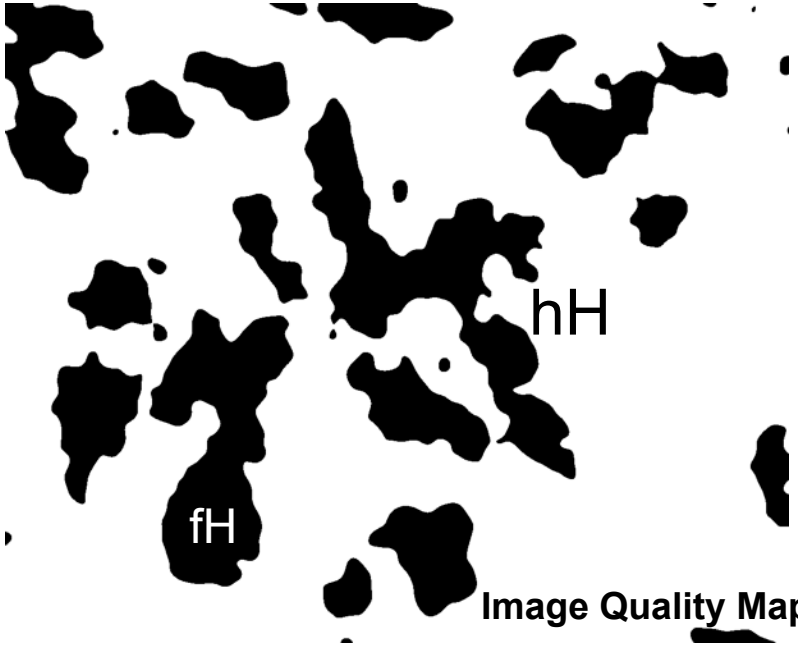


Image Quality Map

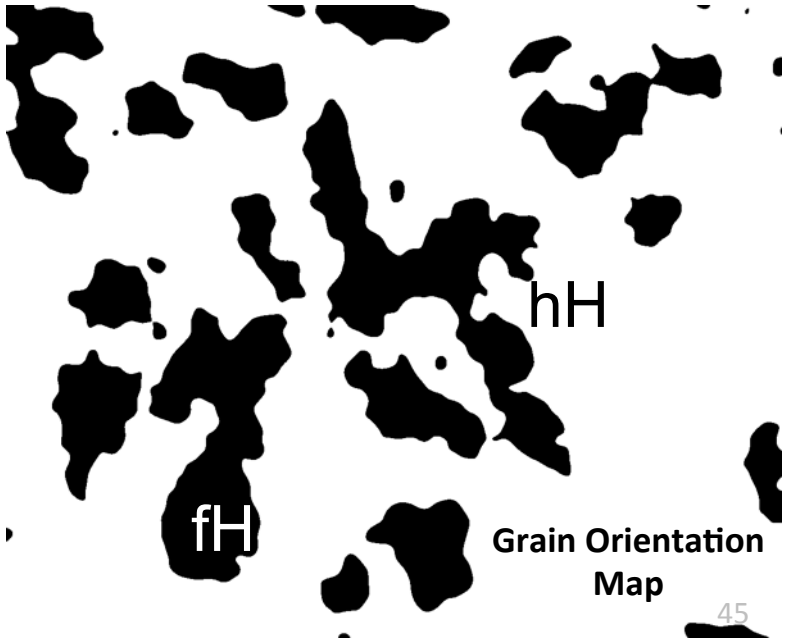


Grain Orientation Map

- Measurement of connectivity of full-Heusler phase requires multimodal EDS/EBSD mapping to distinguish phases
- New algorithms for merging datasets being developed
- Low misorientation (semicoherent) boundaries between fH and hH in many regions

# TriBeam for Tomography

Dataset size: 160 x 120 x 90 um
Rene88DT – Nickel Disk Alloy

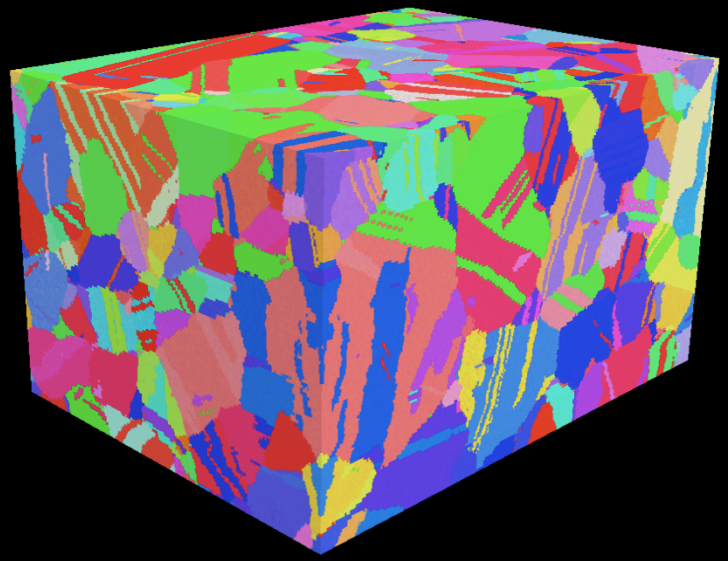

CuW

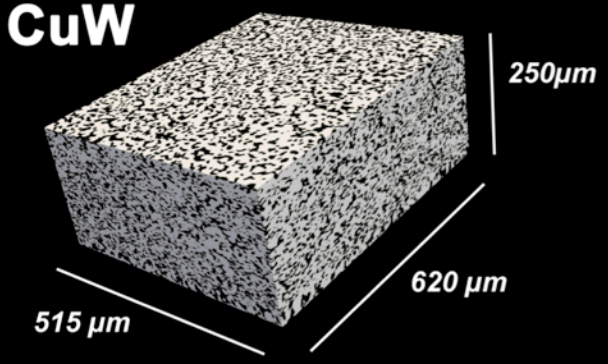


Cu

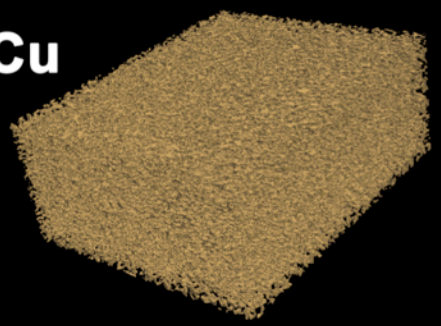

Dataset size: 190 x 250 x 108 um
Alpha grains

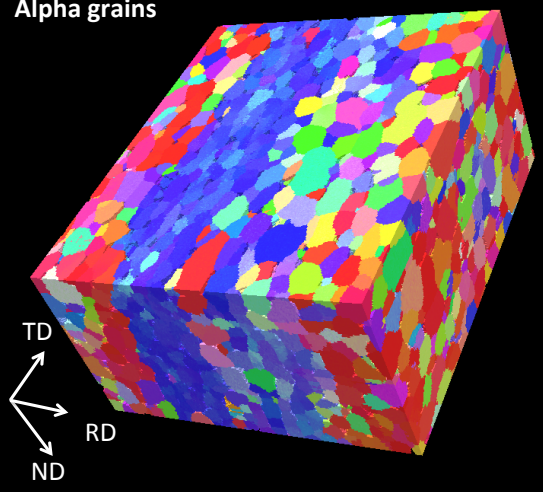


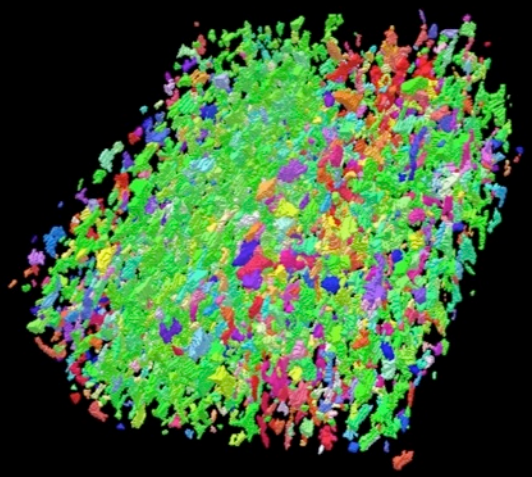

W

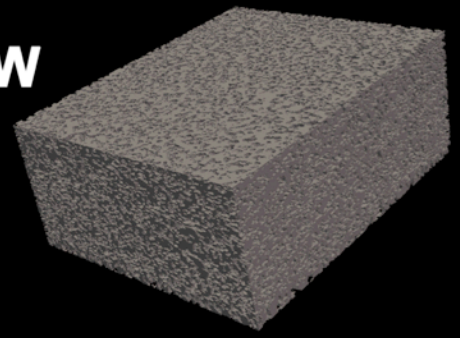

# Schematic of Laser Ablation

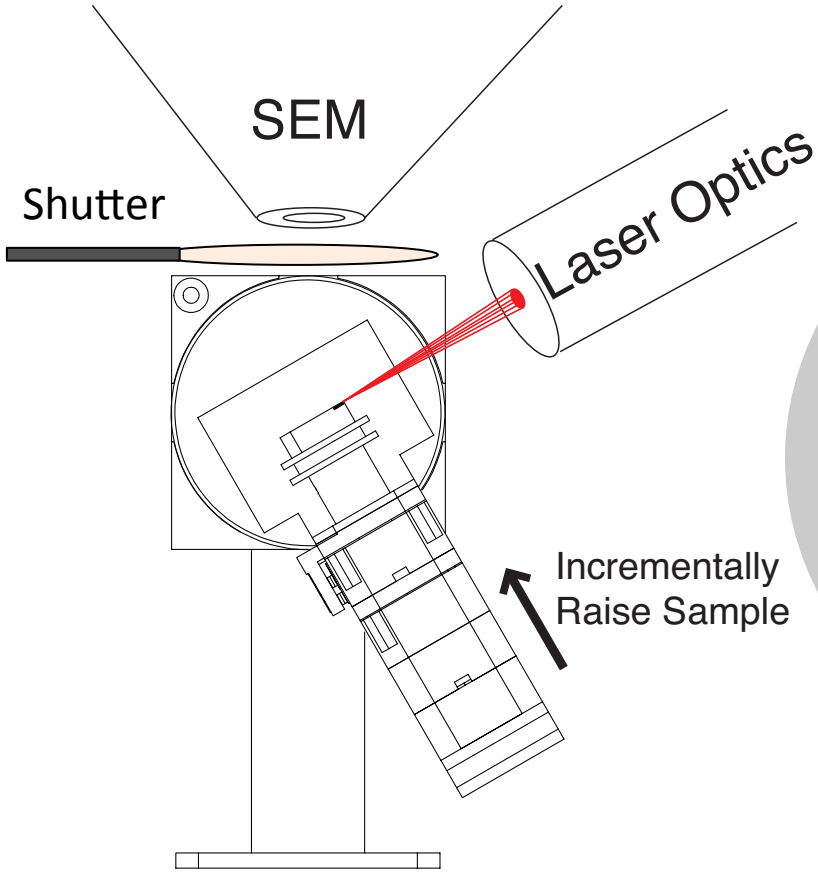


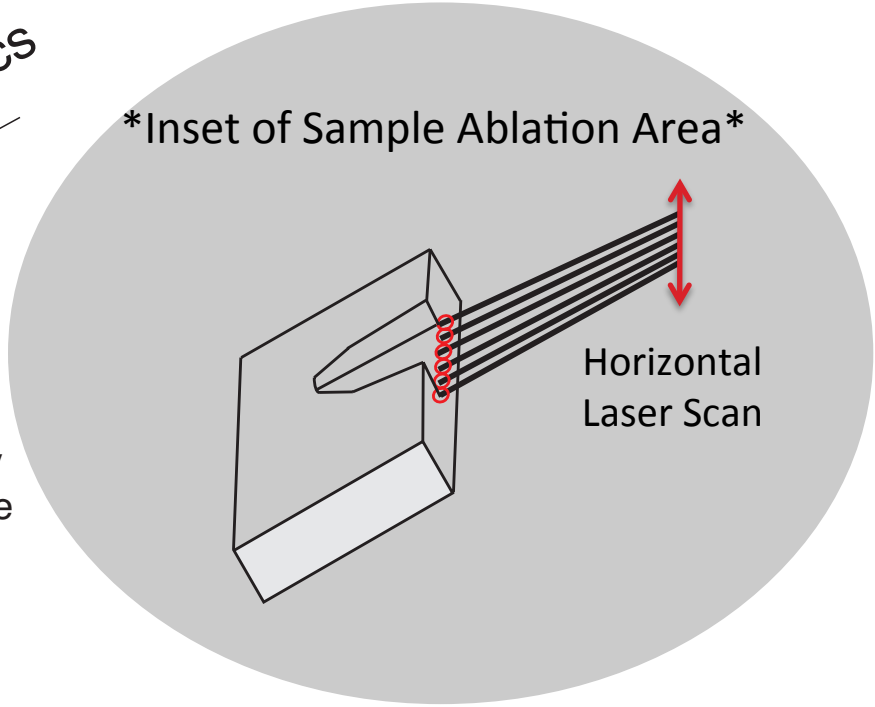


- Sample is incrementally raised into the focus of the beam
- The pole piece is blocked from redeposition by a shutter
- Surface parallel ablation decouples phase removal rate dependence

# High Fluence Fs. Laser Damage

## SCHEMATIC OF LASER MACHINING! – DIFFERENT THAN TRIBEAM

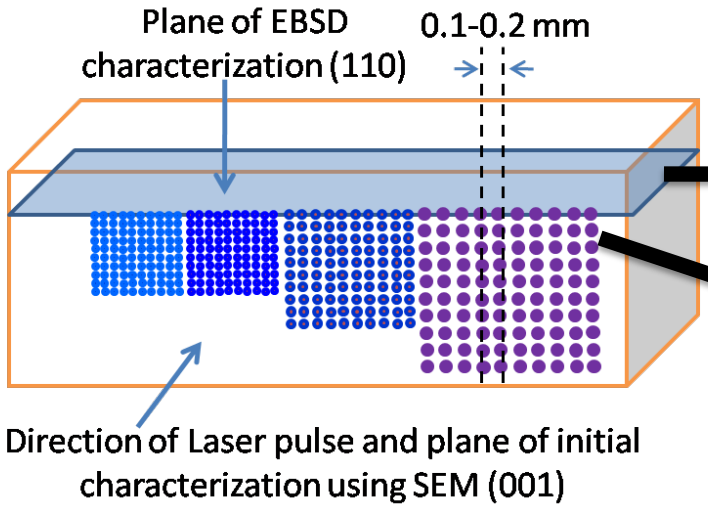


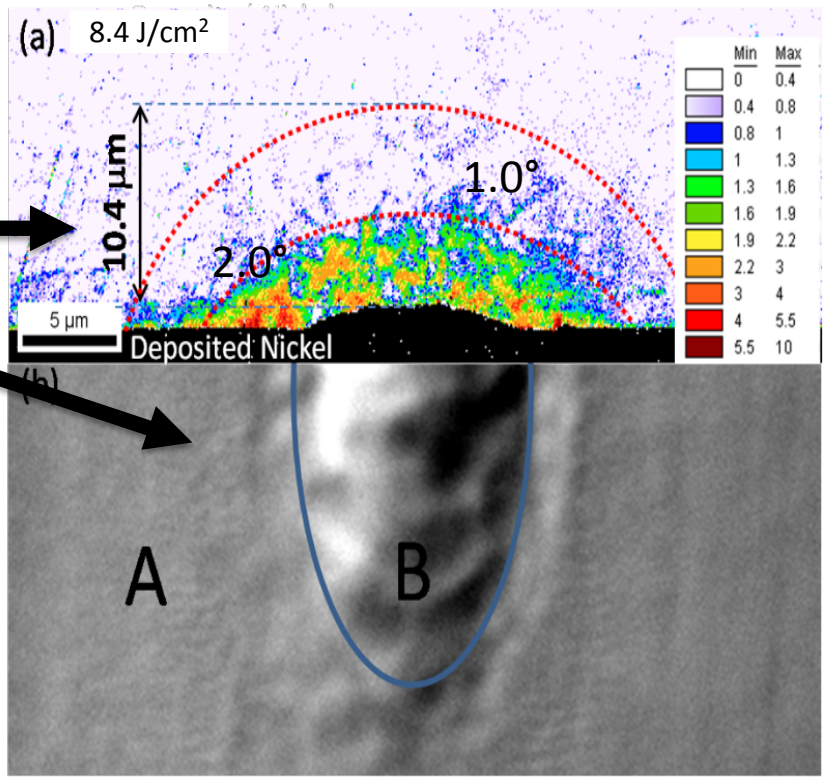


- High Fluence pulses, sample perpendicular to beam
- Most damage limited to less than 3-4µm in depth
- Highest damage < 5.5°
- EBSD patterns can still be obtained
- Dislocation densities of ~2.8 x $10^{10}$ per $cm^3$

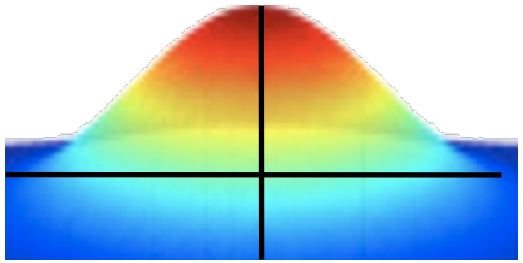

Gaussian Laser Beam

*A. Kumar and T.M. Pollock, Journal of Applied Physics, **110**, (2011)*

# Low Damage with Fs. Laser Ablation

Single crystal Ni-base Superalloy TEM foil

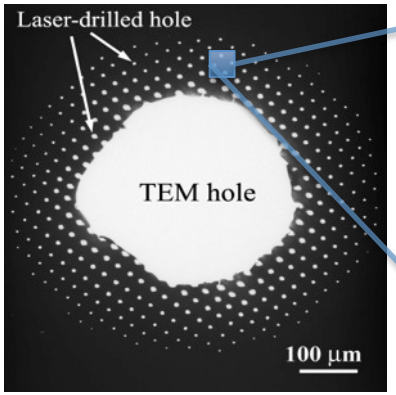


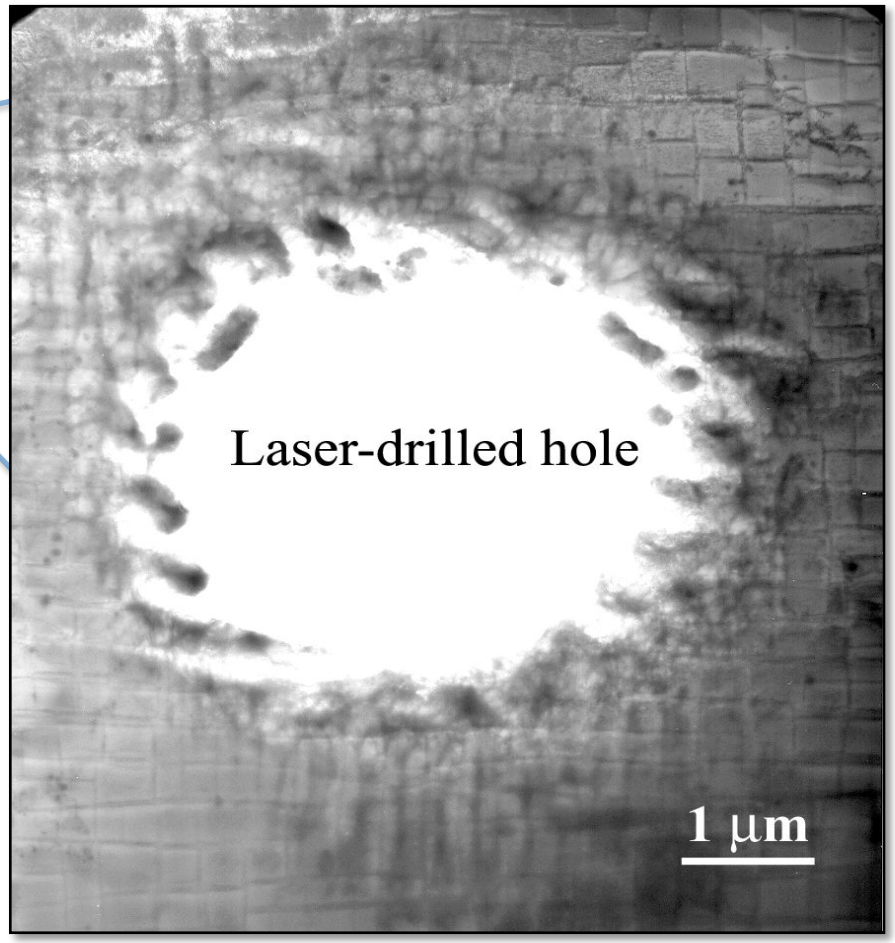


Diffraction patterns sampled near edge of laser-drilled hole

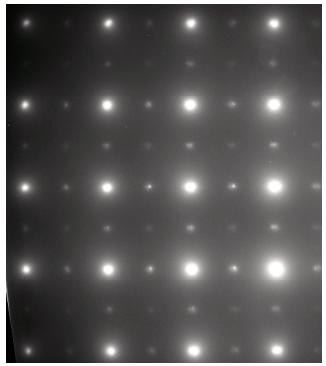

γ' precipitates

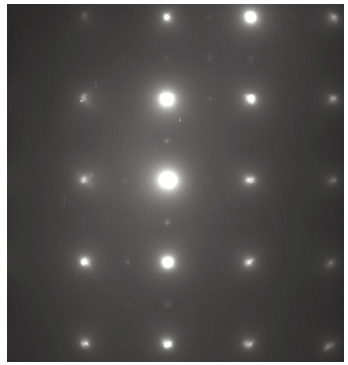

γ matrix

Ni-base Superalloy Unperturbed microstructure

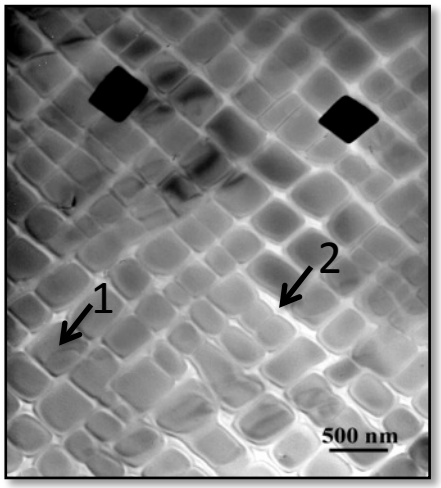


1. $L1_2$ ordered γ' precipitates
2. γ phase matrix

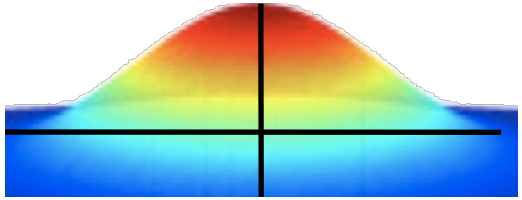

*Feng, Q. et al. Scripta Materialia.* ***53****, 514 (2005)*

# Two Distinct Ablation Rates in Superalloy

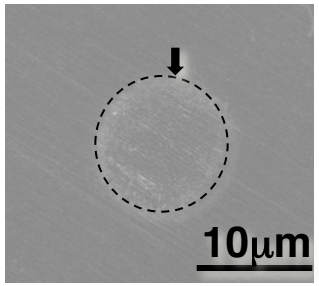


Low Fluence Crater

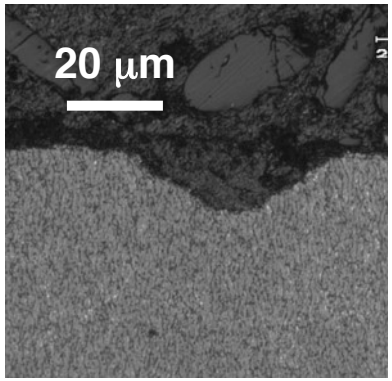


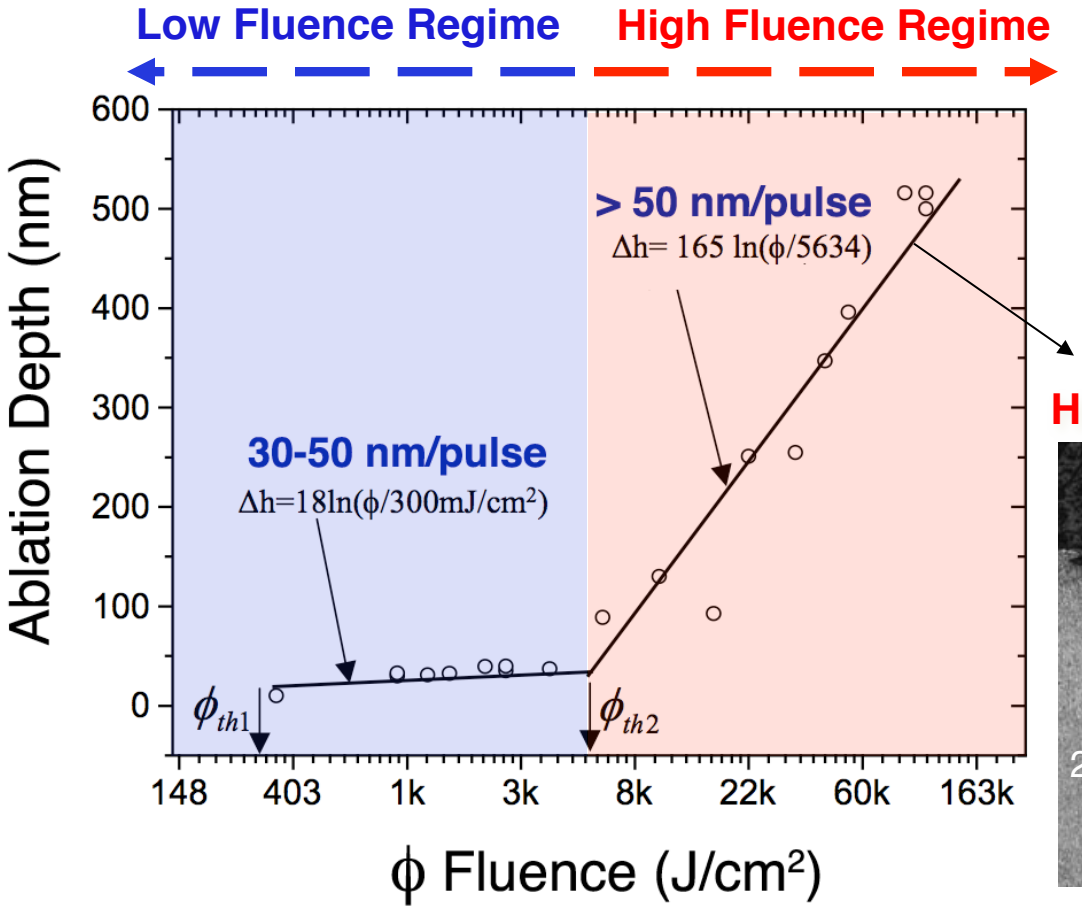


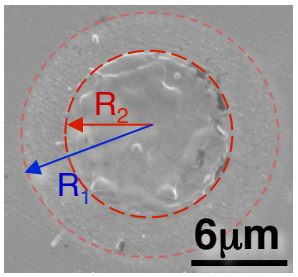


High Fluence Crater

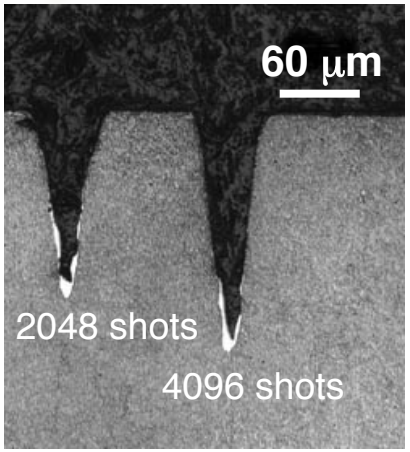


- Single pulse ablation of CMSX-4 Superalloy
- Depth and ablation morphology characterized with AFM
- Two distinct ablation rates and damage

*S. Ma – Met. Trans.* ***38A.*** *2007*

# Fs. Laser Induced Periodic Surface Structures

Si(100)

AFM

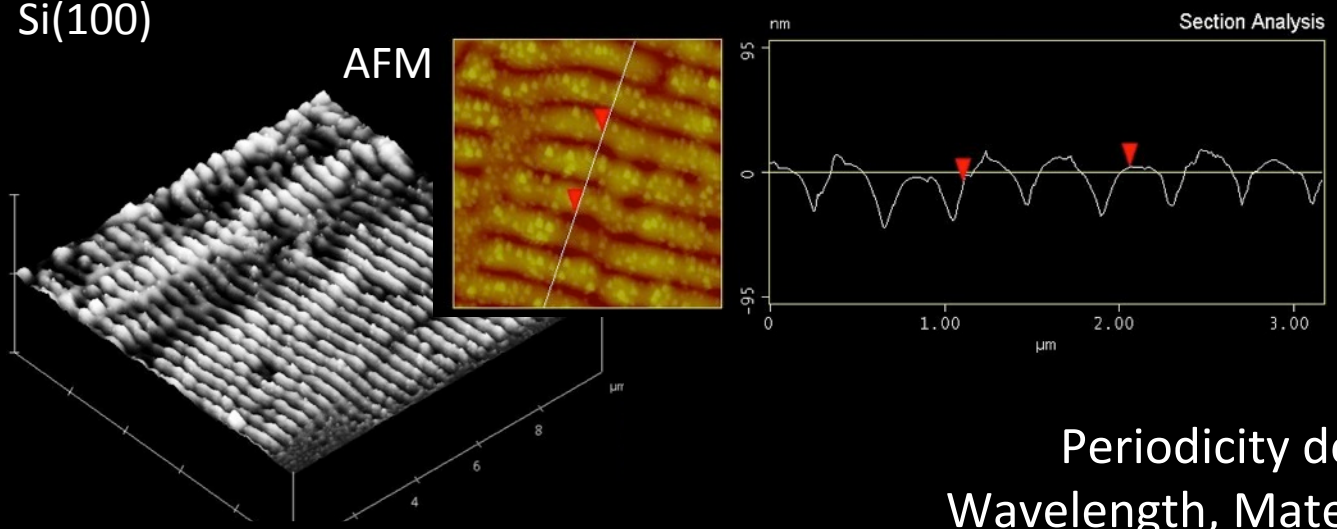


Periodicity dependent on:
Wavelength, Material, Laser Fluence

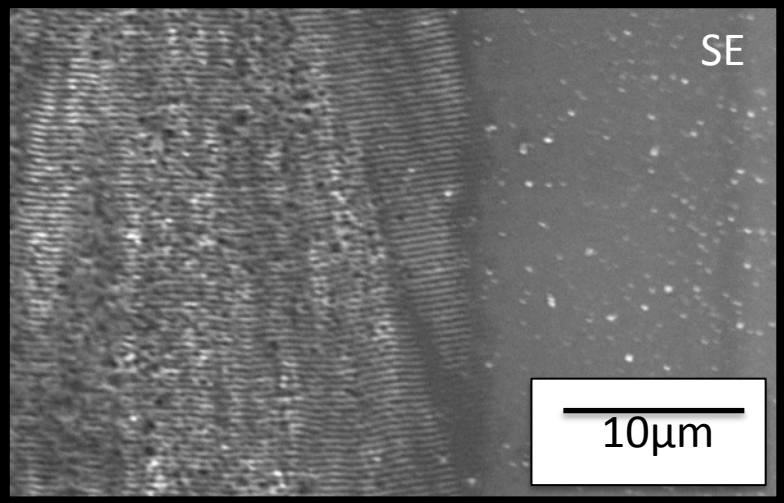


J.P. Mcdonald, S.M. Yalisove, *et al.* MRS Bulletin, 31, 626, (2006).

Ni Alloy - CMSX-4

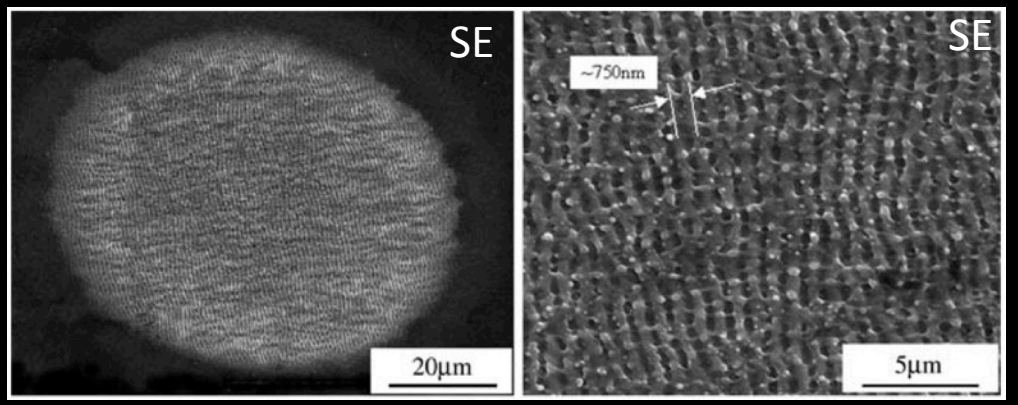


S. Ma *et al.* Metall. Mater. Trans. A 38A, 2349 (2007).

# EBSD Patterns from Fs. Laser Ablated Surfaces

Laser Ablated Mg Alloy - AXJ-530

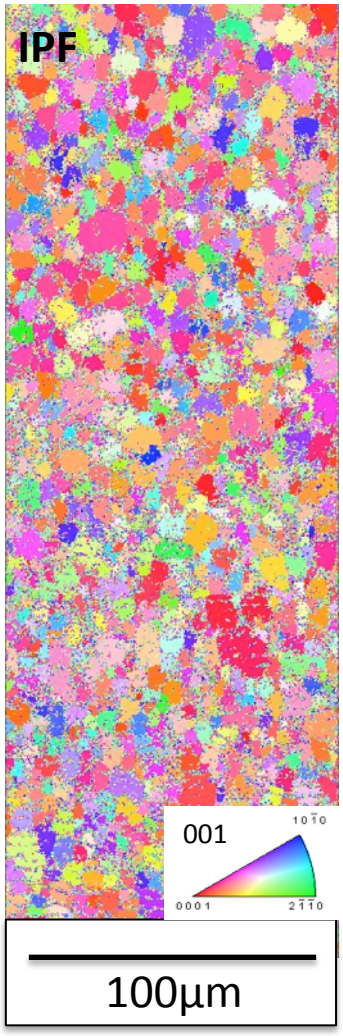


Laser Ablated Ni Alloy - Rene88DT

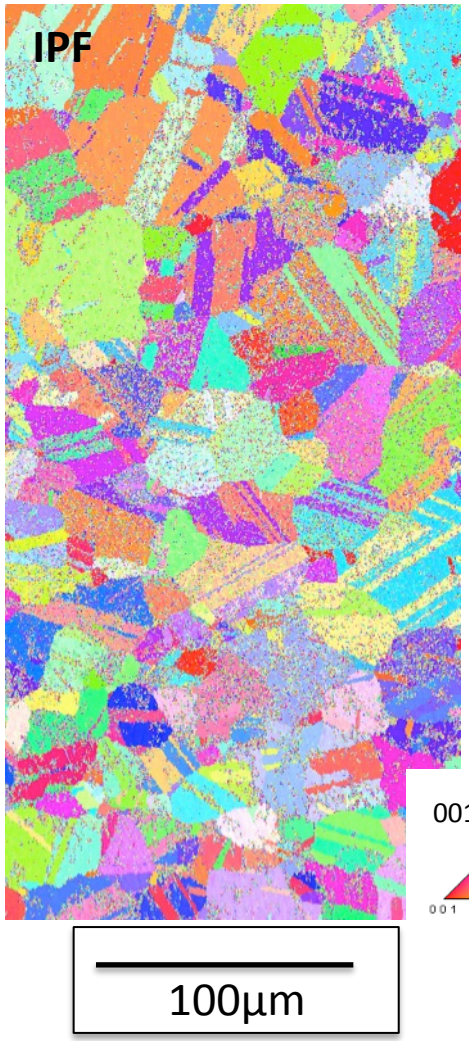


Laser Ablated Strontium Titanate

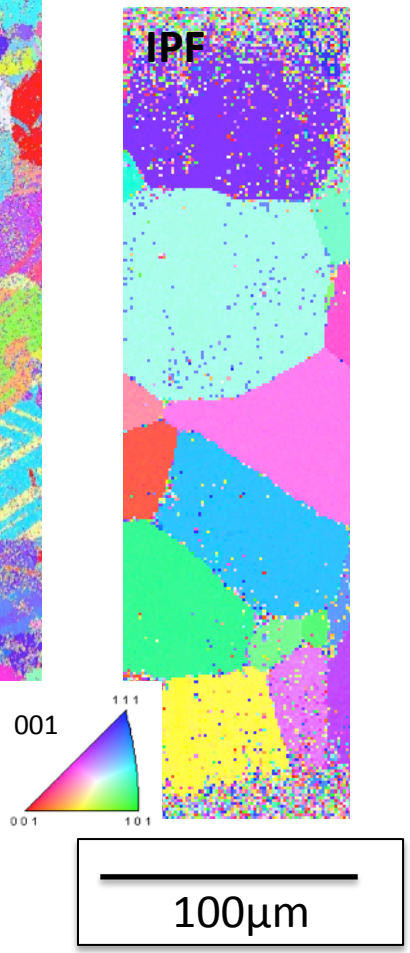


- Direct EBSD mapping of laser ablated surfaces in Ni, Mg, Ti, STO
- Surface laser damage is limited to < the sampling depth for EBSD
- Non-systematic locations of pixels / pixel groups that do not index
- EBSD resolution < 0.5 µm/ pixel

# STO Backscatter Interaction Depth

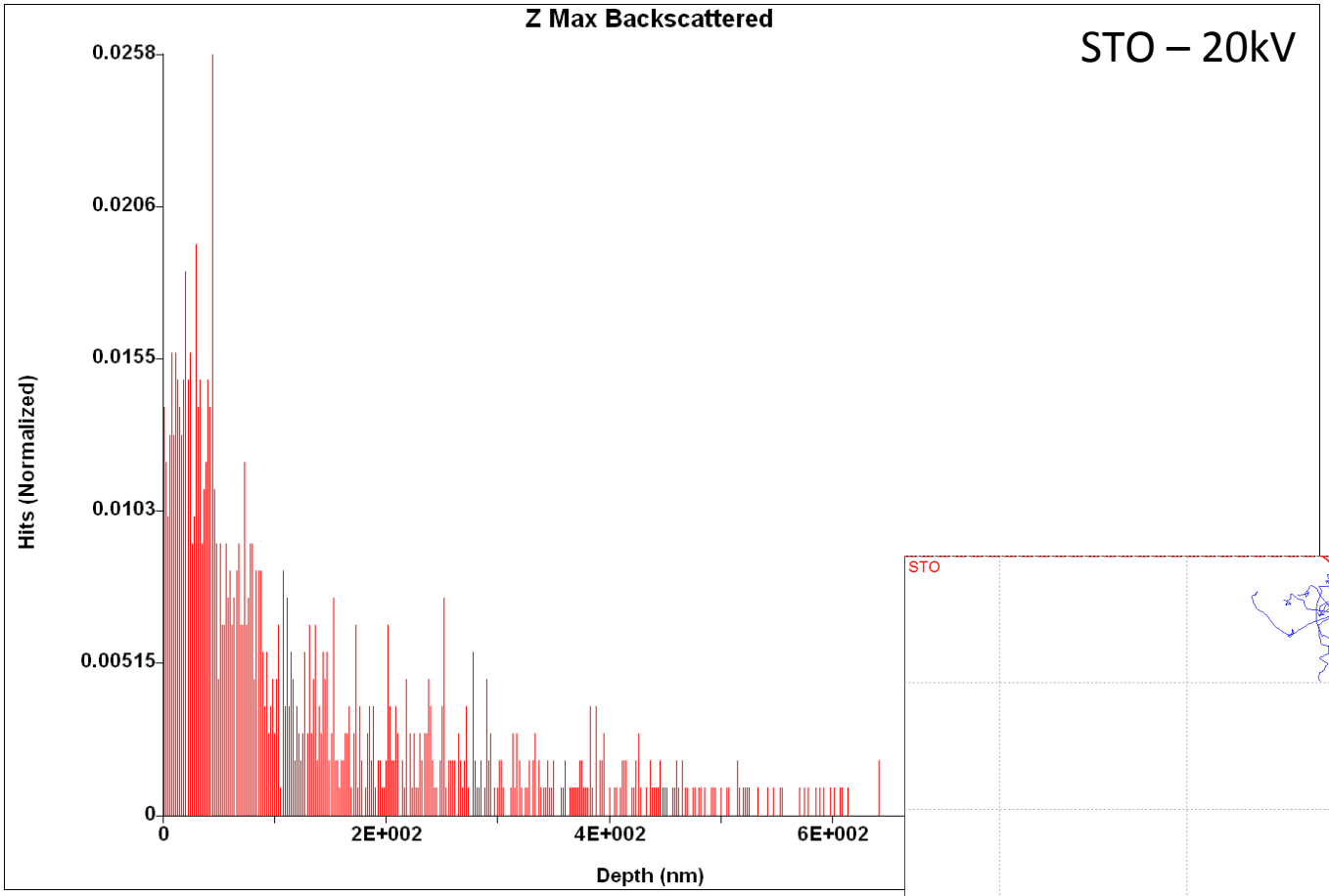


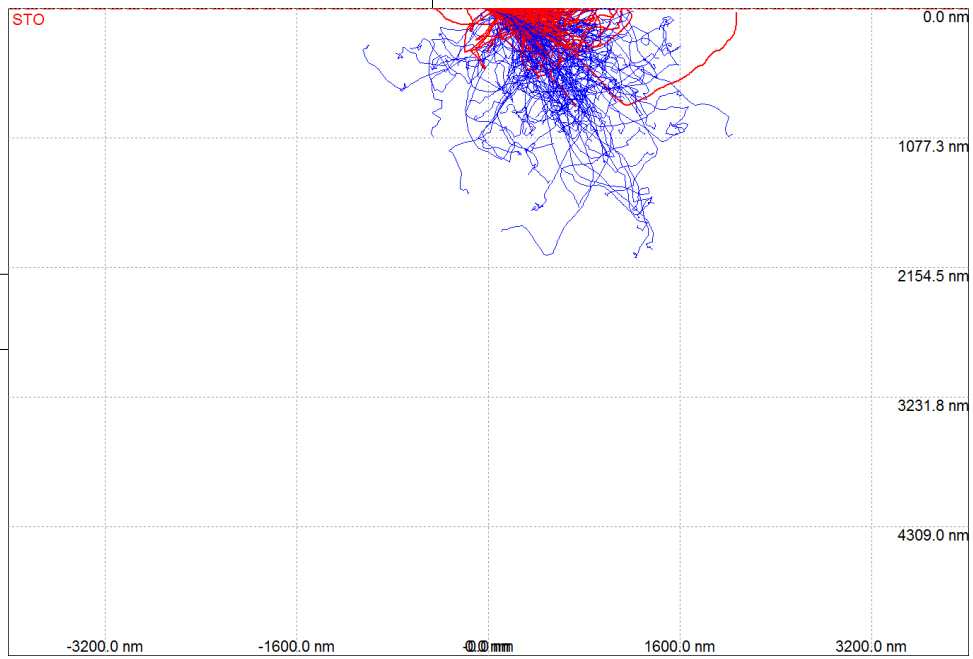


Depth < 150 nm

Casino - Drouin, D. *et al. Scanning 29(3) 2007. 92-101.*

# STO Backscatter Interaction Depth

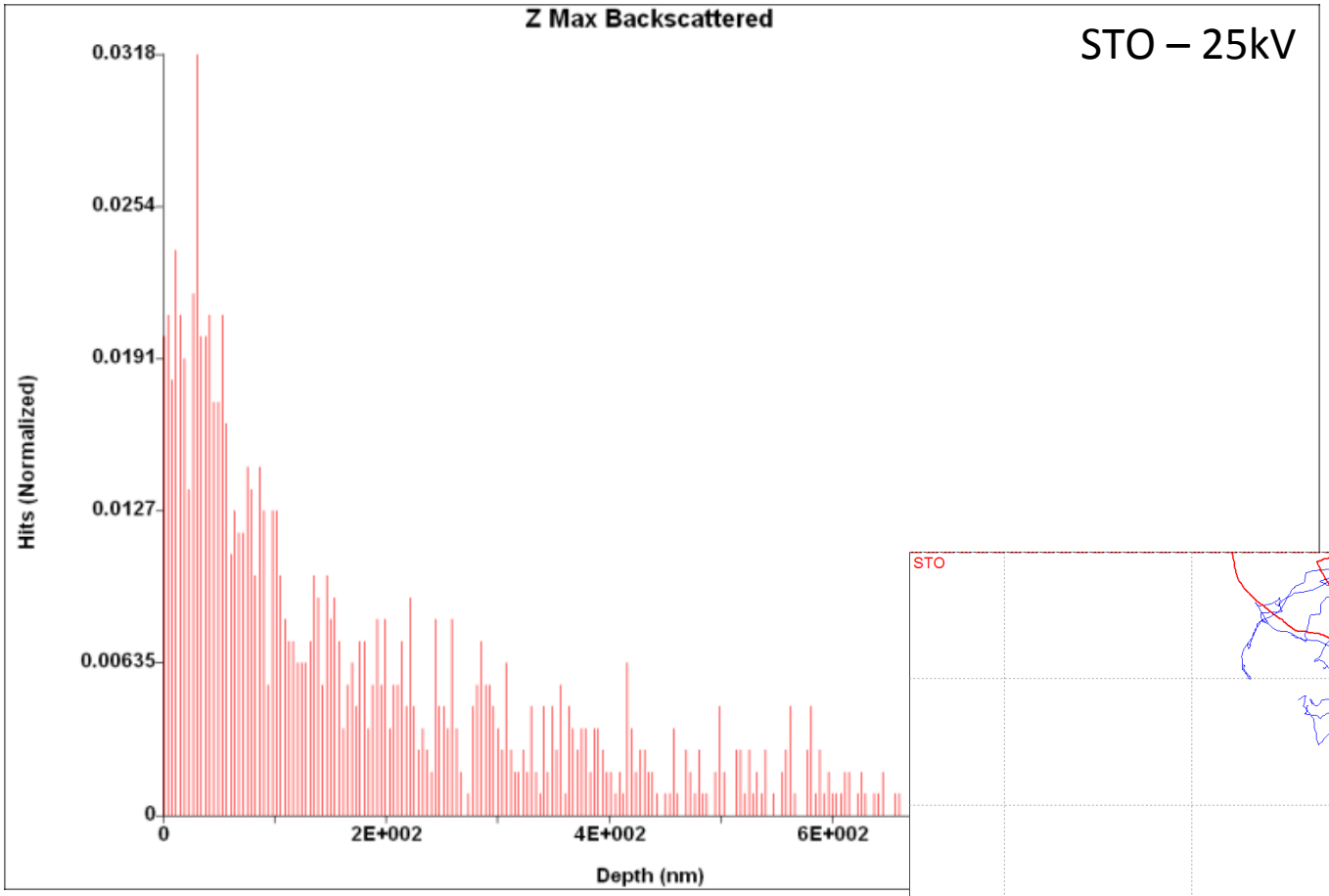


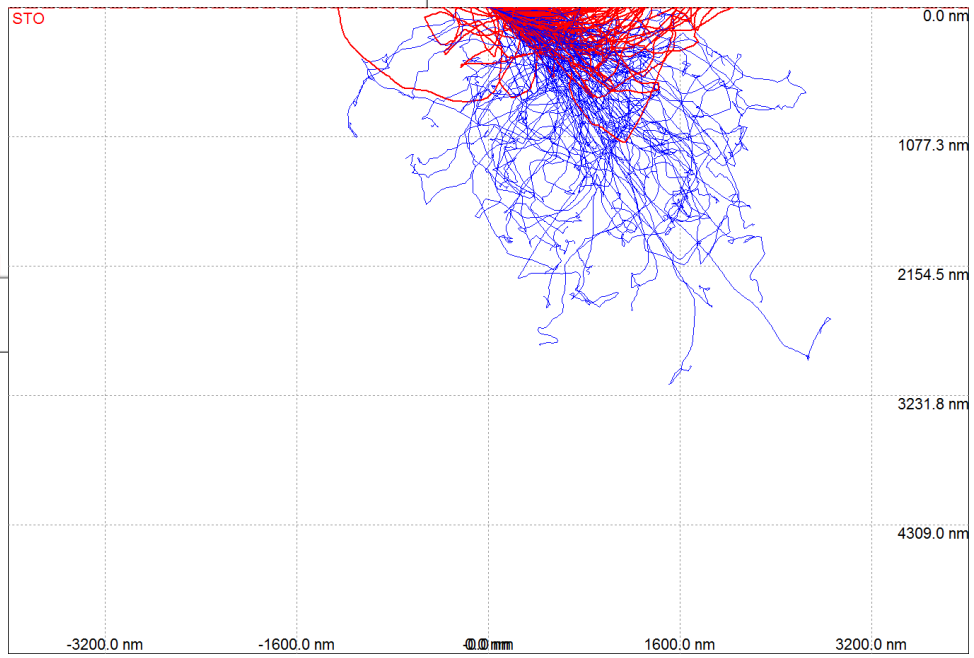


Depth < 200 nm

Casino - Drouin, D. *et al. Scanning 29(3) 2007. 92-101.*

# STO Backscatter Interaction Depth

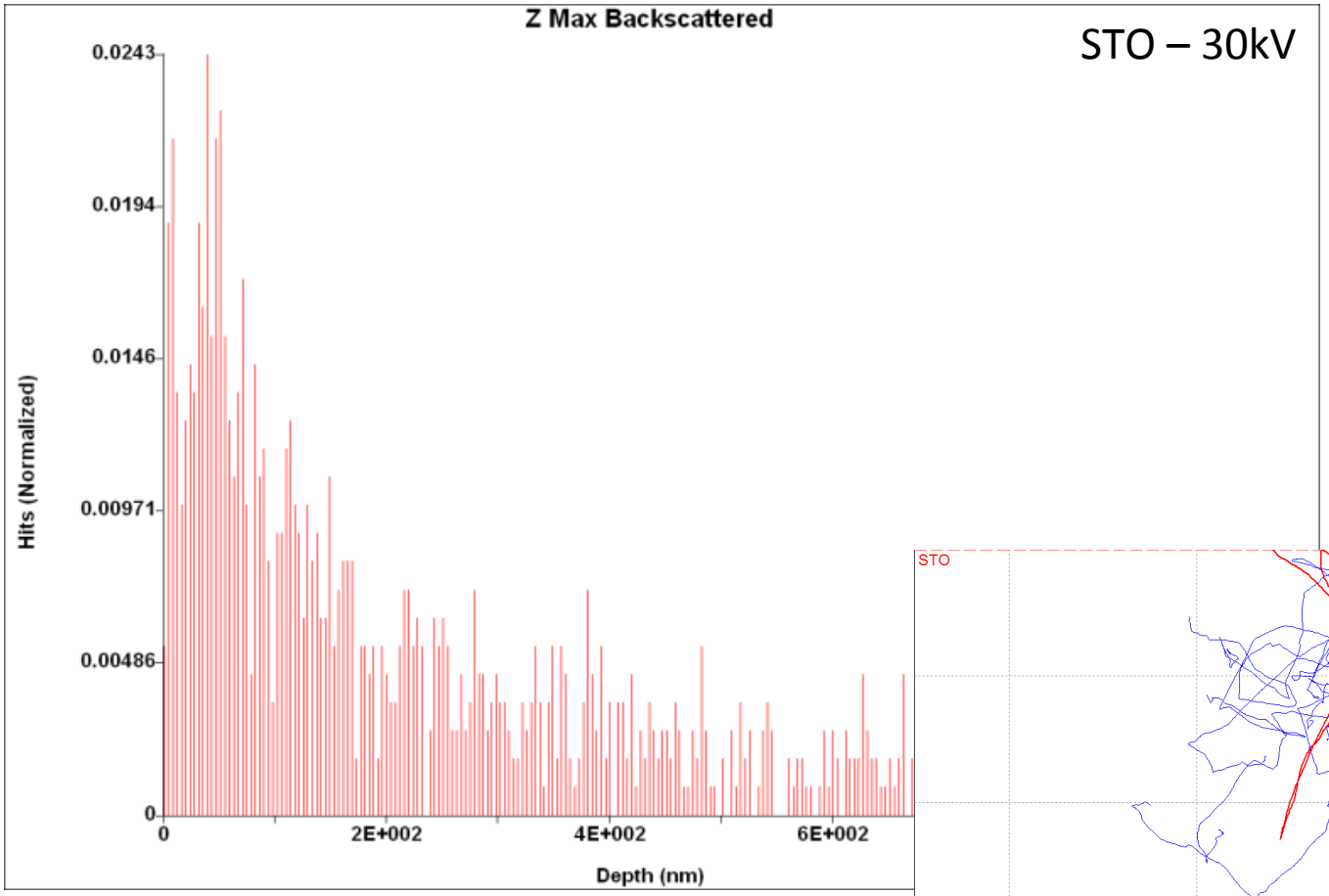


Depth < 250 nm

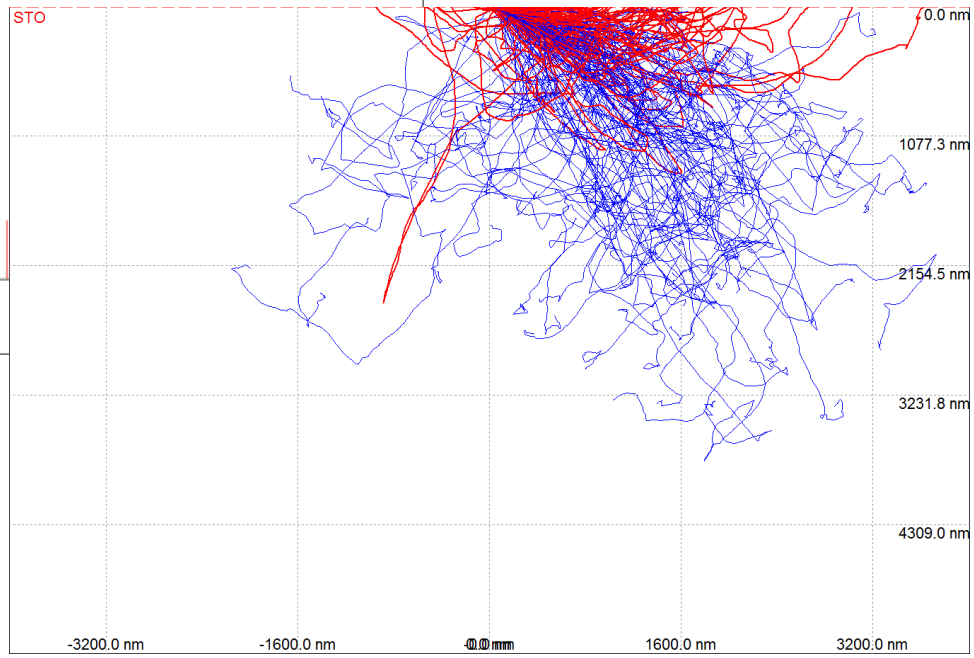


Casino - Drouin, D. *et al. Scanning 29(3) 2007. 92-101.*

# STO Backscatter Interaction Depth

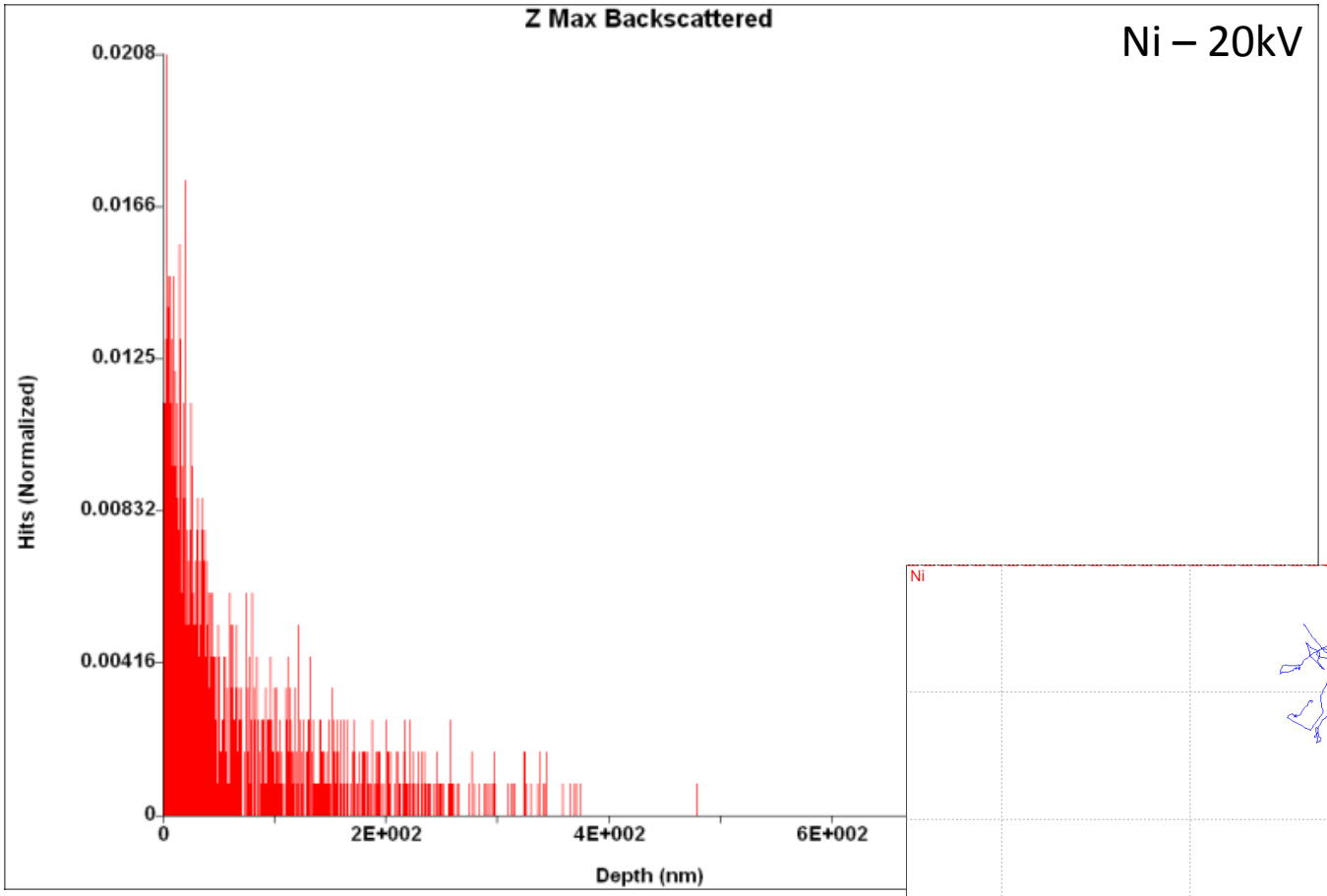


Ni – 20kV

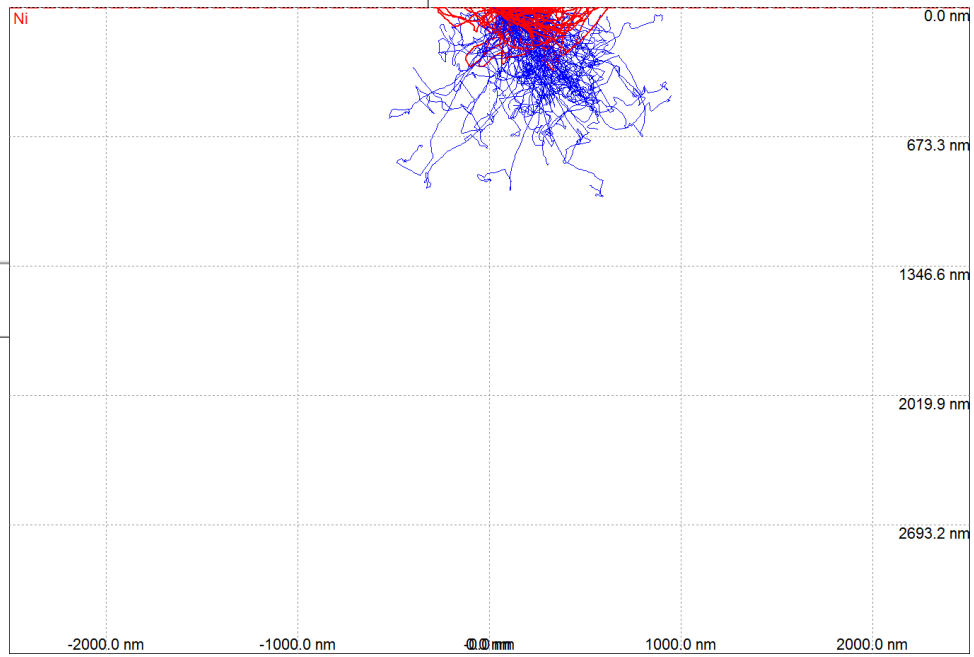


Depth < 100 nm

Casino - Drouin, D. *et al. Scanning 29(3) 2007. 92-101.*

# STO Backscatter Interaction Depth

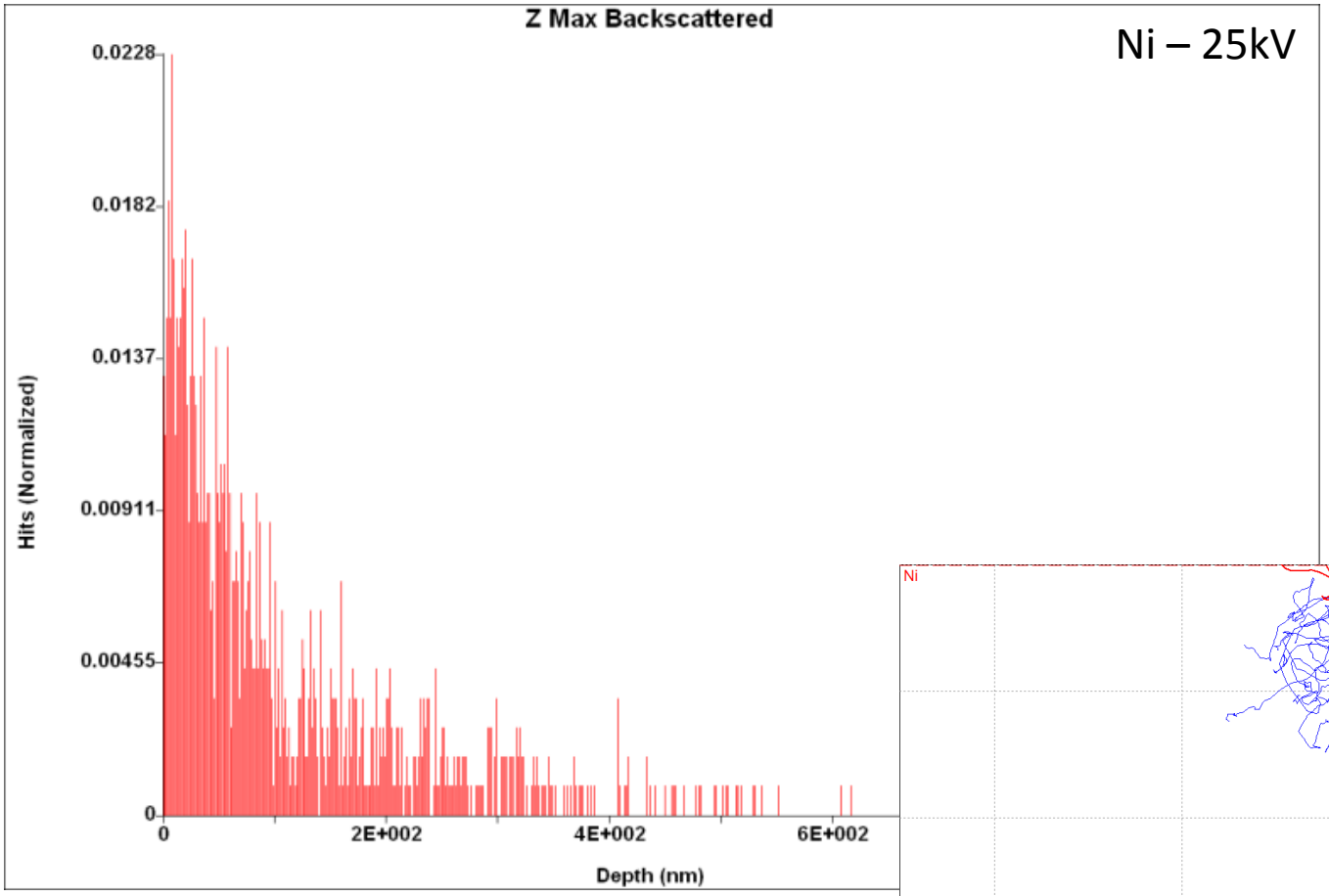


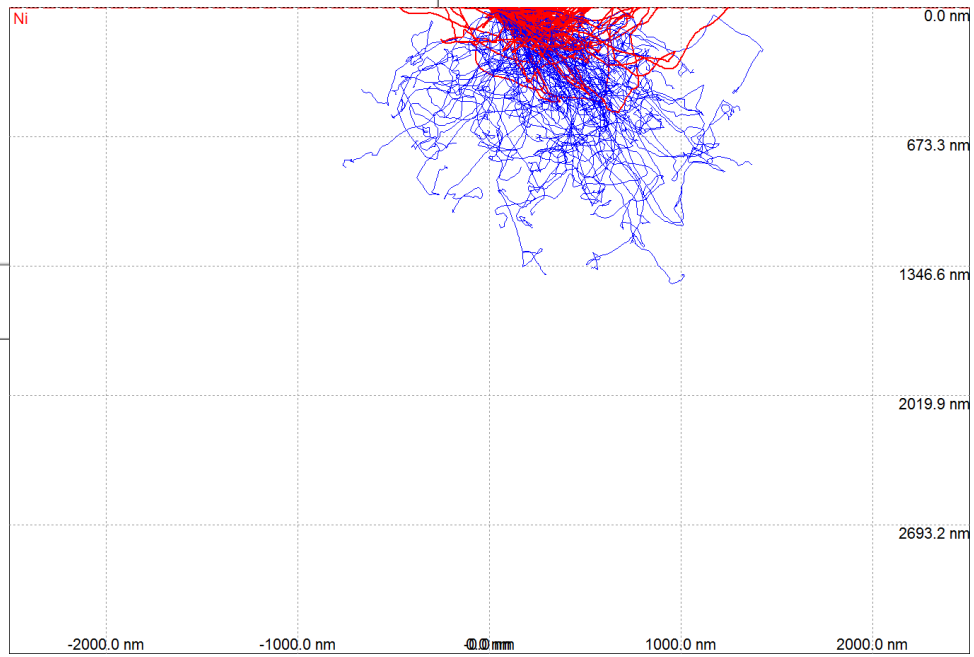


Depth < 150 nm

Casino - Drouin, D. *et al. Scanning 29(3) 2007. 92-101.*

# STO Backscatter Interaction Depth

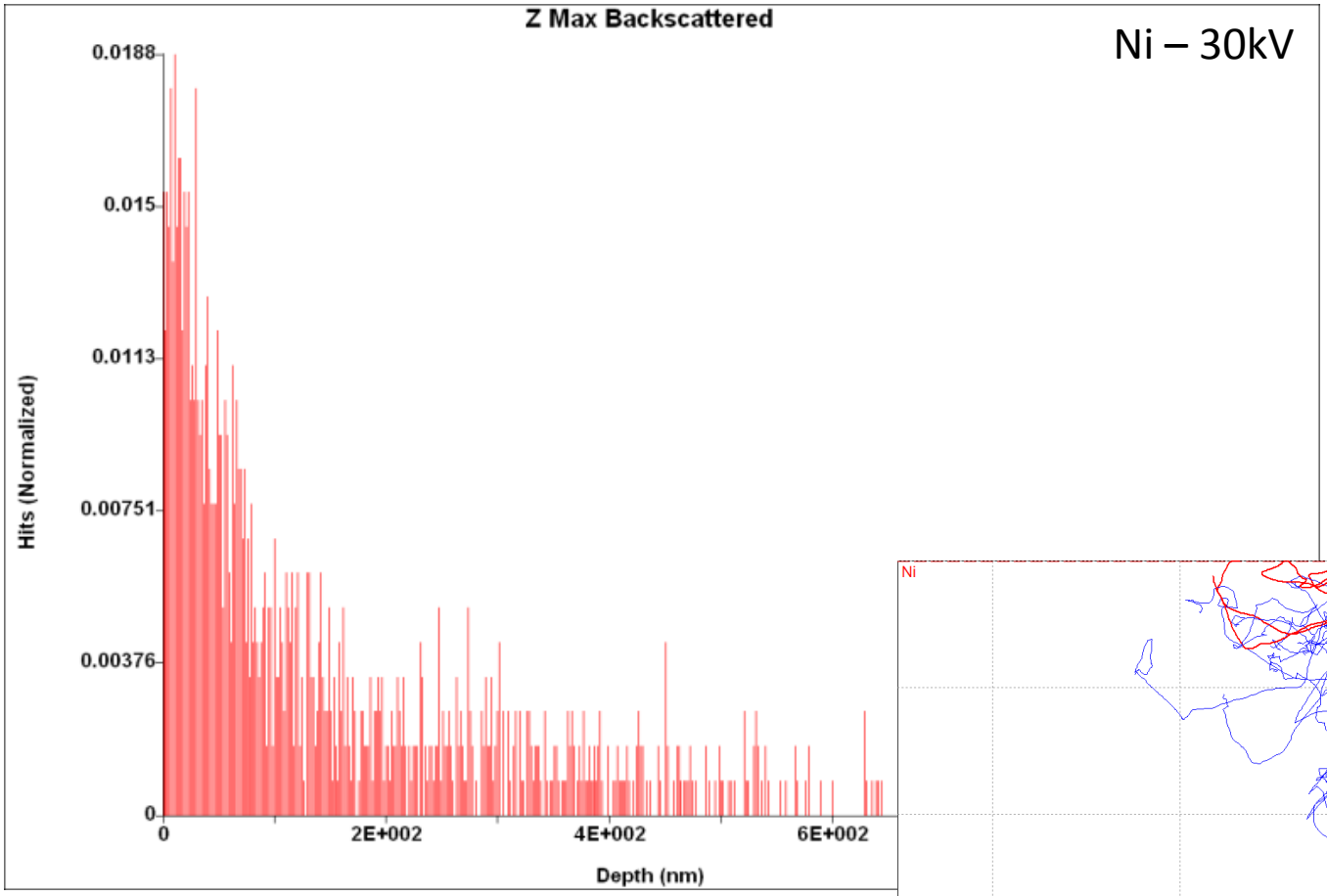


Depth < 200 nm

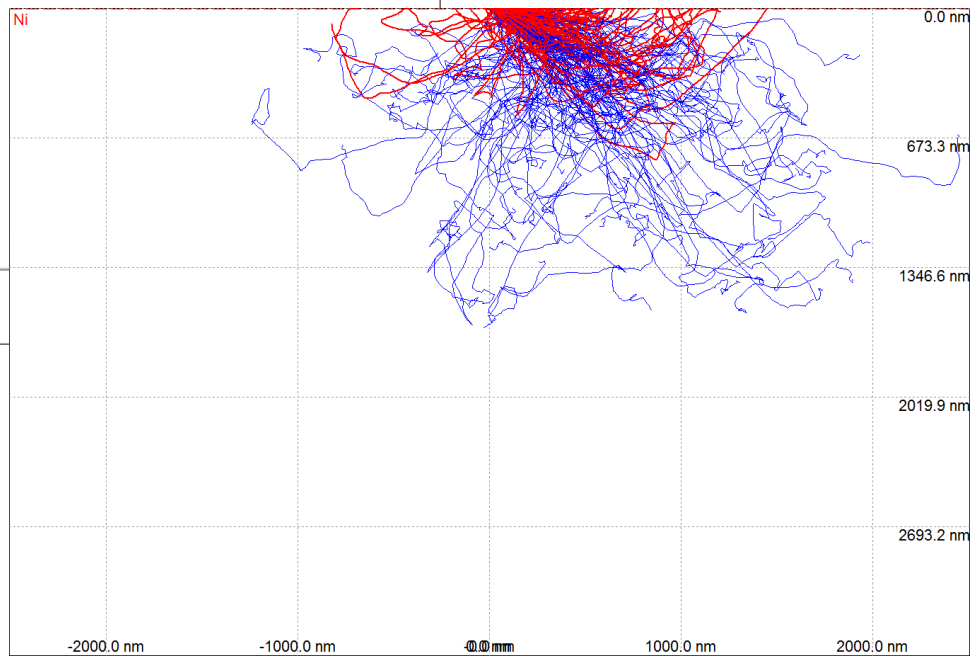


Casino - Drouin, D. *et al. Scanning 29(3) 2007. 92-101.*

# Exit Depth of Backscattered electrons in Ni

Ni

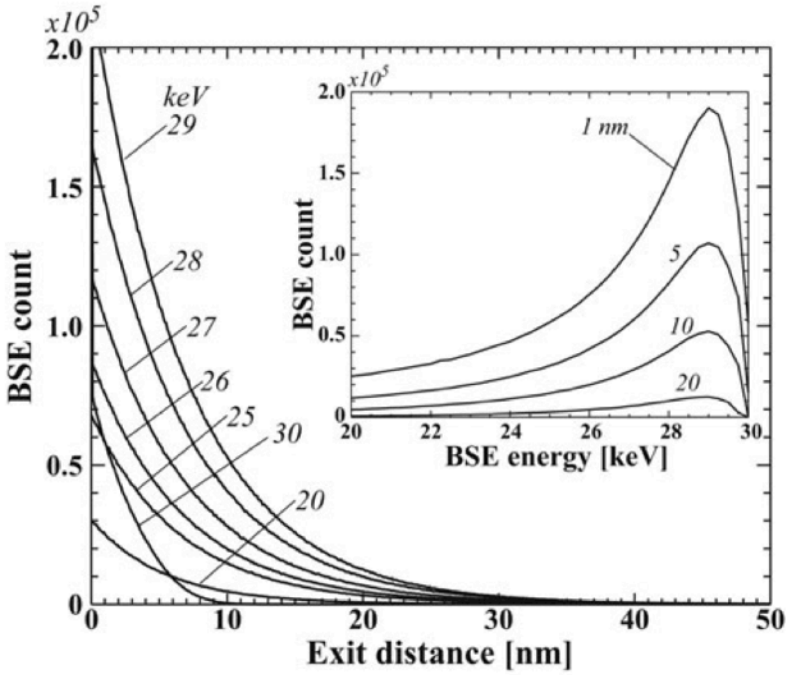


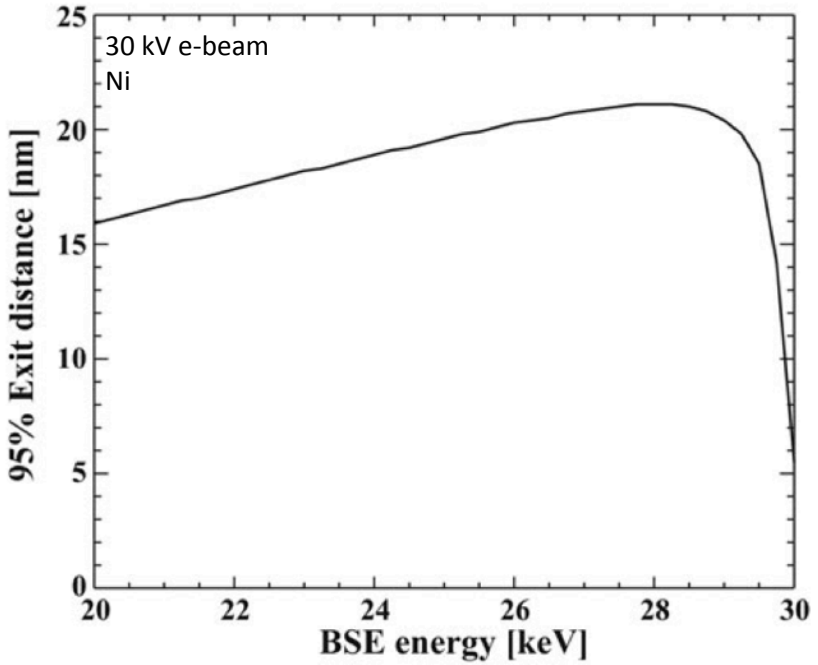


Callaghan, PG and M. De Graef. Microscopy and Microanalysis. 7 (2013) 1-11 .

# EBSD Patterns from Fs. Laser + FIB Surface

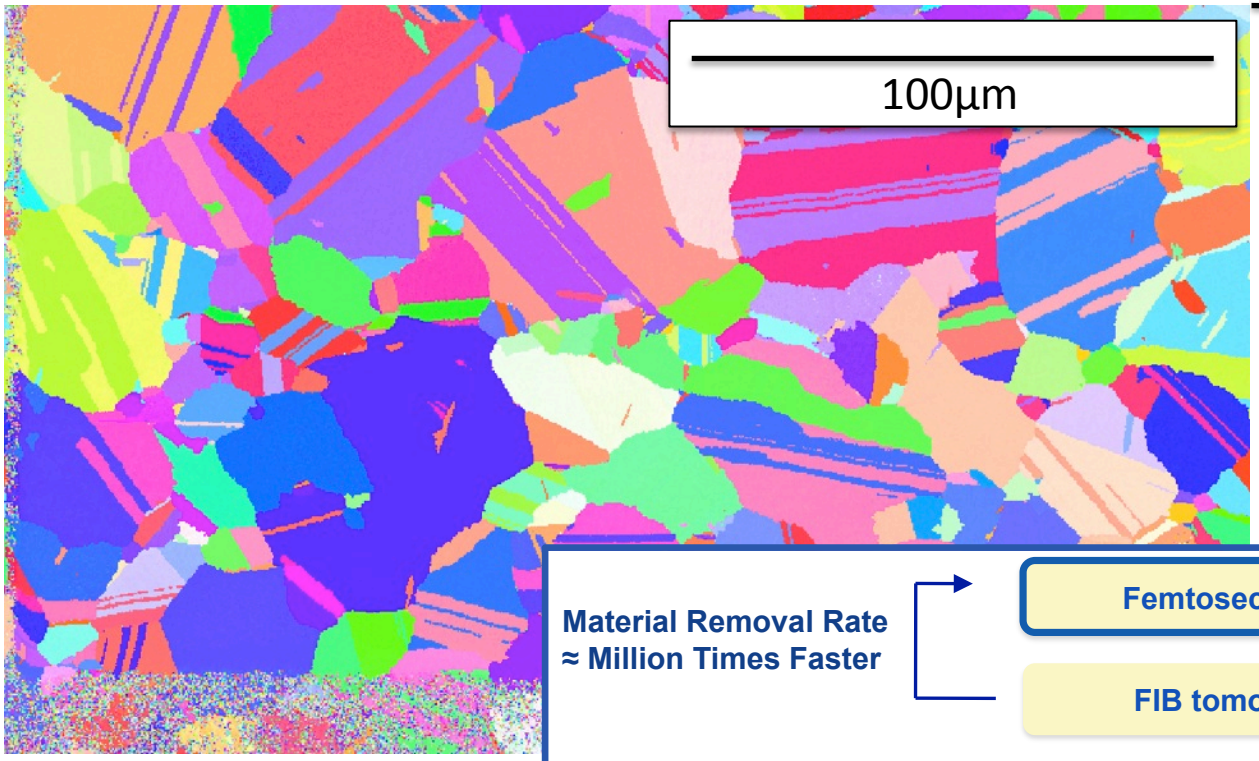


Fs. Laser + FIB

Ion Milling: 30kV, 20nA, <10° p

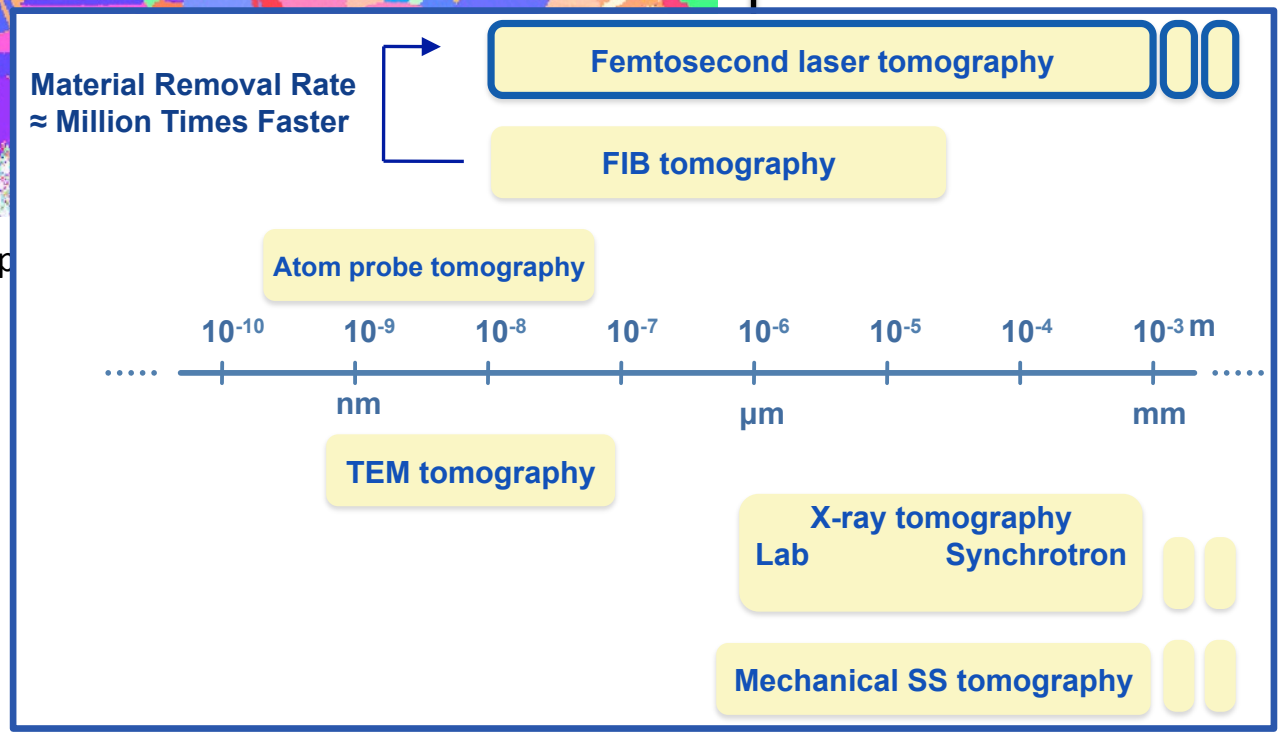

# Fs. Laser + FIB in Rene88DT Ni Alloy

Laser Induced Periodic Structures

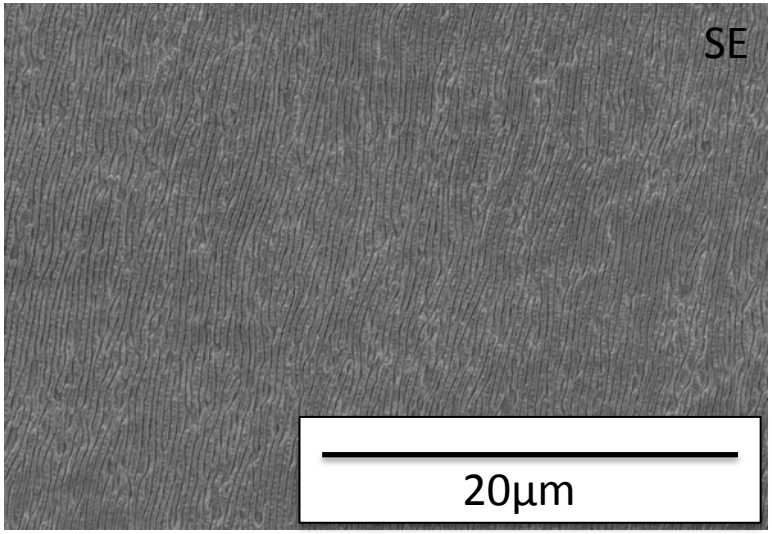


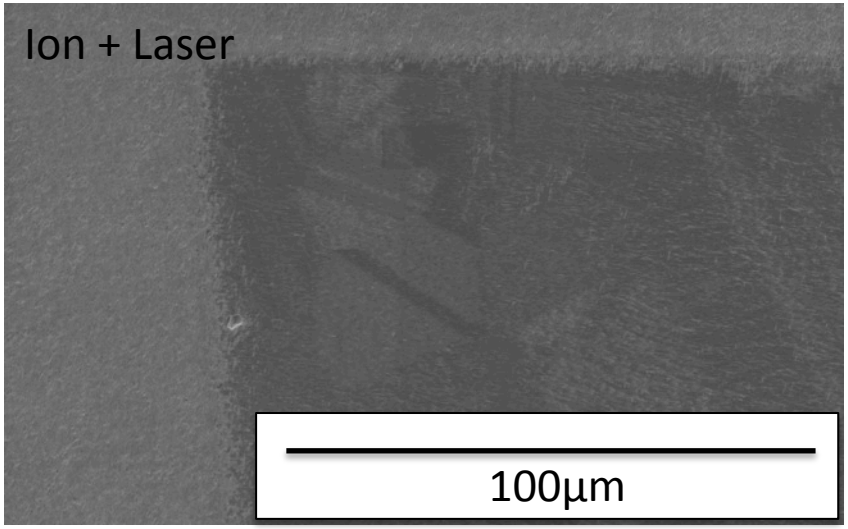


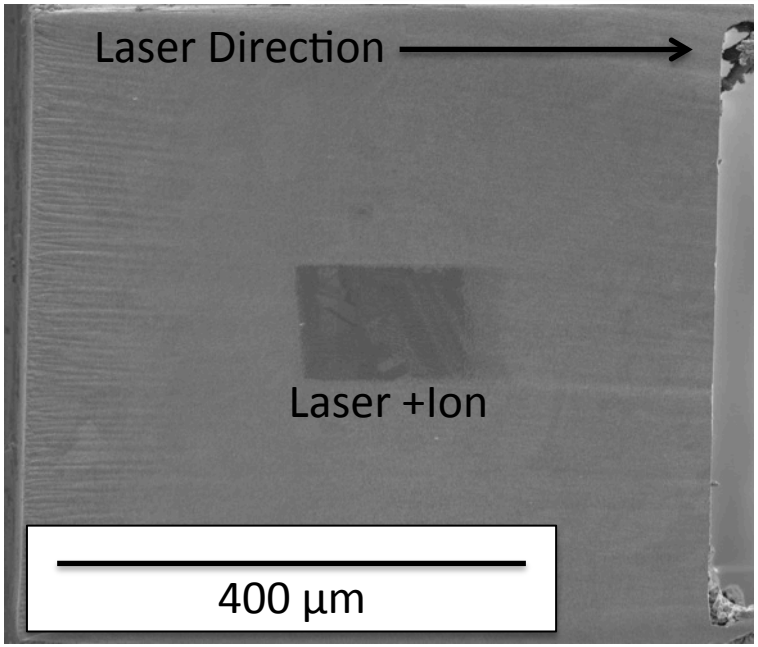


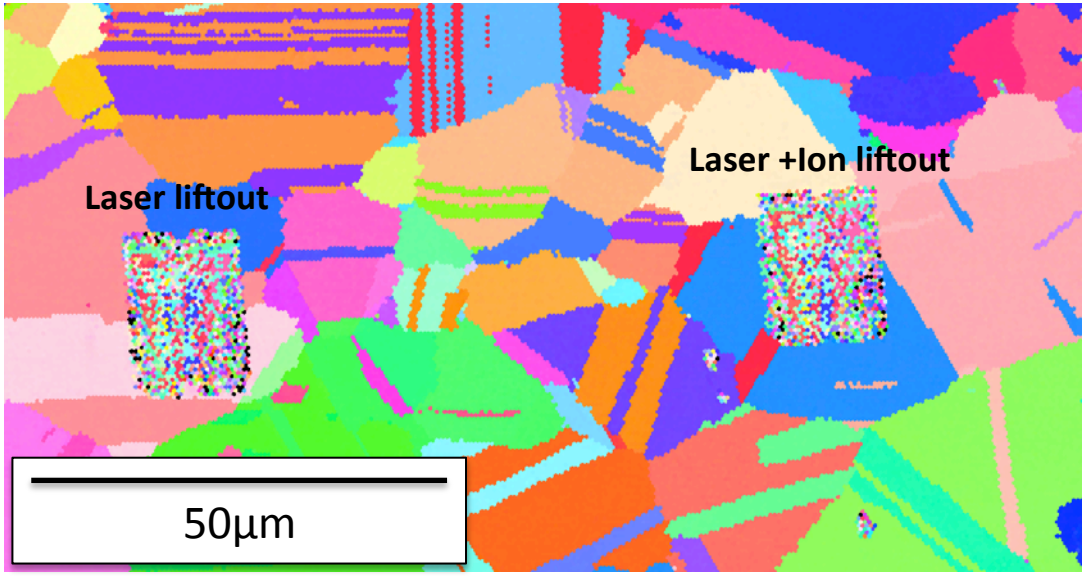

# Femtosecond Laser and Ion Damage

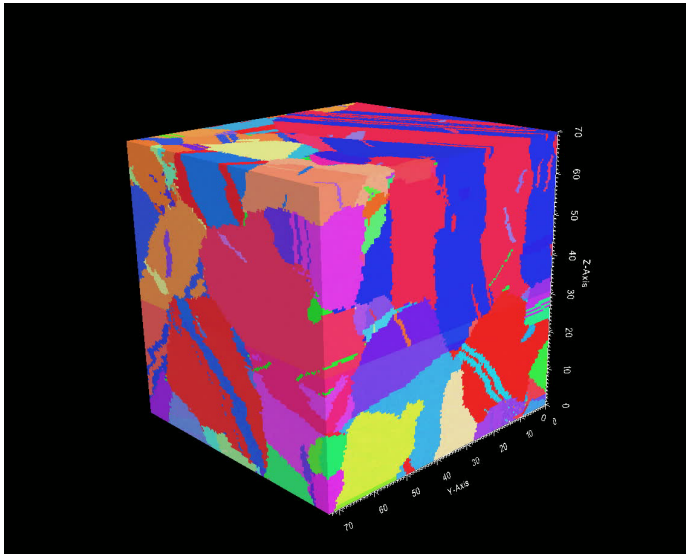

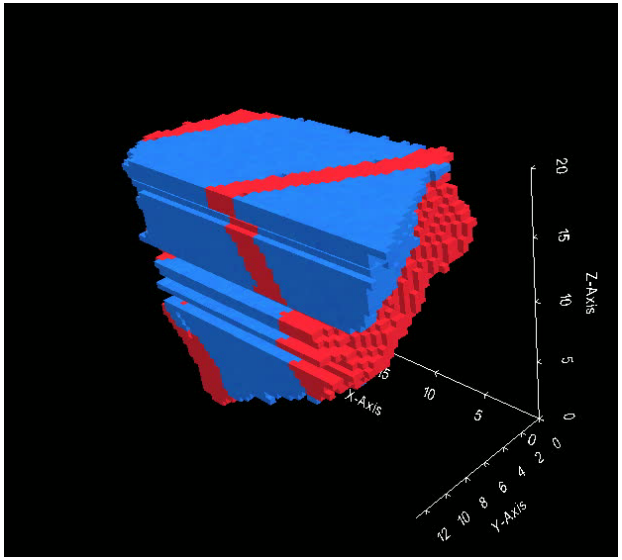


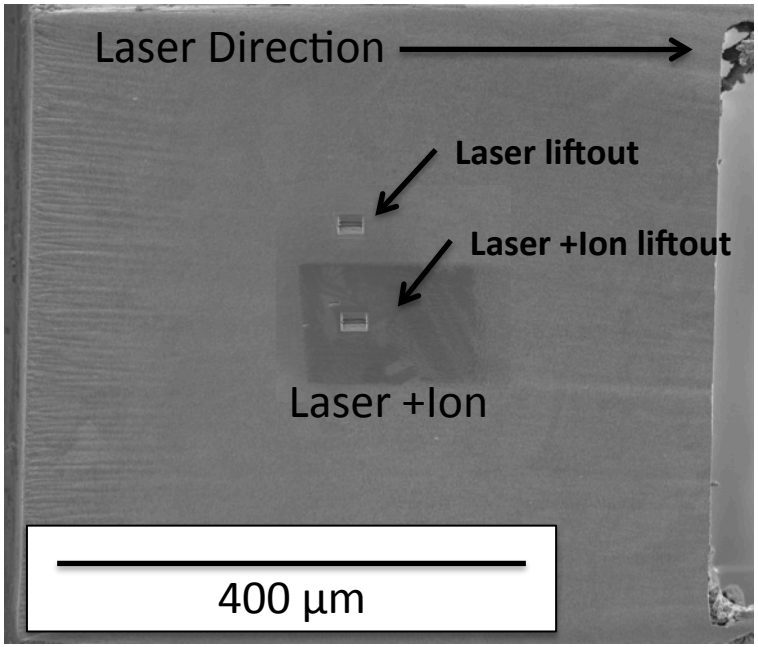


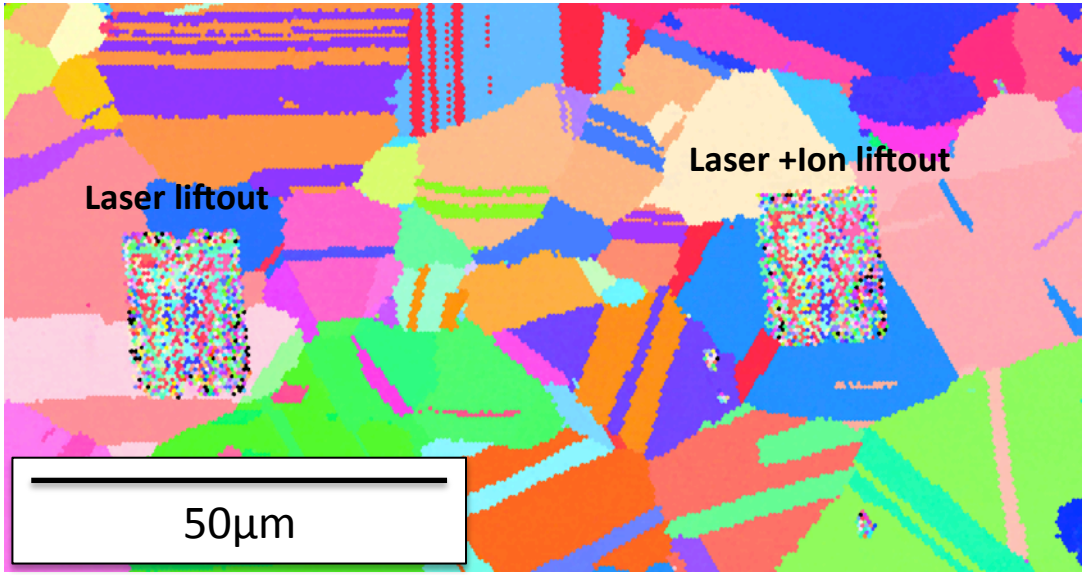

# Removing Roughness with FIB in Rene88DT

**Laser Ablated**

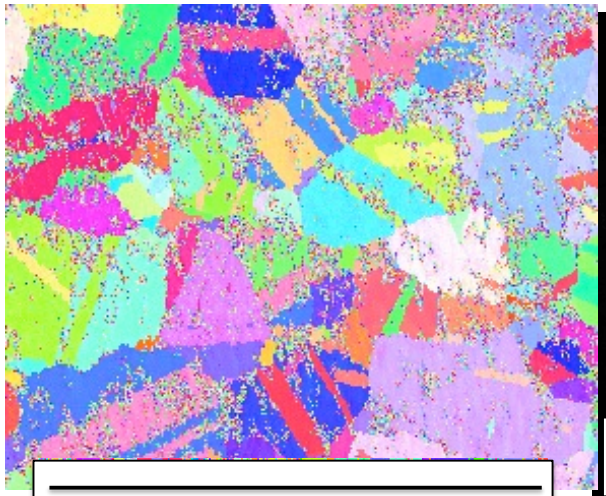


Pt Cap

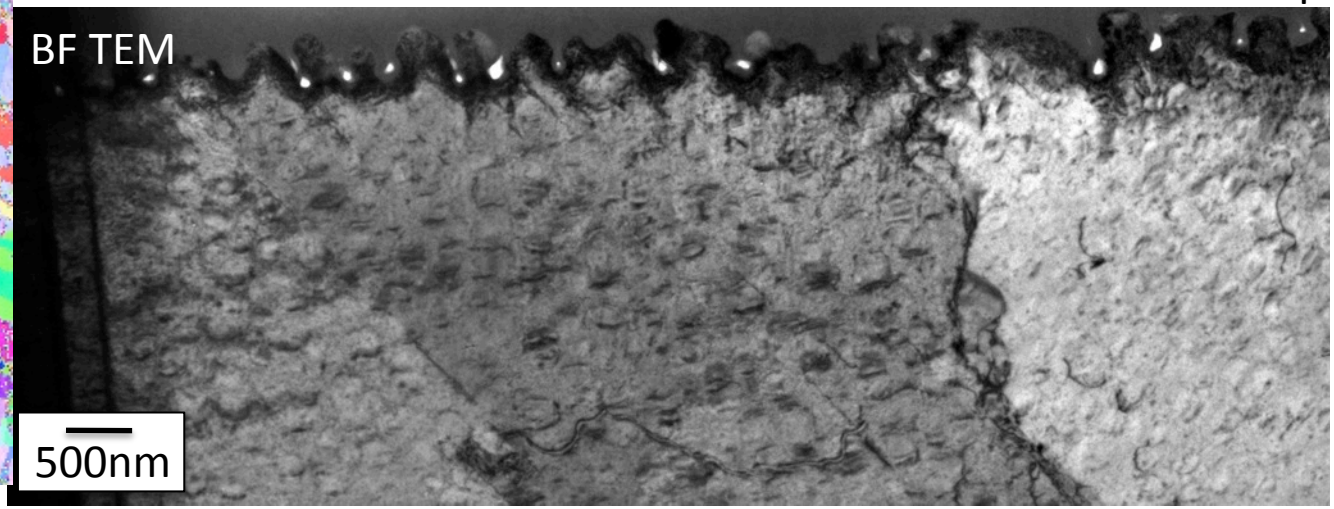


**Laser Ablated + FIB Milled**

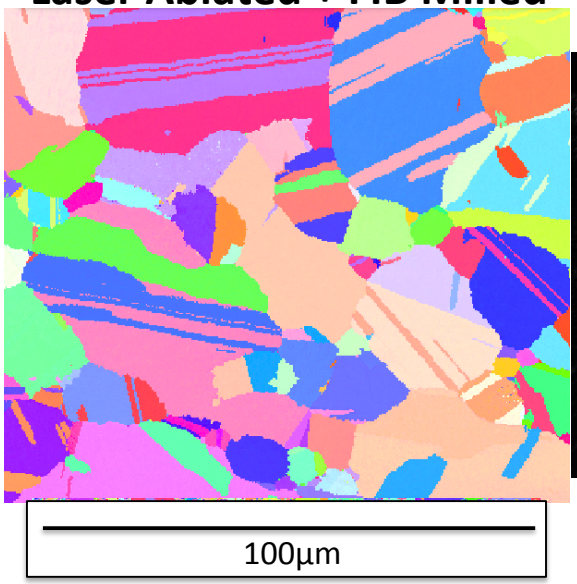


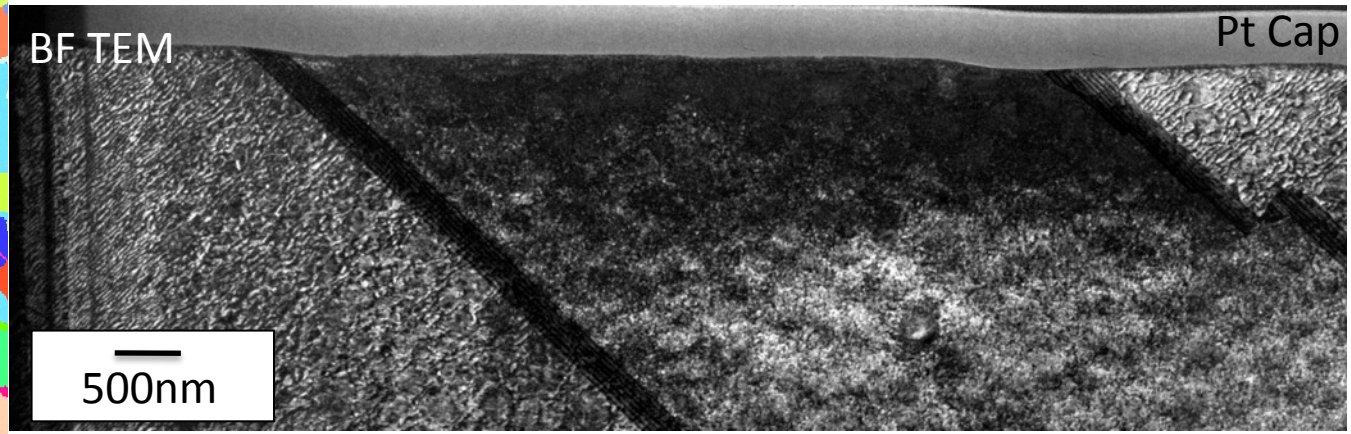


FIB parameters: 30kV, 20nA, <10° glancing angle

UC SANTA BARBARA engineering

The convergence of research and innovation.

# Recrystallization of Grains in Rene88DT

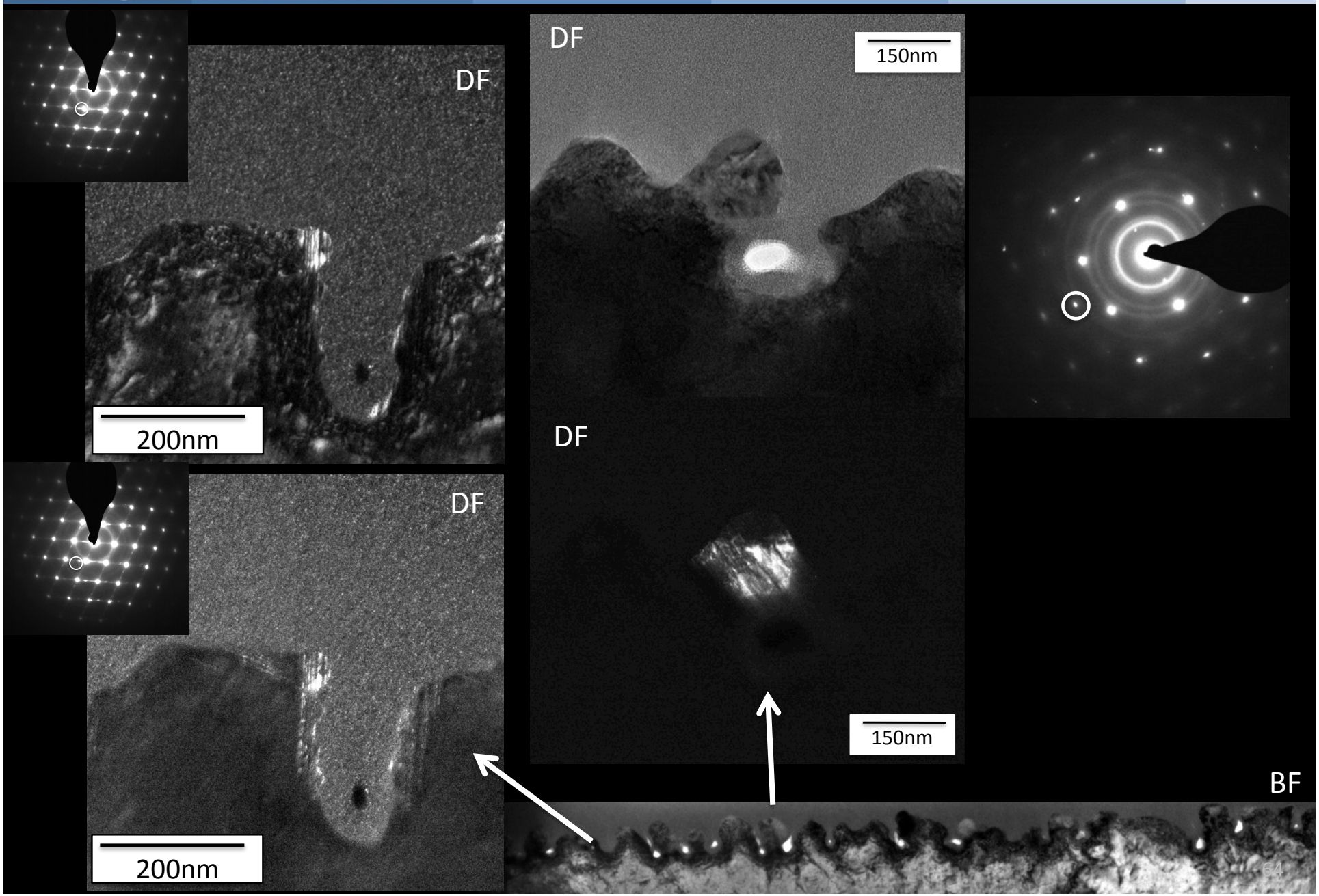

# Origins of Spatially Degraded EBSD Patterns

Rene88DT – Fs. Laser Ablated Surface

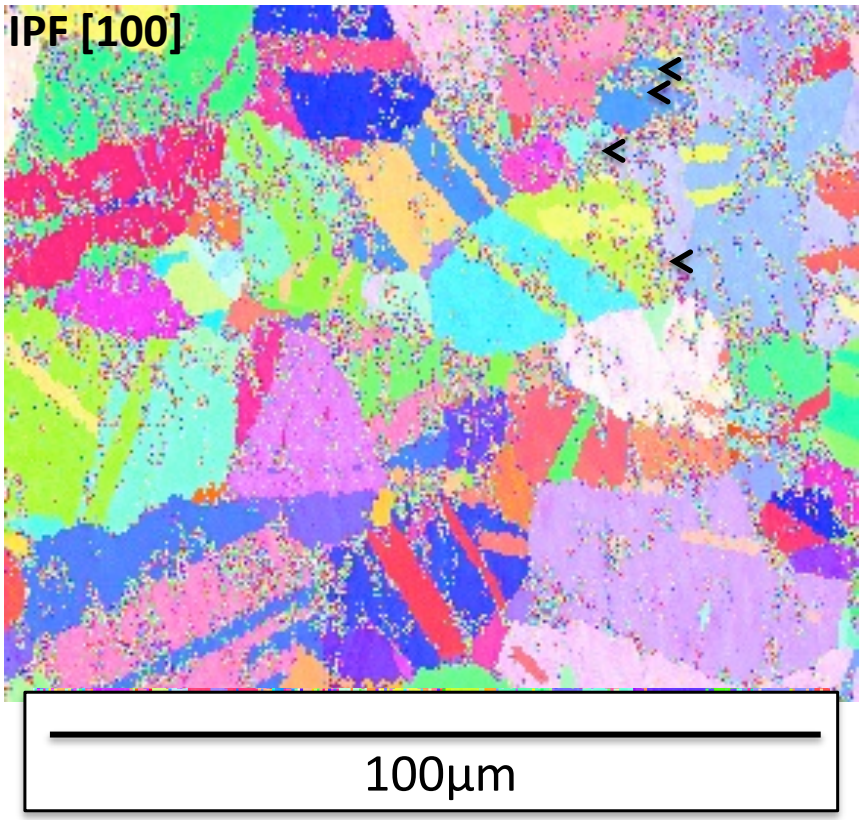


Examples of non-indexed or poorly indexed EBSD patterns

Spatial periodicity of non-indexed points correlates with LIPSS and recrystalization

Need to confirm by EBSD mapping a surface, and liftout TEM from a known location

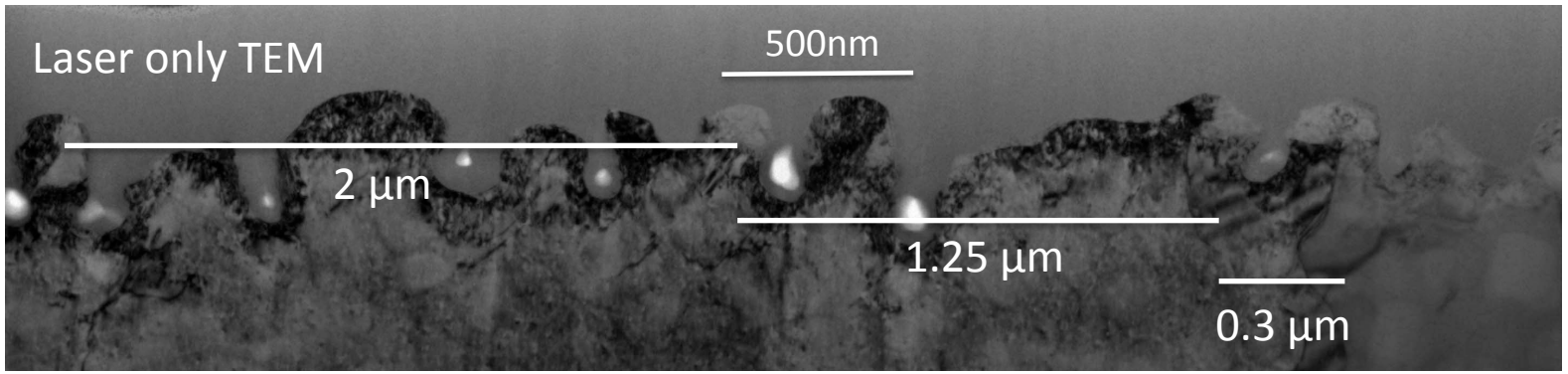

# Optimizing FIB Milling Parameters for EBSD

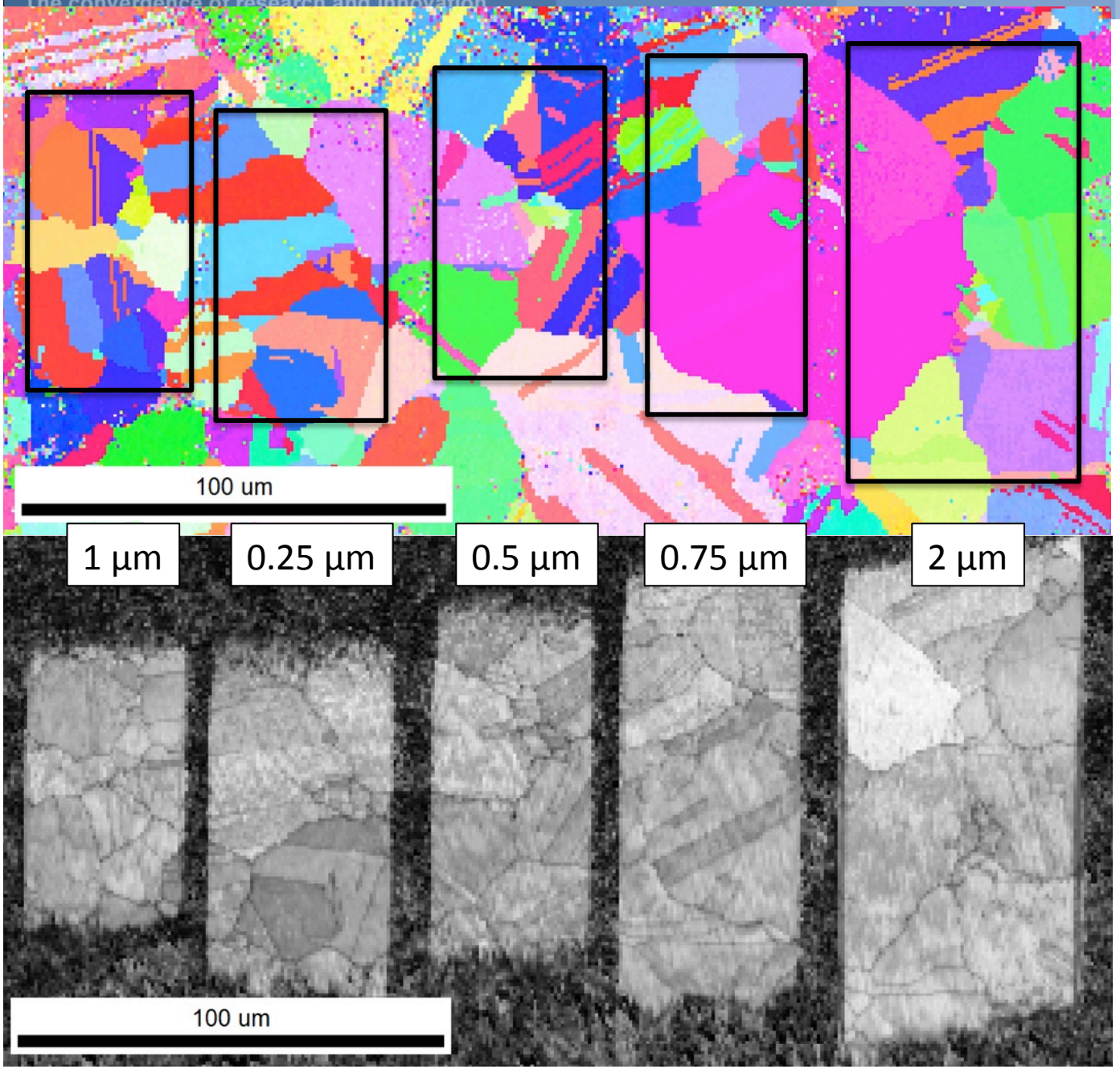


FIB Conditions:
30kV @ 20 nA

Depths calibrated for Si with Normal FIB beam Incidence

Ion mill depth independent of EBSD image quality

< 0.1-0.2 µm threshold FIB mill depth for dramatic improvement in EBSD

Why?

# STO 3D dataset from Pedestal

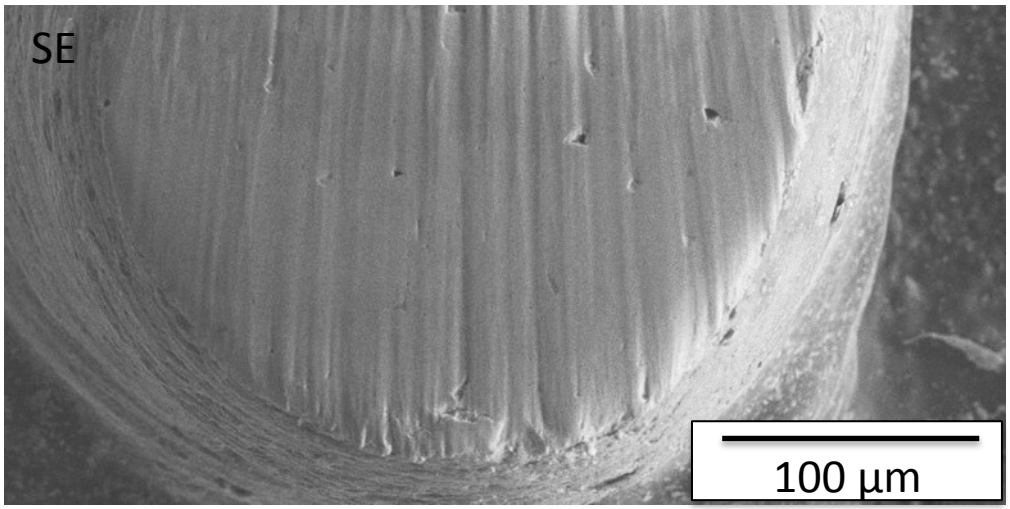


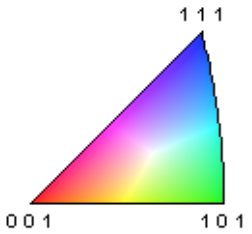


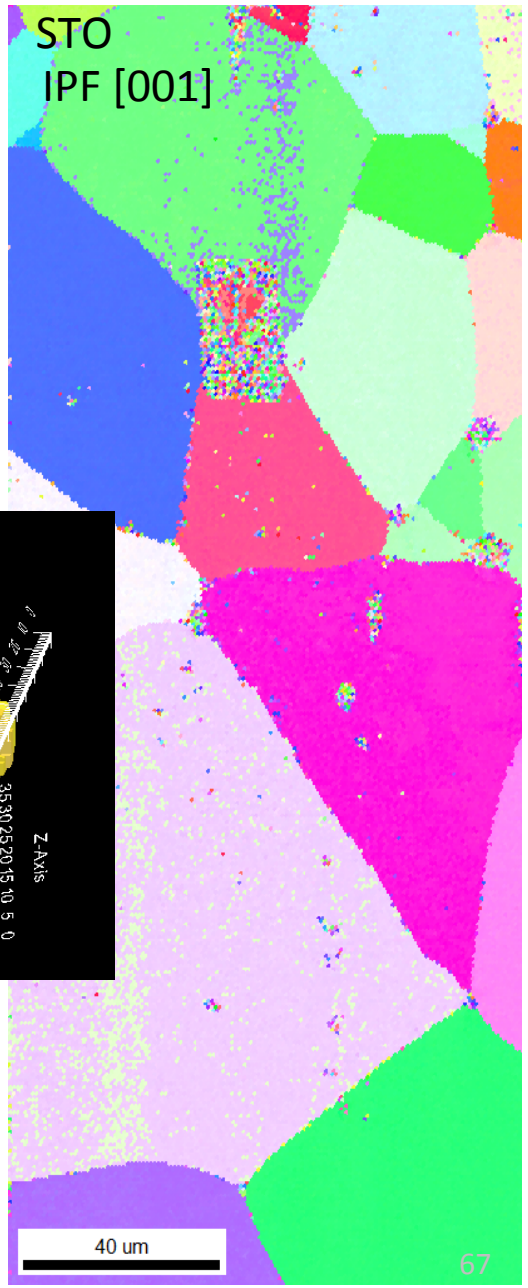


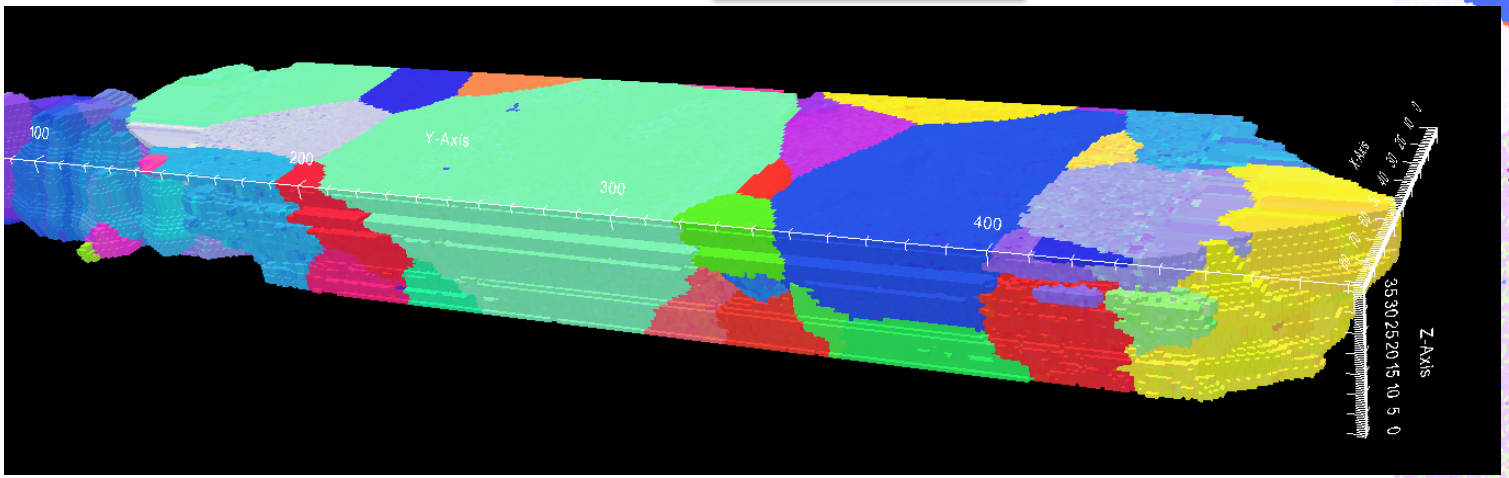


- EBSD patterns can be imaged from a relatively narrow range of Fs. laser machining fluences
- Would like to expand the area over which EBSD patterns can be indexed to the entire pedestal

# STO LIPSS and FIB Liftout

LIPSS depth:
darker contrast – smoother
lighter contrast – rougher

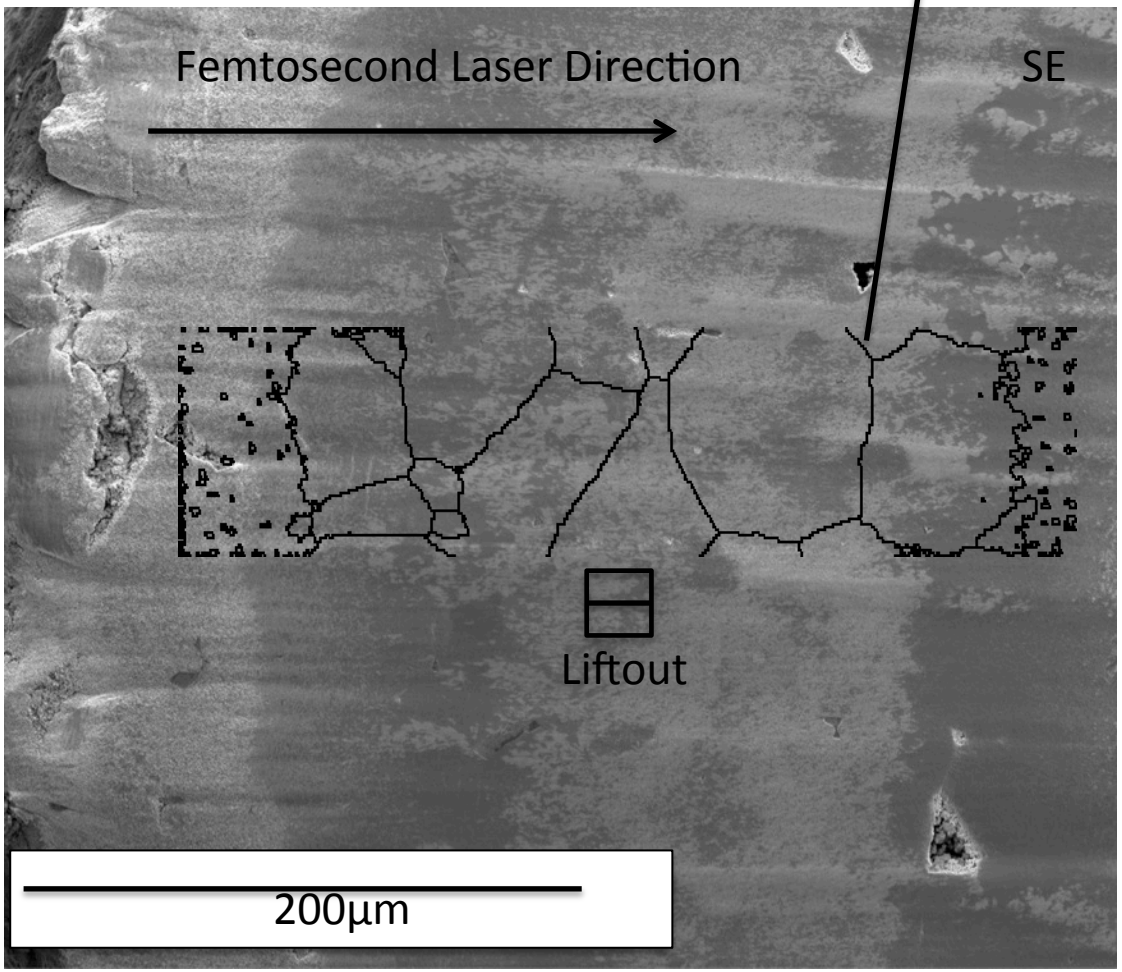


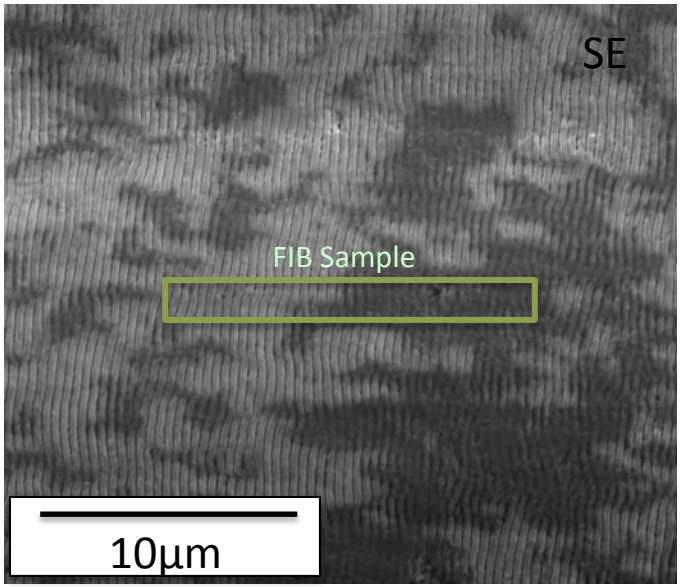


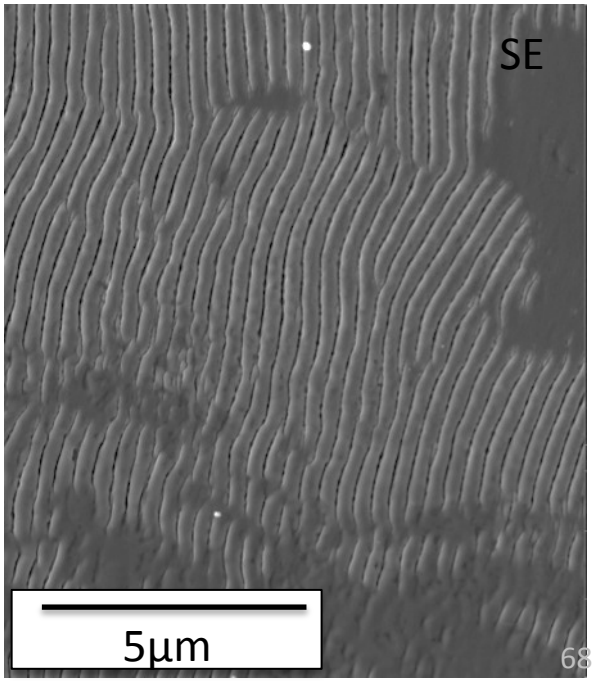

# Near glancing angle FIB milling in STO

5kV 13 nA FIB mil  30 kV 65nA FIB mill

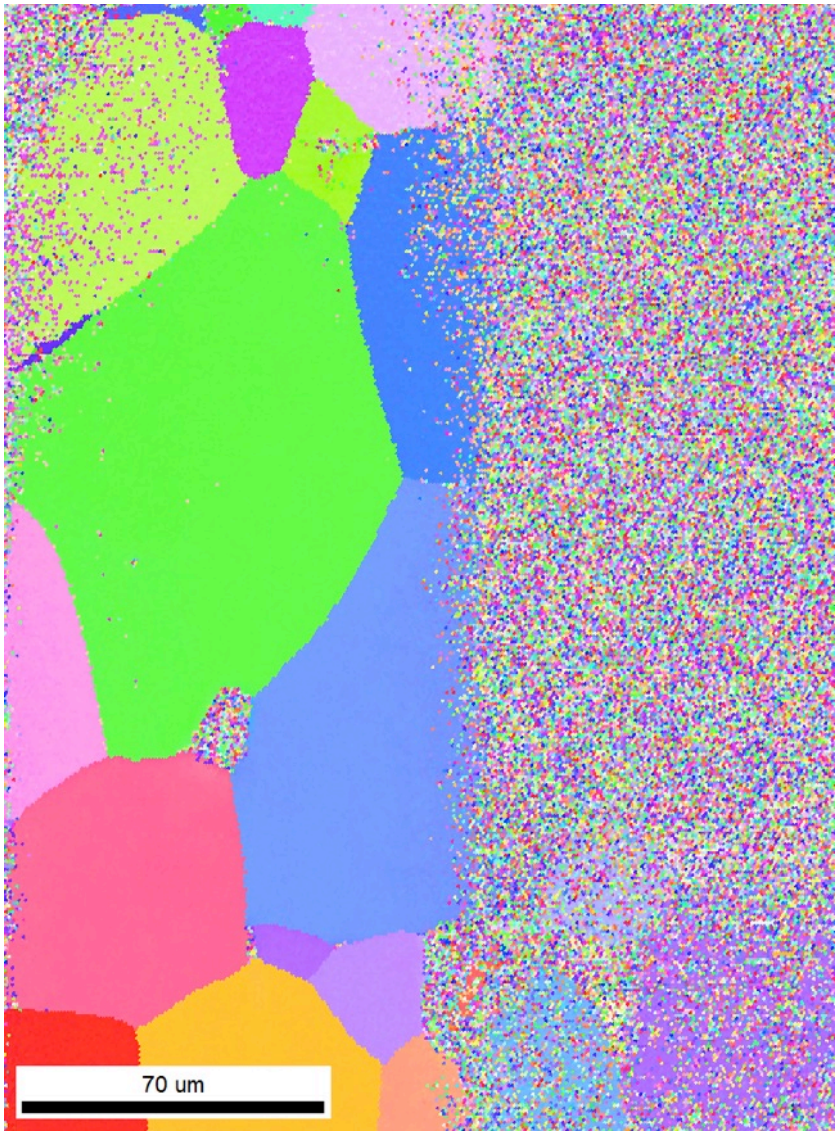


30kV  5kV

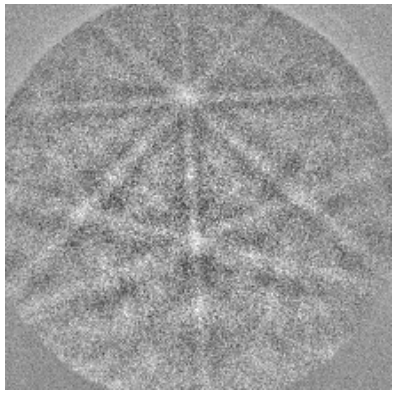

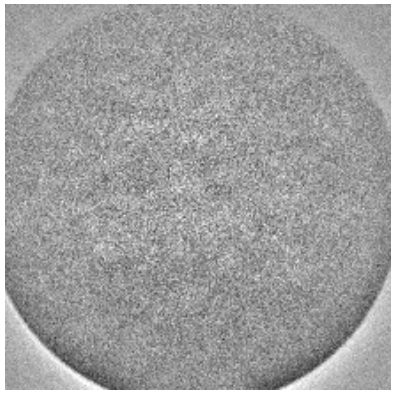

- Laser ablated surface milled at <10° at both 5kV and 30kV
- Diffraction patterns only able to be indexed after 5kV FIB mill
- Current optimized to be highest possible for each accelerating voltage
- TEM foil liftouts required to discern STO Ga+ damage mechanisms

# Removing Roughness with FIB in STO

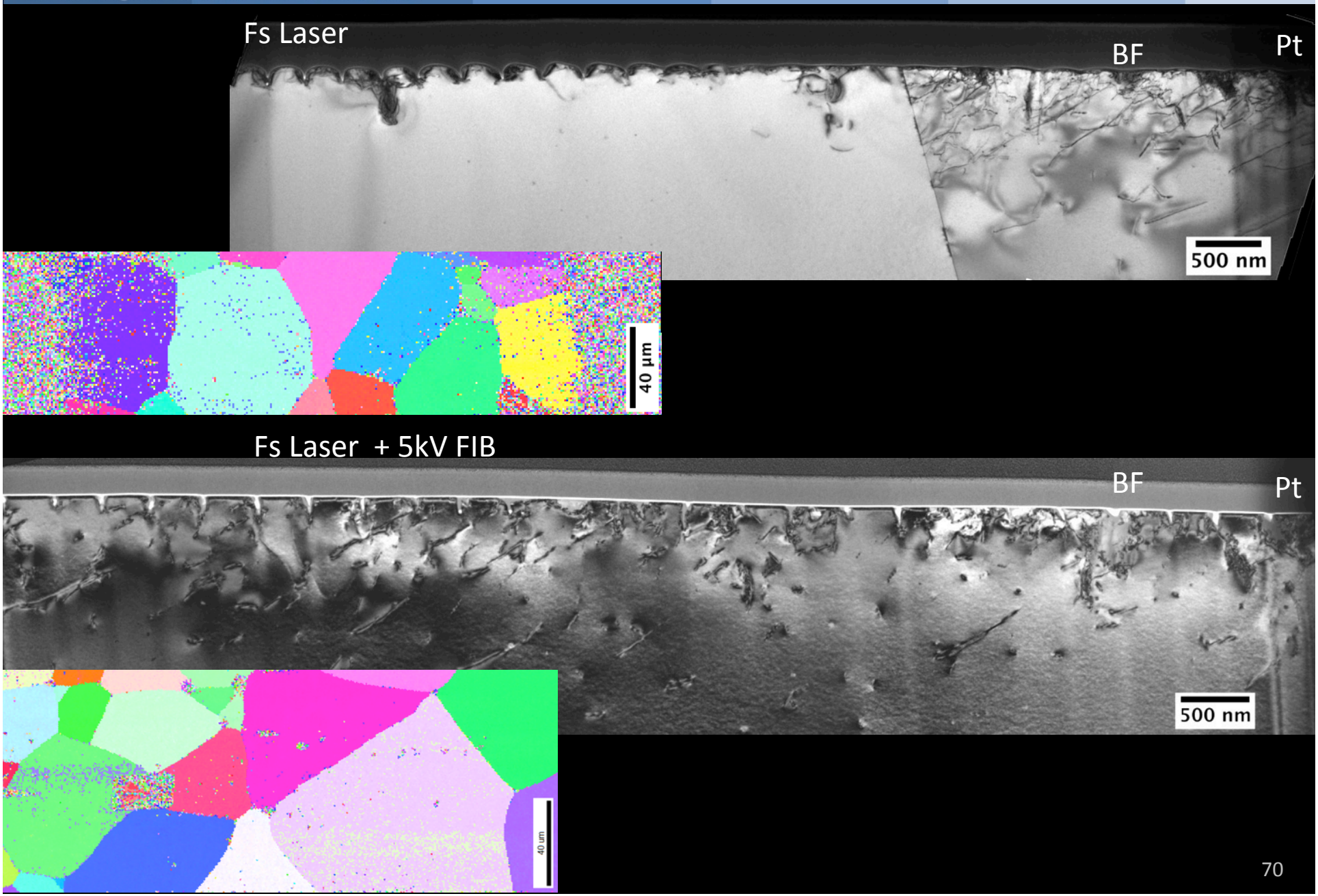

# STO Dislocation Structure

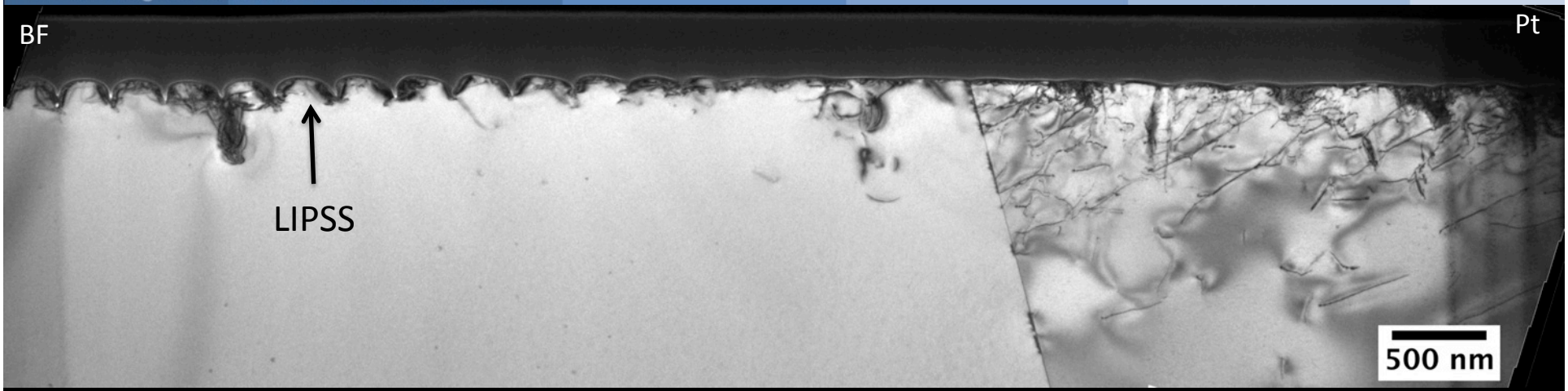


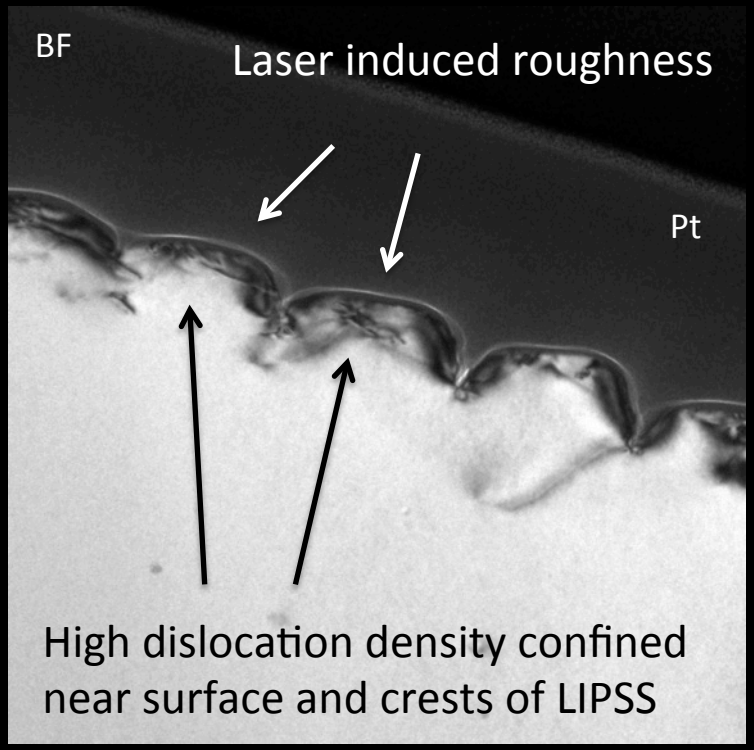


High dislocation density confined near surface and crests of LIPSS

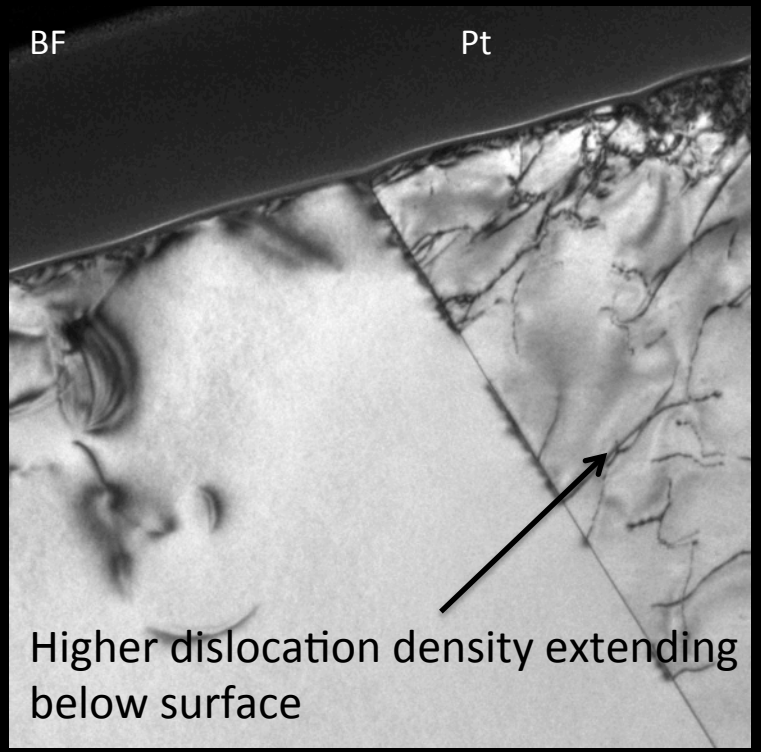


Higher dislocation density extending below surface

# Plasticity as a Function of Grain Orientation

**IPF Map**

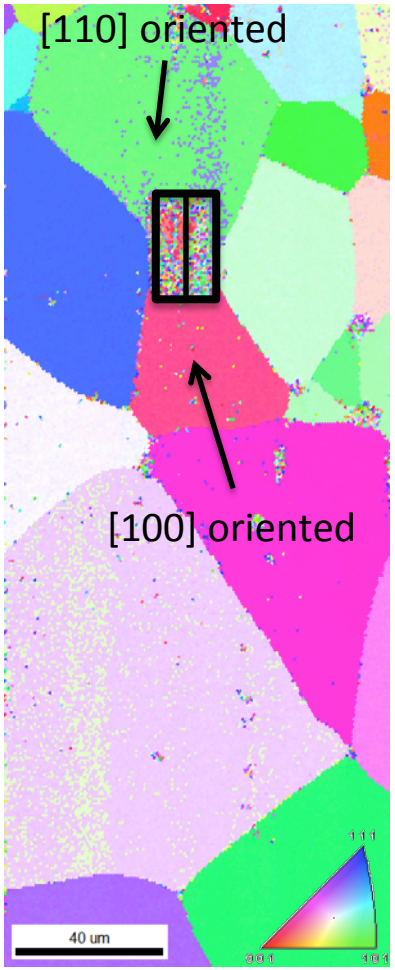


**Schmid Factor**

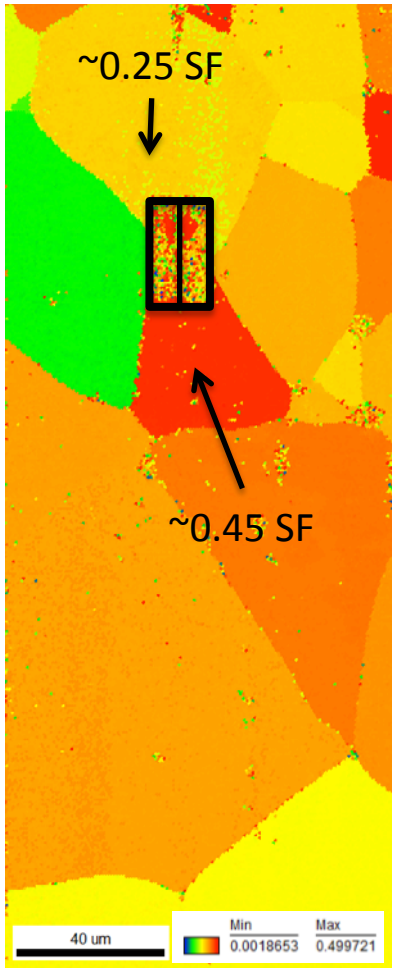


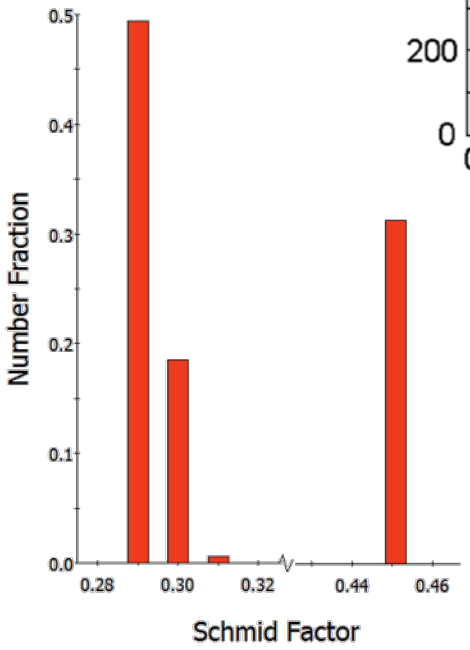


**Flow Stress vs. Temperature in STO**

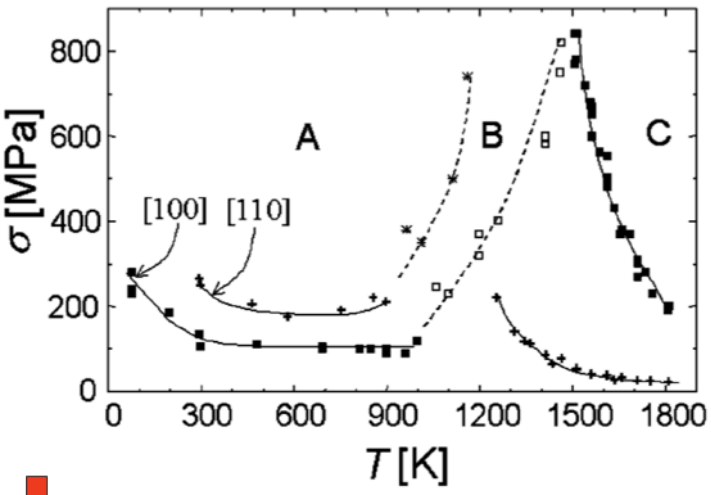


Stresses in [100] crystal are between 100-200 MPa

Enhanced plasticity in [100] grain

| Orientation | Regime A | | Regime C | |
|---|---|---|---|---|
| | Slip system | Schmid factor | Slip system | Schmid factor |
| <100> | <110>{110} | 0.5 | <110>{110} | 0.5 |
| <110> | <110>{110} | 0.25 | <100>{100} | 0.5 |

P. Gumbsch, M. Ruhle *et al*. APS. 87(2001) 8.
S. Taeri, D. Brunner, W. Sigle, M. Ruhle. Z. Metallkd. 6(2004) 95

# Fs. Laser + Ion in STO [100] Oriented Grains

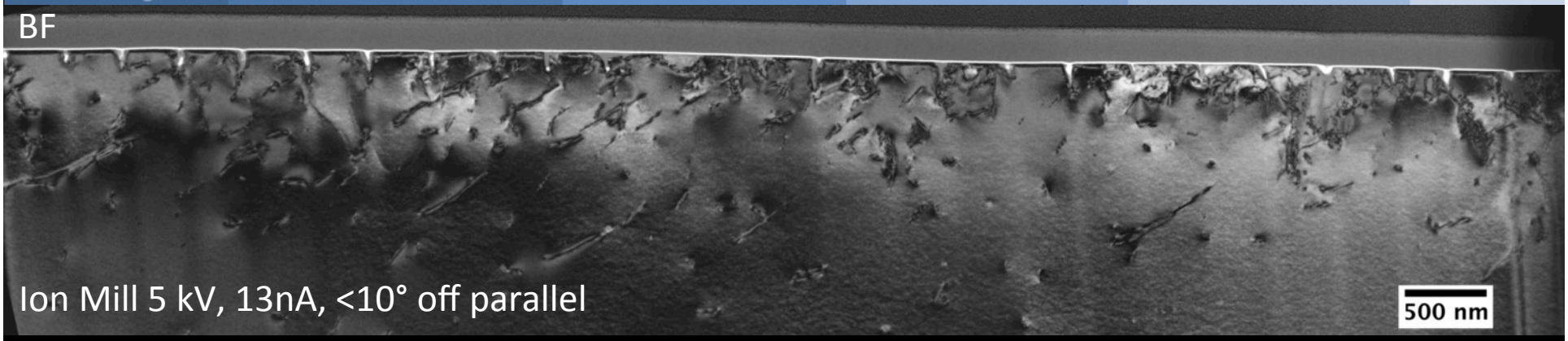


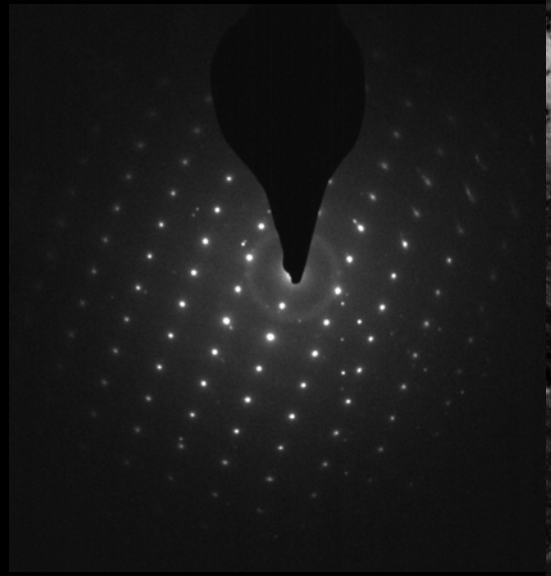

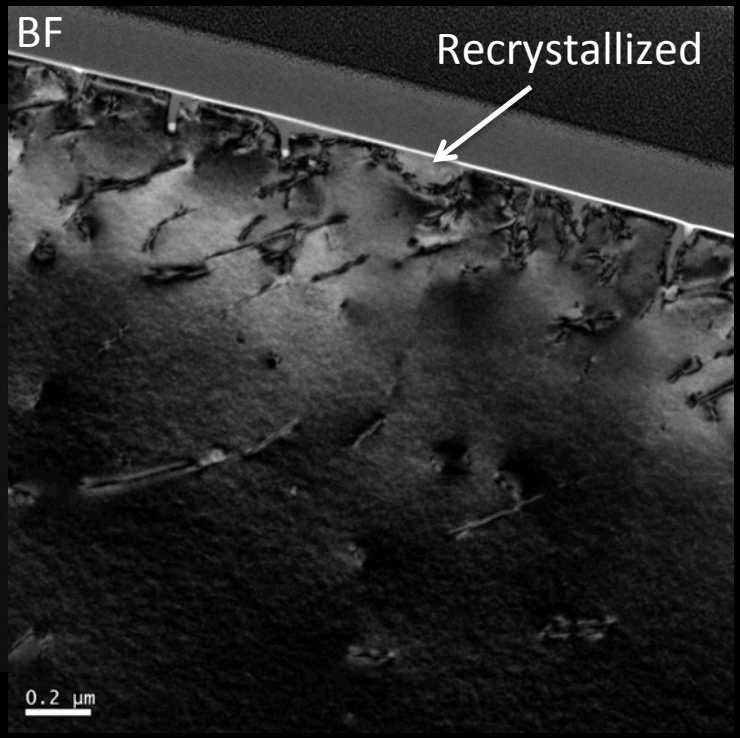

# Conclusions

- Bulk ablation with fs. laser can yield low damage surfaces capable of producing EBSD maps in STO, Ni, Mg, Ti
- FIB milling at near glancing angles in conjunction with fs. laser ablation can produce lower damage surfaces with higher EBSD map quality in both STO and Ni (and Ti)
- In STO dislocation damage is more extensive in grains with preferred orientations for slip, allowing us to characterize the stresses being imparted on the sample

# Questions?

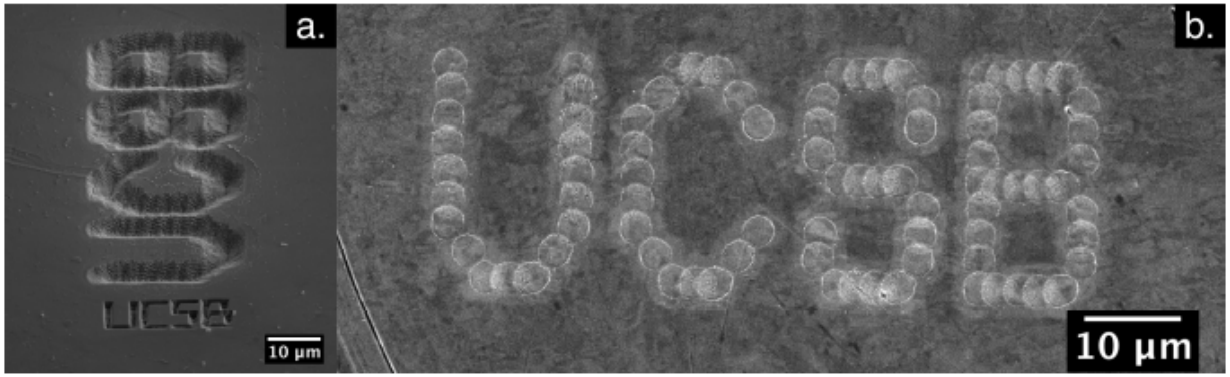


**Funding Sources:**
ONR, AFOSR, NSF, General Electric